UNIVERSIDADE ESTADUAL PAULISTA
"JÚLIO DE MESQUITA FILHO"
Campus de São José do Rio Preto

Ícaro Putinhon Caruso

Estudo de interação dos flavonóides Isovitexina e 2-Fenilcromona com a Albumina do Soro Humano: abordagem experimental e computacional

São José do Rio Preto – SP

2016

Ícaro Putinhon Caruso

Estudo de interação dos flavonóides Isovitexina e 2-Fenilcromona com a Albumina do Soro Humano: abordagem experimental e computacional

Tese apresentada como parte dos requisitos para obtenção do título de Doutor em Biofísica Molecular, junto ao Programa de Pós-graduação em Biofísica Molecular, do Instituto de Biociências, Letras e Ciências Exatas da Universidade Estadual Paulista "Júlio de Mesquita Filho", Campus de São José do Rio Preto.

Orientador: Prof. Dr. Marinônio Lopes Cornélio
Co-orientador: Prof. Dr. Marcelo Andrés Fossey

São José do Rio Preto – SP

2016

Caruso, Ícaro Putinhon.
Estudo de interação dos flavonóides Isovitexina e 2-Fenilcromona com a Albumina do Soro Humano : abordagem experimental e computacional / Ícaro Putinhon Caruso. -- São José do Rio Preto, 2016
97 f. : il., tabs.

Orientador: Marinônio Lopes Cornélio
Coorientador: Marcelo Andrés Fossey
Tese (doutorado) – Universidade Estadual Paulista "Júlio de Mesquita Filho", Instituto de Biociências, Letras e Ciências Exatas

1. Biologia molecular. 2. Biofísica. 3. Flavonóides. 4. Sangue - Proteínas. 5. Albumina. 6. Espectroscopia de fluorescência. 7. Dinâmica molecular. I. Cornélio, Marinônio Lopes. II. Fossey, Marcelo Andrés. III. Universidade Estadual Paulista "Júlio de Mesquita Filho". Instituto de Biociências, Letras e Ciências Exatas. IV. Título.

CDU – 577.3

Ficha catalográfica elaborada pela Biblioteca do IBILCE
UNESP - Câmpus de São José do Rio Preto

Ícaro Putinhon Caruso

Estudo de interação dos flavonóides Isovitexina e 2-Fenilcromona com a Albumina do Soro Humano: abordagem experimental e computacional

Tese apresentada como parte dos requisitos para obtenção do título de Doutor em Biofísica Molecular, junto ao Programa de Pós-graduação em Biofísica Molecular, do Instituto de Biociências, Letras e Ciências Exatas da Universidade Estadual Paulista "Júlio de Mesquita Filho", Campus de São José do Rio Preto.

Comissão Examinadora

Prof. Dr. Marinônio Lopes Cornélio
Professor Adjunto
UNESP - São José do Rio Preto

Prof. Dr. Raghuvir Krishnaswamy Arni
Professor Titular
UNESP - São José do Rio Preto

Prof. Dr. Jorge Chahine
Professor Adjunto
UNESP - São José do Rio Preto

Prof. Dr. Amando Siuiti Ito
Professor Titular
USP - Ribeirão Preto

Prof. Dr. Luiz Claudio Di Stasi
Professor Adjunto
UNESP - Botucatu

São José do Rio Preto – SP
Agosto de 2016

Dedicatória

Dedico este trabalho à minha família que sempre me apoiou e auxiliou na realização dos meus estudos.

Agradecimentos

Ao Prof. Dr. Marinônio Lopes Cornélio, pela valiosa orientação e atenção dedicadas à realização deste trabalho e do meu progresso acadêmico. Obrigado pela confiança depositada em mim durante todos esses anos que trabalhamos juntos, sempre me dando liberdade para desenvolver este projeto e outros trabalhos.

Ao Prof. Dr. Marcelo Andrés Fossey, pela dedicada co-orientação empregada na realização deste projeto, sempre disposto para discutir os resultados com muita atenção e entusiasmo. Obrigado por sempre me incentivar mostrando o valoroso e surpreendente caminho da ciência.

À Profa. Dra. Fátima Pereira de Souza pelo incentivo e sábios conselhos proporcionados ao longo de toda a minha caminhada acadêmica. Obrigado pela confiança que sempre depositou em mim. Admiro sua dedicação a ciência e seu empenho para crescimento do nosso grupo de pesquisa.

Aos Profs. Drs. Wagner Vilegas e José Maria Barbosa Filho, por fornecerem os flavonóides (Isovitexina e 2-Fenilcromona) utilizados no desenvolvimento deste projeto de pesquisa.

A todo o corpo docente do Departamento Física, pelos ricos ensinamentos transmitidos. Não posso deixar de ressaltar a importância desse grupo de pesquisa para o desenvolvimento da Biofísica Molecular no nosso País e no mundo.

Aos amigos de laboratório e departamento, pelas amizades e ajudas proporcionadas ao longo desses anos. Compartilhamos muitas alegrias e angústias que somente a vida acadêmica poderia nos fornecer.

À minha namorada Mariana, que sempre esteve ao meu lado durante toda essa trajetória, tanto nos momentos felizes quanto nos momentos difíceis. Obrigado, por me apoiar em todas as minhas decisões e sempre me fazer acreditar que todos os meus objetivos seriam alcançados. Eu te agradeço por me dar forças para continuar na minha caminhada pessoal e profissional.

À minha mãe Adriana pelos esforços desmedidos dedicados à minha formação. Obrigado por ter desempenhando o papel de mãe e pai que somente uma mulher com sua força e determinação poderia ter desempenhado.

Aos meus avós, Diogo e Alice, que nunca mediram esforços em proporcionar todo o suporte necessário para mais essa conquista em minha vida. Agradeço também aos meus irmãos, Ítalo e Thales, pelo incentivo durante essa jornada.

A toda família da minha namorada pelo apoio e bons conselhos que me transmitiram ao decorrer dessa jornada.

Ao Prof. Daniel, pela ajuda fundamental fornecida no começo da minha jornada acadêmica, mostrando a importância do caminho da educação na vida de uma pessoa.

Aos técnicos Paulinho, Barbosa, Marcelino, Bruno e Fábio, e as secretárias do departamento, Ilva e Valéria, que sempre foram atenciosos e prestativos.

Aos Profs. Drs. Raghuvir Krishnaswamy Arni, Jorge Chahine, Amando Siuiti Ito e Luiz Claudio Di Stasi por terem aceito a participarem da minha banca de avaliação.

À Coordenação e Aperfeiçoamento de Pessoal de Nível Superior (CAPES) e ao Conselho Nacional de Pesquisa (CNPq) pelo apoio financeiro durante minha trajetória acadêmica.

"If I have seen farther than others, it is because I stood on the shoulders of giants."

— Sir Isaac Newton

Resumo

Os flavonóides fazem parte de uma ampla classe de compostos polifenólicos os quais ocorrem naturalmente nas plantas e podem ser encontrados nas sementes, caules, folhas, flores e/ou frutos. Estudos recentes indicam que esses compostos polifenólicos podem apresentar uma variedade significativa de atividades biológicas benéficas para a saúde humana, como por exemplo: antioxidante, anti-inflamatória, antibacteriana, antiviral e anticancerígena. A Albumina do Soro Humano (HSA) é a principal proteína extracelular presente no plasma sanguíneo. A função central dessa proteína é transportar e distribuir ligantes endógenos e exógenos para diferentes alvos moleculares no corpo humano. Por tais aspectos, torna-se importante o desenvolvimento de estudos que caracterizam a interação dos flavonóides com a proteína transportadora HSA. Este trabalho investiga a interação dos flavonóides Isovitexina (ISO) e 2-Fenilcromona (2PHE) com a HSA, utilizando técnicas experimentais de espectroscopia de fluorescência, absorbância UV-Vis, dicroísmo circular (CD) e infravermelho com transformada de Fourier (FT-IR); juntamente com ferramentas computacionais de cálculo *ab initio*, dinâmica molecular e modelagem molecular. A integração dessas abordagens experimentais e computacionais possibilita caracterizar a formação dos complexos HSA-flavonóides, determinando aspectos físico-químicos como: constantes de afinidade, parâmetros termodinâmicos, número de sítios de ligação, perfil de cooperatividade e resíduos de aminoácidos responsáveis pelas interações proteína-flavonóides (hidrofóbicas e eletrostáticas).

Palavras-chave: Flavonóide. Isovitexina. 2-Fenilcromona. Albumina do Soro Humano. Espectroscopia de fluorescência. Função de densidade de ligação. Dinâmica molecular. Modelagem molecular.

Abstract

Flavonoids belong to a large class of polyphenolic compounds which occur naturally in plants and can be found seeds, stems, leaves, flowers and/or fruits. Recent studies indicate that these polyphenolic compounds can present a significant variety of beneficial biological activities on human health, such as: antioxidant, anti-inflammatory, antibacterial, antiviral, and anticancer. Human Serum Ambumin (HSA) is the main extracellular protein presents in blood plasma. The core function of this protein is to carry and distribute endogenous and exogenous ligands to different molecular targets in the human body. For these aspects, it is important to develop studies that characterize the interaction of the flavonoids with the carrier protein HSA. This work investigates the interaction of the flavonoids Isovitexin (ISO) and 2-Phenylchromone (2PHE) with the HSA, using experimental techniques of fluorescence, UV-Vis absorbance, circular dichroism (CD), and Fourier transform infrared (FT-IR) spectroscopy; along with computational tools of ab initio calculation, molecular dynamics, and molecular modeling. The integration of these experimental and computational approaches allows to characterize the formation of the HSA-flavonoids complexes, determining physicochemical aspects, sucha as: affinity constants, thermodynamic parameters, number of binding sites, cooperativity profile and aminoacid residues responsable for the protein-flavonoids interactions (hydrophobic and electrostatic).

Keywords: Flavonoid. Isovitexin. 2-Phenylchromone. Human Serum Albumin. Fluorescence spectroscopy. Bindind density function. Molecular dynamics. Molecular modeling.

Lista de Figuras

Lista de Tabelas

Lista de Abreviaturas

2PHE – *2-Phenylchromona* (2-Fenilcromona)

AhR – *Aryl Hydrocarbon Receptor* (Receptor de Hidrocarboneto Aromático)

ASA – *Accessible Superficial Area* (Área de Acessibilidade Superficial)

BDF – *Binding Density Function* (Função de Densidade de Ligação)

CD – *Circular Dichroism* (Dicroísmo Circular)

COX-2 – Cicloxigenase-2

DFT – *Density Functional Theory* (Teoria do Funcional de Densidade)

DNA – *Deoxyribonucleic Acid* (Ácido Desoxirribonucleico)

DSC – Differential Scanning Calorimetry (Calorimetria de Varredura Diferencial)

ER – Estrogen Receptor (Receptor de Estrogênio)

FT-IR – *Fourier Transformed Infrared* (Infravermelho com Transformada de Fourier)

HSA – *Human Serum Albumin* (Albumina do Soro Humano)

IBU – Ibuprofen (Ibuprofeno)

ISO – Isovitexin (Isovitexina)

JPBA – *Journal Pharmaceutical and Biomedical Analysis*

LPS – Lipopolissacarídeos

MCF-7 – Michigan Cancer Foundation-7

MEP – *Molecular Electrostatic Potential* (Potencial Eletrostático Molecular)

MTO – Methyl Orange (Laranja de Metila)

NaCl – Cloreto de Sódio

NF-κB – Nuclear Factor κB (Fator Nuclear κB)

NMR – *Nuclear Magnetic Resonance* (Ressonância Magnética Nuclear)

PDB – *Protein Data Bank* (Banco de Dados de Proteína)

PGE_2 – Prostaglandina E2

RNA – *Ribonucleic Acid* (Ácido Ribonucleico)

ROS – Reactive Oxygen Species (Espécies Reativas de Oxigênio)

STD – *Saturation-Transfer Difference* (Diferença de Transferência de Saturação)

TNFα – *Tumor Necrosis Factor* α (Fator de Necrose Tumoral α)

UV-Vis – *Ultraviolet-Visible* (Ultravioleta-Visível)

WAR – Warfarin (Varfarina)

Lista de Símbolos

F_0 – Intensidade de fluorescência na ausência de supressor

F – Intensidade de fluorescência na presença do supressor

K_q – Constante de supressão bimolecular

τ_0 – Tempo de vida de fluorescência na ausência do supressor

$[Q]$ – Concentração do supressor

K_{SV} – Constante de supressão de Stern-Volmer

n – Número de sítios de ligação

K_b – Constante de ligação

$[P]$ – Concentração total de proteína

λ_{ex} – Comprimento de onda de excitação

ΔH^o – Variação de entalpia

ΔS^o – Variação de entropia

R – Constante universal dos gases ideais

T – Temperatura

ΔG^o – Variação da energia livre de Gibbs

$\sum \nu_i$ – Distribuição de ligantes ligados por macromoléculas em i estados diferentes

L_F – Concentração de ligante livre

L_T – Concentração total de ligante

M_T – Concentração total de macromolécula

ΔS_{obs} – Variação de sinal fracional observado

$S_F M_T$ – Sinal observado para a macromolécula na ausência de ligante

K_a – Constante de associação

k_1 – Constante de associação do primeiro sítio

k_2 – Constante de associação do segundo sítio

n_H – Coeficiente de Hill

ΔG_B^T – Energia de ligação teórica

K_B^T – Constante de ligação teórica

k_1^T – Constante de associação teórica do primeiro sítio

k_2^T – Constante de associação teórica do segundo sítio

Sumário

1 Organização do trabalho

Neste trabalho serão apresentados os estudos de interação dos flavonóides Isovitexina (ISO) e 2-Fenilcromona (2PHE) com a Albumina do Soro Humano (HSA). Para a realização desses estudos foram utilizadas as técnicas experimentais de espectroscópica de fluorescência, absorbância UV-Vis, dicroismo circular (CD) e infravermelho com transformada de Fourier (FT-IR), assim como os métodos computacionais de cálculo *ab initio*, dinâmica molecular e modelagem molecular. Os trabalhos realizados com os flavonóides ISO [1] e 2PHE [2] foram publicados no *Journal Pharmaceutical and Biomedical Analysis* (JPBA) e *Food Chemistry*, respectivamente. Deste modo, este trabalho será organizado em uma seção de introdução sobre os flavonóides (ISO e 2PHE) e a HSA, e outra como os principais resultados experimentais e teóricos para a interação HSA-flavonóides. Os detalhes das metodologias empregadas nos estudos de interação podem ser encontrados nos Anexos I, II, III e IV.

O Anexo V apresenta as primeiras páginas dos artigos publicados em colaboração durante o doutoramento. As contribuições para os trabalhos envolveram a obtenção e/ou interpretação de dados de caracterização biofísica por espectroscopia de fluorescência, dicroísmo circular, calorimetria de varredura diferencial (DSC), diferença de transferência de saturação por ressonância magnética nuclear (STD-NMR) e modelagem molecular.

2 Introdução

2.1 Flavonóides

O primeiro registro de uma substância natural que posteriormente seria reconhecida como flavonóide foi descrito por Nehemiah Grew no século XVII. Em artigos para a *Royal Society* em Londres, Grew analisava as diferenças nas propriedades de solubilidade de pigmentos de plantas, dos quais alguns apresentavam-se solúveis em óleo e outros em água [3].

Os flavonóides são compostos polifenólicos que ocorrem naturalmente nas plantas, sendo encontrados nas sementes, caules, folhas, flores e/ou frutas. Os flavonóides são responsáveis por efeitos importantes na bioquímica e fisiologia das plantas atuando como antioxidantes, inibidores de enzimas, precursores de substâncias tóxicas e pigmentos (tons de amarelo, laranja e vermelho). Em adição, esses compostos polifenólicos estão envolvidos na fotossensibilização e transferência de energia, ações de hormônios e reguladores de crescimento, controle de respiração, fotossíntese, morfogênese, determinação de sexo e defesa contra infecções [4].

O termo "flavonóide" é usado geralmente para descrever uma ampla coleção de moléculas polifenólicas que contêm um esqueleto de carbono C6 – C3 – C6 (fenil-benzopirano). Dependendo da posição da ligação do anel aromático à porção benzopirano, esse grupo de compostos fenólicos pode ser dividido em três classes: flavonóides (2-fenil-benzopiranos), isoflavonóides (3-benzopiranos) e neoflavonóides (4-benzopiranos) (Figura 1) [5].

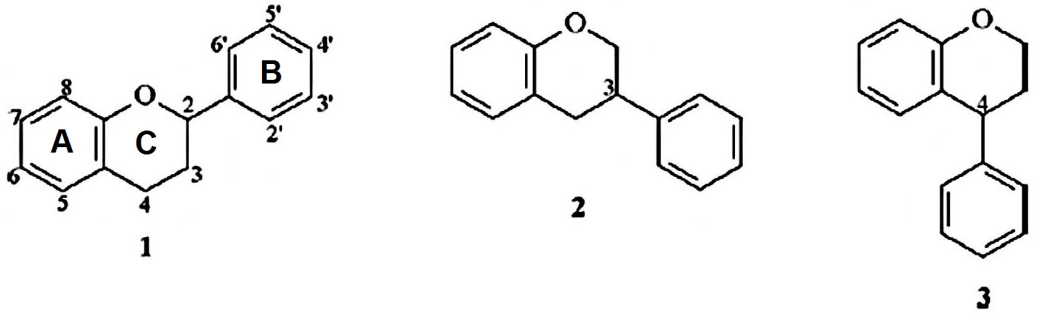

Figura 1: Estrutura molecular básica dos flavonóides (1), isoflavonóides (2) e neoflavonóides (3).

As várias classes de flavonóides diferem quanto ao nível de oxidação e/ou saturação presente no anel heterocíclico C. Dentre as várias classes de flavonóides podem ser citadas as flavanas, flavanonas, flavonas, flavonóis e flavanóis (flavan-3-ol, flavan-4-ol e flavan-3,4-diol) (2) [5]. Os compostos individuais dentro de uma classe diferenciam-se pelo padrão de substituição dos anéis A e B, tais como: substituintes hidroxilas (OH) e óxidos de metal (OMe), glicosilações e acilações [5, 6].

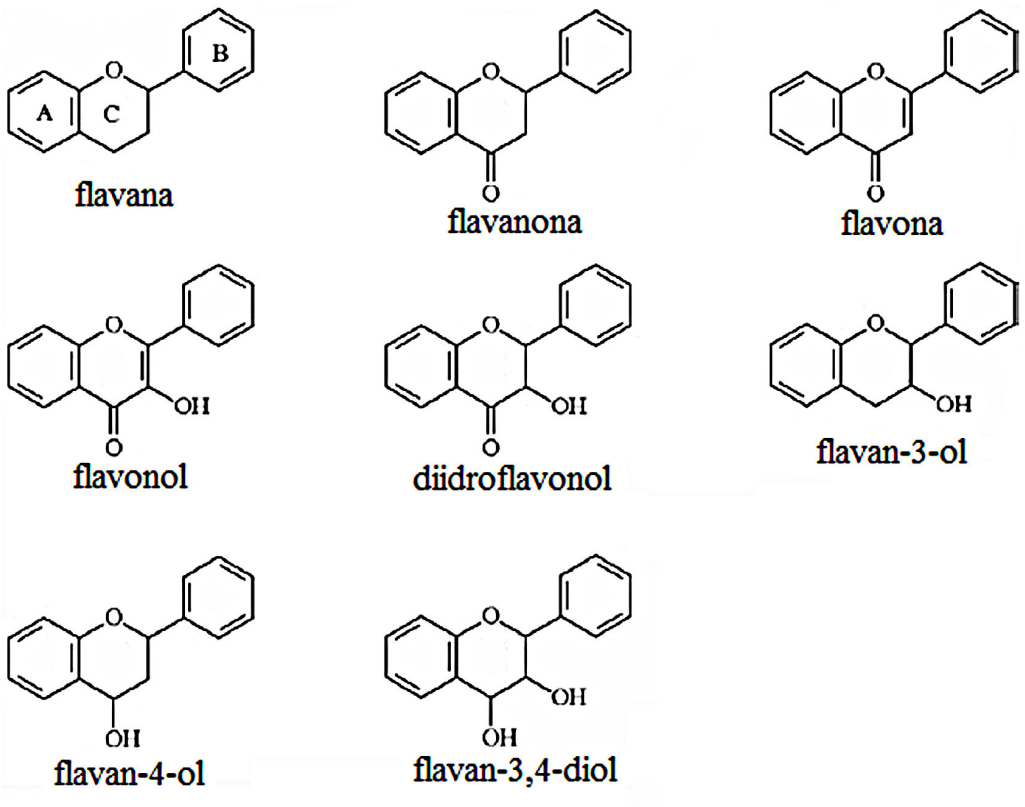

Figura 2: Diferentes classes de flavonóides. Essas classes se diferenciam com relação ao nível de oxidação e/ou saturação no anel heterocíclico C.

Além do seu importante papel biológico nas plantas e interações entre essas com insetos, os flavonóides têm sido extensivamente estudados nas últimas décadas devido aos seus possíveis benefícios para a saúde humana, como consequência de uma dieta rica em produtos de plantas [6]. Nutricionistas estimam que o consumo médio de flavonóides em uma dieta normal humana é de cerca de um a dois gramas por dia [7]. Suas propriedades farmacológicas e bioquímicas incluem: atividade anti-inflamatória, antioxidante, anticancerígena, antibacteriana, antiplaquetária, antiviral e de proteção contra doenças

cardiovasculares [4, 8–10]. Os flavonóides também são responsáveis pela inibição de varias enzimas, tais como: hidrolases, oxidoredutases, DNA sintetases, RNA polimerases, fosfatases e fosfoquinases [9, 11–13].

2.2 Isovitexina (ISO)

A Isovitexina (Apigenina-6-C-β-*D*-glicopiranosídeo) é um flavonóide glicosilado que consiste da união da flavona Apigenina e o sacarídeo glicose (Figura 3). Esse composto polifenólico pode ser encontrado na casca do arroz (*Oryza sativa* L.) [14], na planta Sempre-Vivas Chapadeira (*Syngonanthus bisulcatus* Rul.) [15] e *Tanxiang* (*Santalum album* L.) [16].

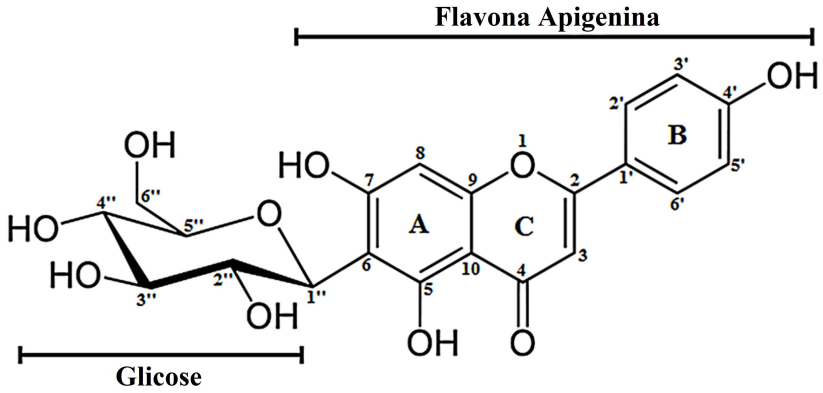

Figura 3: Estrutura química da Isovitexina (Apigenina-6-C-β-*D*-glicopiranosídeo).

Como muitos antioxidantes que apresentam atividade anti-inflamatória, a ISO também exibe um potente efeito antioxidante comparável com atividade do α-tocoferol (Vitamina E). Estudos demonstram que, em processos inflamatórios induzidos por lipopolissacarídeos (LPS) em macrófago de rato, essa flavona é capaz de inibir a produção e/ou liberação do fator de necrose tumoral α (TNFα), cicloxigenase-2 (COX-2) e prostaglandina E2 (PGE_2). O provável mecanismo de atividade anti-inflamatória da Isovitexina estaria relacionado com a inibição da ativação do fator nuclear κB (NF-κB), como consequência da atividade antioxidante desenvolvida por esse flavonóide. NF-κB é um fator de transcrição essencial na via de transdução do sinal inflamatório e sua ativação é fortemente associada com a produção de espécies reativas de oxigênio (ROS) intracelular, como peróxido de

hidrogênio, óxido nítrico e radical hidroxila. Esses efeitos antioxidante e anti-inflamatório da ISO poderia ter implicações em carcinogênese [14].

Trabalhos também demonstram que a Isovitexina apresentaria uma possível atividade antiulcerogênica e, dessa forma, poderia ajudar no tratamento de úlcera péptica . Lesões gástricas podem surgir como consequência de um dano direto das células da mucosa gástrica. Esse processo resulta no desenvolvimento de radicais livres e hiperoxidação de lipídeos. O flavonóides ISO poderia agir como composto antiulcerogênico provavelmente por causa de sua potente atividade antioxidante, que poderia prevenir a formação de radicais livres e também minimizar as injúrias causadas por reações oxidativas [15].

2.3 2-Fenilcromona (2PHE)

A 2-Fenilcromona é o composto polifenólico que apresenta a base estrutural das flavonas (Figura 4), as quais representam uma das principais classes de flavonóides. A 2PHE pode ser encontrada principalmente em cereais e ervas [17]. Em adição à sua atividade antioxidante, estudos indicam que a 2-Fenilcromona poderia exibir uma atividade anti-estrogênio, visto que, esse composto polifenólico apresenta uma propriedade inibitória da ação de estrogênio em células de câncer de mama humano MCF-7, sem se ligar ao receptor de estrogênio (ER). O mecanismo proposto para a atividade anti-estrogênio sugere que a 2PHE atuaria como um competidor agonista para o receptor de hidrocarboneto aromático (AhR) e, dessa forma, interromperia a atividade de transcrição do ER, degradando-o. AhR é um fator de transcrição ativado por ligante que estimula a expressão gênica [18].

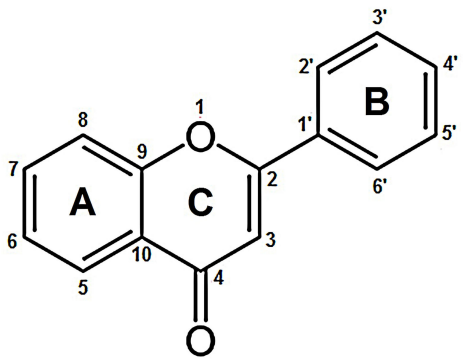

Figura 4: Estrutura química da 2-Fenilcromona, a base estrutural das flavonas.

O flavonóide 2PHE presente na *Primula macrophylla* (Primulaceae) é o principal composto polifenólico responsável pela atividade antileishmanea da planta, a qual é comparável a atividade do fármaco Anfotericina B. A 2-Fenilcromona apresentou uma concentração inibitória que induz metade do efeito máximo (IC_{50}) igual a 25 μg/mL contra *Leishmania major* [19].

2.4 Albumina do Soro Humano (HSA)

A Albumina do Soro Humano (HSA) é a proteína mais abundante no plasma sanguíneo, em concentração de aproximadamente 40 mg/mL. A HSA é uma das proteínas mais bem estudadas na literatura. Um levantamento da quantidade de artigos publicados que apresentam o tema *human serum albumin*, utilizando o banco de dados do *Scopus* [20], contabiliza um total de 86.804 documentos publicados entre os anos de 1915 e 2016 (Figura 5a). O número de publicações com o tema HSA apresenta um crescimento significativo por volta do ano de 1965 e um ápice em 2014. De acordo com os dados levantados, Medicina, Bioquímica, Genética, Biologia Molecular, Farmacologia, Toxicologia, Farmacêutica e Química são as principais áreas do conhecimento que contribuem para desenvolvimento científico do tema. Esse levantamento evidencia a relevância científica que a HSA tem para a ciência mundial.

Como destacado previamente, a HSA tem atraído a atenção e o interesse da comunidade científica por gerações. Dentre os vários estudos desenvolvidos com a HSA, um dos principais alvos de investigação é a sua surpreendente capacidade de ligação para uma ampla variedade de compostos endógenos (ácidos graxos não esterificados e compostos lipofílicos) e exógenos (fármacos). Este fato confere a HSA um papel preponderante no transporte e regulação do fluxo intercelular de pequenas moléculas, assim como na farmacocinética e farmacodinâmica de diferentes drogas [21–24]. A partir de um levantamento feito usando o banco de dados do *Scopus* [20], no qual se cruza as palavras-chave *human serum albumin* e *ligand binding* é possível quantificar um total de 6.814 documentos publicados entre os anos de 1967 e 2016. O perfil de crescimento do número desses documentos é semelhante aos dados obtidos para ao tema *human serum albumin*, assim como, as áreas do conhecimento nas quais as publicações se inserem (Figura 5b). Esse levantamento cruzado retifica a

importância do tema HSA-ligantes.

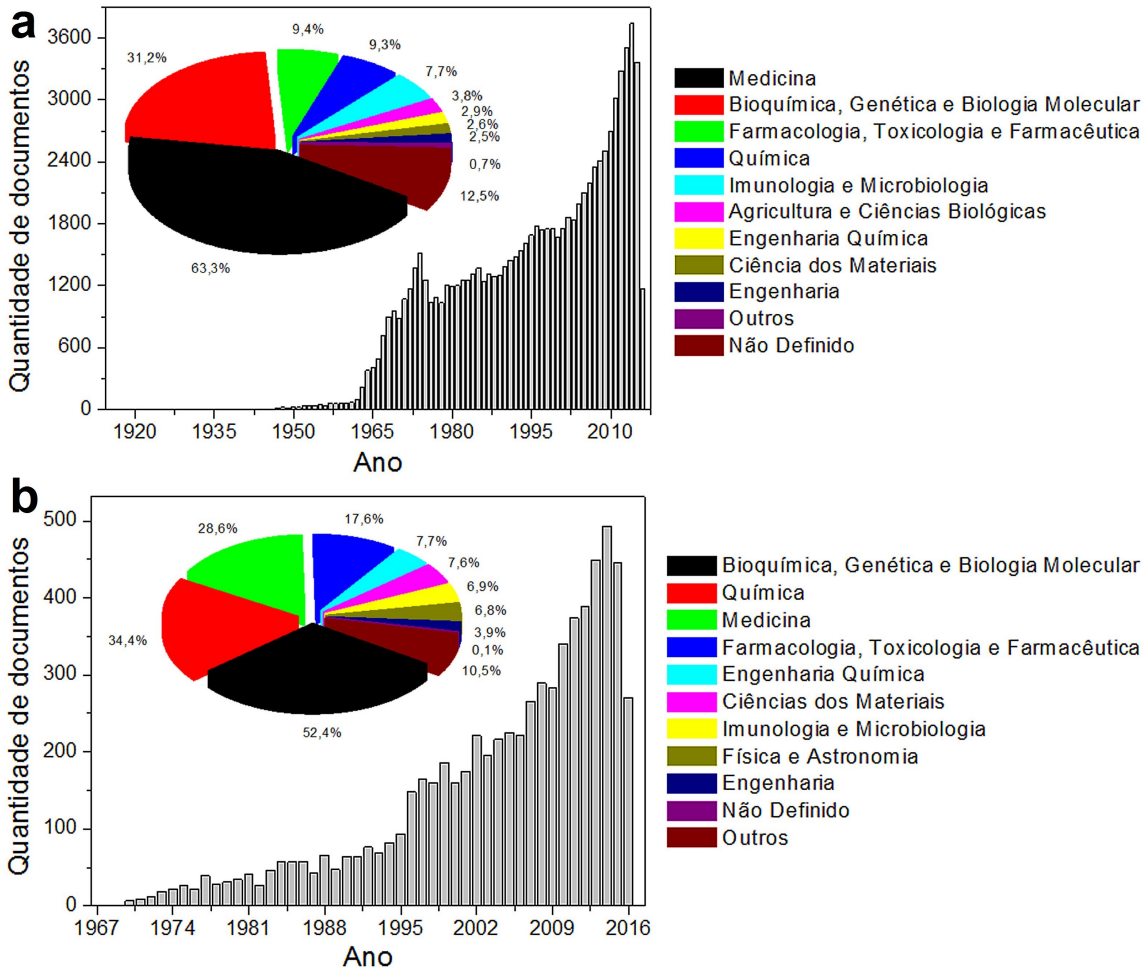

Figura 5: Levantamento de dados utilizando o banco de dados do *Scopus*. (a) Dados obtidos usando o tema *human serum albumin* entre os anos de 1915 e 2016. (b) Dados adquiridos utilizando o cruzamento entre as palavras-chave *human serum albumin* e *ligand binding* para o período de tempo de 1915-2016. Os insertos apresentam as porcentagens de publicações relacionadas com as áreas do conhecimento científico nas quais os estudos se inserem.

A HSA é composta por uma única cadeia polipeptídica não glicosilada, a qual apresenta em sua sequência 585 resíduos de aminoácidos (66 kDa). Essa proteína é divida em três domínios (I, II e III), com cada um contendo dois subdomínios (A e B) (Figura 6, código de entrada no PDB 1AO6) [25]. Cada domínio da HSA contém dez α-hélices que são divididos por seis hélices antiparalelas, formando subdomínios com quatro α-hélices cada. A estrutura tridimensional da proteína é estabilizada por 17 pontes dissulfeto (em amarelo

na Figura 6). A HSA tem um único resíduo de triptofano (Trp214) na sua sequência, localizando-se em uma α-hélice do subdomínio IIA da proteína que se encontra na interface com o subdomínio IIIA (Figura 6) [25].

Ligantes aromáticos e heterocíclicos se ligam primariamente nos bolsos hidrofóbidos dos subdomínios IIA e IIIA da HSA, os quais são nomeados como sítio 1 e 2, respectivamente (Figura 6). O sítio 1 é a região específica de ligação primária para fármacos como varfarina e fenilbutazona, enquanto que drogas como diazepam e ibuprofeno se ligam primariamente ao sítio 2. Além dos sítios de ligação mencionados anteriormente, estudos recentes indicam que o subdomínio IB é o principal sítio de ligação para compostos como bilirrubina, hemina e laranja de metila. Esse fato confere ao subdomínio IB a nomeação como sítio 3 (Figura 6) [26].

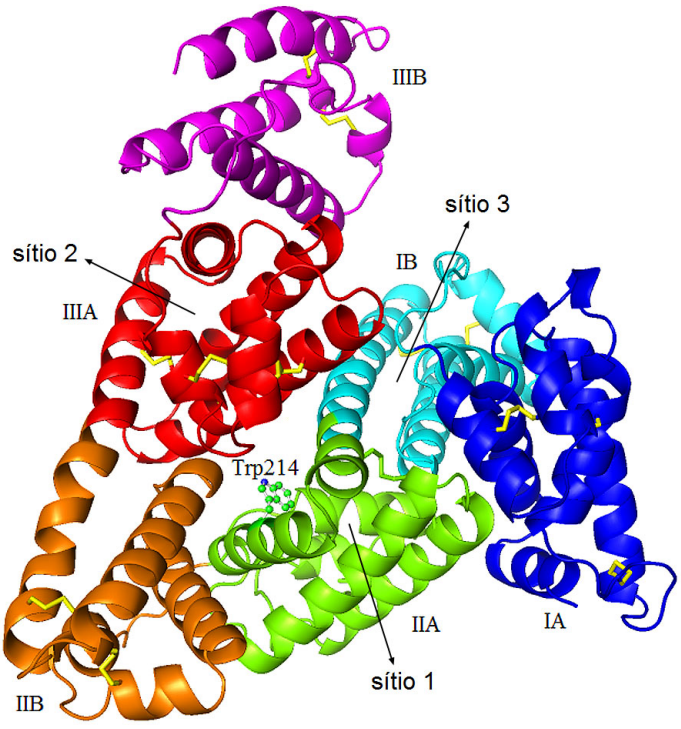

Figura 6: Estrutura tridimensional da HSA determinada por Cristalografia de Raios-X (código de entrada no PDB 1AO6). A proteína é representada utilizando o modelo de *cartoon* e os domínios são indicados com cores diferentes (IA, azul; IB, ciano; IIA, verde; IIB, laranja; IIIA, vermelho; IIIB, purpura). O único resíduo de triptofano (Trp214) da HSA que está localizado no bolso hidrofóbico do subdomínio IIA é demonstrado por meio do modelo de *stick-ball*. As pontes dissulfeto são denotadas em amarelo.

3 Motivação

Devido à tendência intrínseca dos núcleos fenólicos para desenvolver interações moleculares, não é surpresa que um dos grandes alvos atuais de estudos da comunidade científica seja a interação dos flavonóides com proteínas. Dentre as proteínas estudas, a Albumina do Soro Humano merece destaque, tendo em vista, seu importante papel no transporte e disposição de ligantes endógenos (ácidos graxos não esterificados, bilirrubina e composto lipofílicos) e exógenos (varfarina, diazepam e ibuprofeno), os quais estão presentes no plasma sanguíneo e atuam em diferentes alvos moleculares no corpo humano.

Um levantamento realizado usando o banco de dados do *Scopus* entre os anos de 1963 e 2016 contabiliza um total de 973 documentos quando é cruzado o tema *human serum albumin* com *flavonoid* [20]. A partir desse levantamento de dados realizado é possível verificar que após o ano de 1995 ocorreu um significante crescimento do número de publicações relacionadas aos temas, o que demonstra o quanto esses estudos de interação HSA-flavonóides são recentes. Os dados obtidos também indicam que as principais áreas do conhecimento interessadas por esses estudos de interação são as áreas de Química, Bioquímica, Genética, Biologia Molecular, Medicina, Farmacologia, Toxicologia e Farmacêutica.

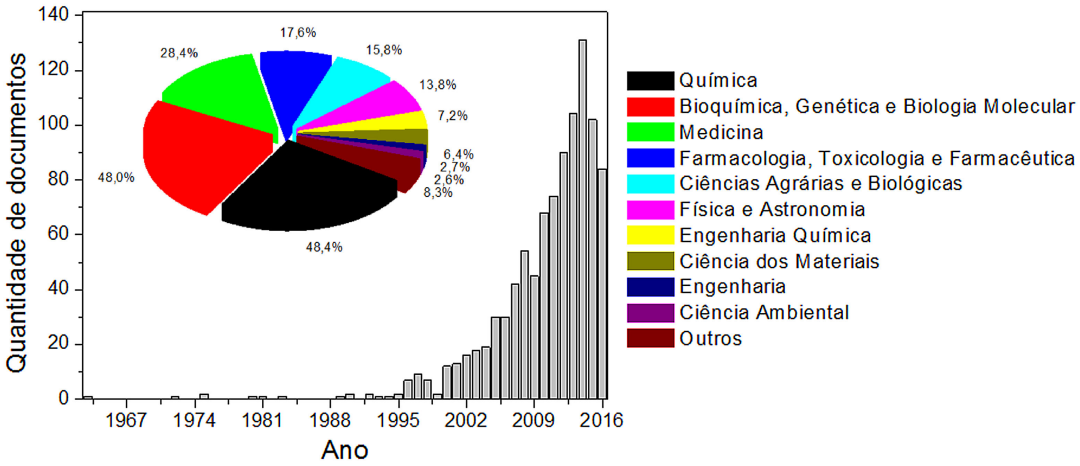

Figura 7: Levantamento de dados realizado usando o bando de dados do *Scopus*. Dados obtidos a partir do cruzamento da palavra-chave *human serum albumin* com *flavonoid* entre os anos de 1963 e 2016. O inserto apresenta as porcentagens de publicações relacionadas com as áreas do conhecimento científico nas quais os estudos se inserem.

Os estudos de interação HSA-flavonóide mencionados anteriormente sugerem esses compostos polifenólicos poderiam ser transportados pela HSA [27–29]. Esse fato garantiria aos flavonóides alcançarem os alvos moleculares e, assim, desempenharem suas atividades biológicas. Dessa forma, é de suma importância a descrição a nível molecular das interações entre os flavonóides (ISO e 2PHE) e a HSA, uma vez que esses compostos polifenólicos apresentam numerosas e promissoras atividades benéficas a saúde humana. Além disso, o avanço desses estudos de interação HSA-flavonóides ajudam a construir as bases fundamentais para o possível desenvolvimento de novos fármacos.

4 Resultados principais

O estudo detalhado da interação dos flavonóides Isovitexina e 2-Fenilcromona com a HSA foi realizado utilizando técnicas experimentais de espectroscopia de fluorescência, absorbância UV-Vis, dicroísmo circular (CD) e espectroscopia de infravermelho com transformada de Fourier (FT-IR); juntamente com métodos computacionais de cálculos *ab initio*, dinâmica molecular e modelagem molecular. Nas próximas seções serão apresentados os principais resultados obtidos para formação dos complexos HSA-flavonóides, assim como uma comparação entre eles.

4.1 Supressão de fluorescência

O processo de supressão de fluorescência pode ocorrer quando a intensidade do sinal de fluorescência diminui com a presença de uma molécula supressora. Muitas interações moleculares podem resultar em um processo de supressão, tais como: reações com estado excitado, rearranjo molecular, transferência de energia, formação de complexo de estado fundamental e processo colisional. Esses diferentes mecanismos são geralmente classificados como dinâmico ou estático. Eles podem ser distinguidos por suas dependências com a temperatura, viscosidade e/ou tempo de vida de fluorescência. Altas temperaturas resultam em difusões mais rápidas e, portanto, uma extensão maior do processo de supressão por colisão (supressão dinâmica). Ao mesmo tempo, temperaturas elevadas também implicam em dissociação de complexos fracamente ligados, conduzindo a uma redução no processo de supressão estática [30].

Os dados de supressão de fluorescência mostram que a emissão da HSA ($\lambda_{ex} = 295\,nm \rightarrow$ Trp214) diminui com o aumento da concentração dos flavonóides ISO e 2PHE (Figura S1 no Anexo II e Figura 1a no Anexo III, respectivamente). O efeito do etanol na intensidade de fluorescência da HSA é negligenciável (Figura S2 no Anexo IV). Estes resultados indicam que os flavonóides interagem nas proximidades do microambiente do único resíduo de triptofano (Trp214) da HSA, o qual encontra-se localizado no subdomínio IIA (sítio 1). As análises dos dados de supressão de fluorescência foram realizadas utilizando

a equação de Stern-Volmer [30]:

$$\frac{F_0}{F} = 1 + K_q\tau_0[Q] = 1 + K_{SV}[Q] \quad (1)$$

sendo que F_0 e F são as intensidades de fluorescência de estado estacionário da HSA na ausência e presença do supressor (ISO e 2PHE), respectivamente. K_q é a constante de supressão bimolecular, τ_0 é o tempo de vida de fluorescência na ausência do supressor (10^{-8}s para a HSA [30]), $[Q]$ é a concentração do supressor e K_{SV} é a constante de supressão de Stern-Volmer. Nos intervalos de concentrações investigadas para ambos flavonóides, os resultados de supressão de fluorescência em 288, 298 e 308 K estão em concordância com a equação de Stern-Volmer (ver Figura S3 no Anexo II e Figura S2 no Anexo IV, respectivamente).

Tabela I: Constante de supressão de Stern-Volmer (K_{SV}), constante de supressão biomolecular (K_q), constante de ligação (K_b) e número de sítios de ligação (n) da interação entre a HSA e os flavonóides em 288, 298 e 308 K, pH 7,0. Os coeficientes de correlação (R) são $> 0{,}995$.

Flavonóide	$T(K)$	$K_{SV}(\times 10^4 M^{-1})$	$K_q(\times 10^{13} M^{-1})$	$K_b(\times 10^5 M^{-1})$	n
ISO	288	$7,20$	$7,20$	$1,05$	$1,16$
	298	$5,91$	$5,91$	$0,83$	$1,09$
	308	$4,67$	$4,67$	$0,58$	$1,01$
2PHE	288	$12,9$	$12,9$	$1,80$	$0,92$
	298	$13,1$	$13,1$	$1,79$	$0,91$
	308	$13,1$	$13,1$	$1,77$	$0,93$

Os resultados apresentados na Tabela I mostram que os valores das constantes de Stern-Volmer (K_{SV}) para a Isovitexina são inversamente correlacionadas com o aumento de temperatura. Enquanto que os valores de K_{SV} para a 2-Fenilcromona não se alteram com o incremento de temperatura. Os valores das constantes de supressão bimolecular (K_q) para ambos flavonóides são maiores do que $2,0\times 10^{10}\ M^{-1}cm^{-1}$, o qual representa a taxa de colisão máxima por difusão de vários supressores com biopolímeros [30]. Além disso, os espectros de absorção da HSA apresentaram mudanças devido à interação com

a ISO e 2PHE (Figura S4 no Anexo II e Figura S3 no Anexo IV, respectivamente). Portanto, os mecanismos de supressão de fluorescência da HSA pela ISO e 2PHE são caracterizados principalmente por processos estáticos (complexo de estado fundamental não fluorescente) [30].

A partir de uma comparação entre os valores de K_{SV} para os processos de supressão estática promovidos pela ISO e 2PHE é possível observar que a interação entre a HSA e o flavonóide 2-Fenilcromona apresenta valores das constantes de Stern-Volmer maiores, aproximadamente o dobro, do que os valores registrados para a Isovitexina. Esse fato sugere que a 2PHE promove uma supressão de fluorescência da HSA mais eficiente.

4.2 Análise de equilíbrio de ligação

Para processos de supressão estática, se é assumido que os sítios de ligação são os mesmos e independentes na proteína, a constante de ligação (K_b) e o número de sítios de ligação (n) podem ser calculados usando a seguinte equação [31]:

$$log\left(\frac{F_0 - F}{F}\right) = n\ logK_b - n\ log\left(\frac{1}{[Q] - (F_0 - F)[P]/F}\right) \quad (2)$$

sendo que $[P]$ é a concentração total de proteína em solução.

A Figura 8 apresenta os gráficos de equilíbrio de ligação para a supressão de fluorescência da HSA pela ISO e 2PHE em 288, 298 e 308 K. A dependência de $log((F_0 - F)/F)$ com relação a $log(1/([Q] - (F_0 - F)[P]/F))$ é linear para ambos flavonóides, sendo a inclinação da reta igual a n e o intercepto com a ordenada igual ao valor de $n\ logK_b$. Os valores de K_b e n para os complexos HSA-flavonóides em três temperaturas diferentes são mostrados na Tabela I. O número médio de sítios de ligação determinado para o complexo HSA-ISO e HSA-2PHE é 1,09 e 0,92, respectivamente. As constantes de ligação do complexo HSA-2PHE apresentam valores maiores comparados com aqueles do complexo HSA-ISO, sugerindo a 2-Fenilcromona tem uma afinidade pela HSA maior do que a Isovitexina. Com relação a temperatura, os valores de K_b apresentam a mesma tendência que K_{SV}. Esse fato sugere que, no intervalo de temperatura trabalhado (15 - 35 °C), a ligação do complexo HSA-2PHE é mais estável termicamente.

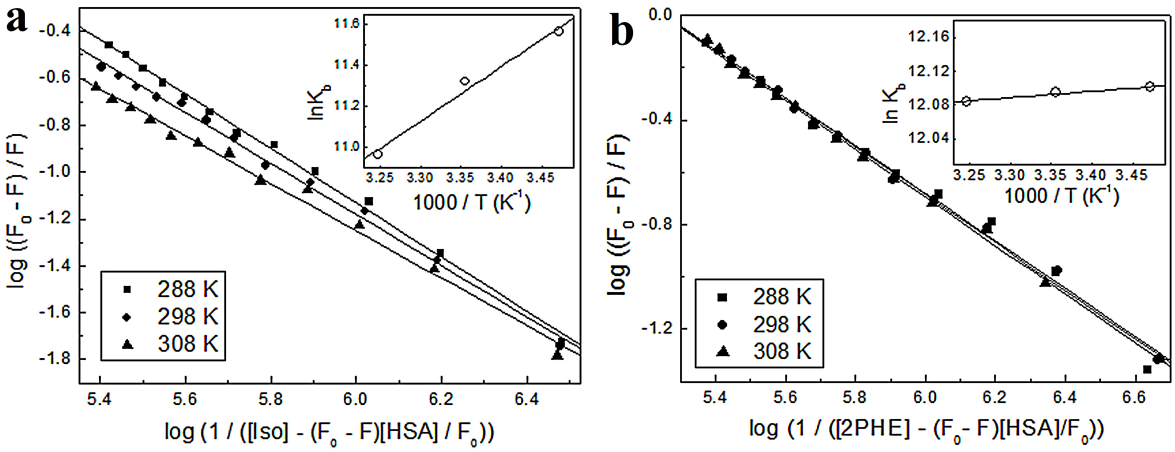

Figura 8: Gráficos duplo-log para a supressão de fluorescência da HSA ($\lambda_{ex} = 295\,nm$ (Trp214)) pela Isovitexina (a) e 2-Fenilcromona (b) em 288, 298 e 308 K. $[HSA] = 4\ \mu M$ em tampão fosfato 50 μM com 150 mM de NaCl e pH 7,0. Os insertos correspondem aos gráficos de van't Hoff para as interações HSA-flavonóides.

4.3 Análise termodinâmica

Para investigar as interações responsáveis pela formação e estabilização dos complexos HSA-flavonóides, análises termodinâmicas foram realizadas a partir da equação de van't Hoff:

$$lnK_b = -\frac{\Delta H^o}{RT} + \frac{\Delta S^o}{R} \tag{3}$$

sendo que ΔH^o é a variação de entalpia, ΔS^o a variação de entropia, R a constante universal dos gases ideais e K_b a constante de ligação em uma correspondente temperatura (T). A Tabela II mostra os valores de ΔH^o e ΔS^o obtidos através da inclinação da reta e extrapolação para a ordenada (relação de van't Hoff, inserto na Figura 8), respectivamente. Também são listados na Tabela II, os valores da variação de energia livre de Gibbs (ΔG^o) calculados pela seguinte relação:

$$\Delta G^o = \Delta H^o - T\Delta S^o \tag{4}$$

Os valores de $\Delta G^o < 0$ sugerem que os processos de interação entre HSA e os flavonóides são espontâneos. A análise dos parâmetros termodinâmicos indica valores de $\Delta H^o < 0$ e $\Delta S^o > 0$ para o complexo HSA-ISO, e $\Delta H^o < 0$ ($|\Delta H^o| \approx 0$) e $\Delta S^o > 0$

para a interação HSA-2PHE. A partir dessa análise é possível identificar que a reação de formação do complexo HSA-ISO é dirigida entalpicamente, com o termo entálpico negativo (processo exotérmico) fornecendo a maior contribuição para a variação de energia livre de Gibbs. Enquanto que os valores de ΔH^o e ΔS^o para a formação do complexo HSA-2PHE sugerem uma reação dirigida entropicamente, com o termo entrópico positivo proporcionando a maior contribuição para os valores de ΔG^o. O balanço entalpia-entropia indica que as interações hidrofóbicas oferecem a principal contribuição para a formação dos complexos HSA-flavonóides, haja vista a estrutura polifenólica destes compostos. Em particular, o complexo HSA-2PHE apresenta valores de ΔH^o e ΔS^o que são característicos para uma interação hidrofóbica clássica [32–34], semelhante a registrada para a formação do complexo HSA-porfirina [35]. No entanto, a contribuição hidrofóbica não é a única interação intermolecular existente entre a HSA e os flavonóides ISO e 2PHE, a interação eletrostática deve ser considerada para a estabilização dos complexos formados [36].

Tabela II: Parâmetros termodinâmicos dos complexos HSA-flavonóides em 288, 298 e 308 K, pH 7,0. Variação de entalpia ΔH^o é a , variação de energia livre de Gibbs (ΔG^o) e variação de entropia (ΔS^o). R é o coeficiente de correlação.

Flavonóide	$T(K)$	$\Delta H^o(kJmol^{-1})$	$\Delta G^o(kJmol^{-1})$	$\Delta S^o(Jmol^{-1}K^{-1})$	R
ISO	288	$-22,1$	$-27,7$	$19,6$	$0,992$
	298		$-27,9$		
	308		$-28,1$		
2PHE	288	$-0,6$	$-28,9$	$98,4$	$0,978$
	298		$-29,9$		
	308		$-30,9$		

4.4 Função de densidade de ligação

O método da função de densidade de ligação (*Binding Density Function* - BDF) baseia-se na distribuição de ligantes ligados por macromolécula em i estados diferentes ($\sum \nu_i$), a qual é estritamente determinada no equilíbrio pelas concentrações de ligantes livres (L_F). Dessa forma, se L_F é a mesma para duas (ou mais) soluções em diferentes

concentrações totais de macromolécula (M_T), então $\sum \nu_i$ também será a mesma em cada solução. Como resultado, valores constantes de L_F e $\sum \nu_i$ ocorrerem para um número de diferentes combinações de concentrações totais de ligante (L_T) e macromolécula (M_T), os quais satisfazem a equação de conservação de massa [37]:

$$L_T = L_F + \left(\sum \nu_i\right) M_T \tag{5}$$

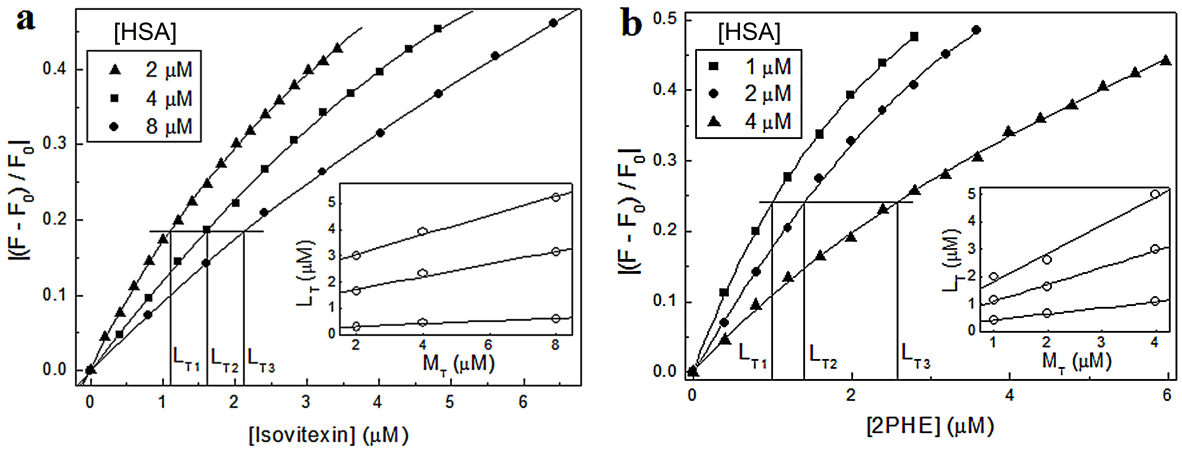

Figura 9: Titulações dos flavonóides ISO (a) e 2PHE (b) em solução de HSA (tampão fosfato 50 μM com 150 mM de NaCl, pH 7,0), as quais foram monitoradas pela supressão de fluorescência para três concentrações diferentes de proteína ($[HSA] = 1, 2, 4$ e/ou 8 μM) em 298 K. L_{T1}, L_{T2} e L_{T3} representam as concentrações de ligantes para um valor de ΔS_{obs} constante em três concentrações de proteína (M_{T1}, M_{T2} e M_{T3}). O inserto corresponde a três pares de concentrações (L_T;M_T) que exemplificam a utilização da Equação 5 para o cálculo dos valores de L_F e $\sum \nu_i$.

Considerando a relação geral entre a concentração de cada espécie de macromolécula com i ligantes ligados e o sinal observado experimentalmente (S_{obs}, fluorescência e/ou absorbância UV-Vis) da macromolécula, as variações molares de sinal fracional (ΔS_{obs}) observadas na presença de L_T e M_T serão dadas por (Figure 9):

$$\Delta S_{obs} = \frac{S_{obs} - S_F M_T}{S_F M_T} \tag{6}$$

sendo que $S_F M_T$ é o sinal observado para a macromolécula na ausência de ligante (F_0, seção 4.1). Então, para os experimentos de supressão de fluorescência têm-se a relação $\Delta S_{obs} = (F - F_0)/F_0$ [37]. Uma linha horizontal foi traçada intersectando as três curvas de

titulação na Figura 9, definindo um valor constante de ΔS_{obs} e três conjuntos de (L_{Tx};M_{Tx}) (x = 1, 2 e 3) para o qual L_F e $\sum \nu_i$ são constantes (insertos na Figura 9).

A partir dos valores de L_F e $\sum \nu_i$ obtidos da Equação 5 é possível construir o gráfico de Scatchard ($\sum \nu_i / L_F$ versus $\sum \nu_i$) sem utilizar qualquer modelo de ligação *a priori*. Os gráficos de Scatchard para a interação entre a HSA e os flavonóides são apresentados da Figura 10.

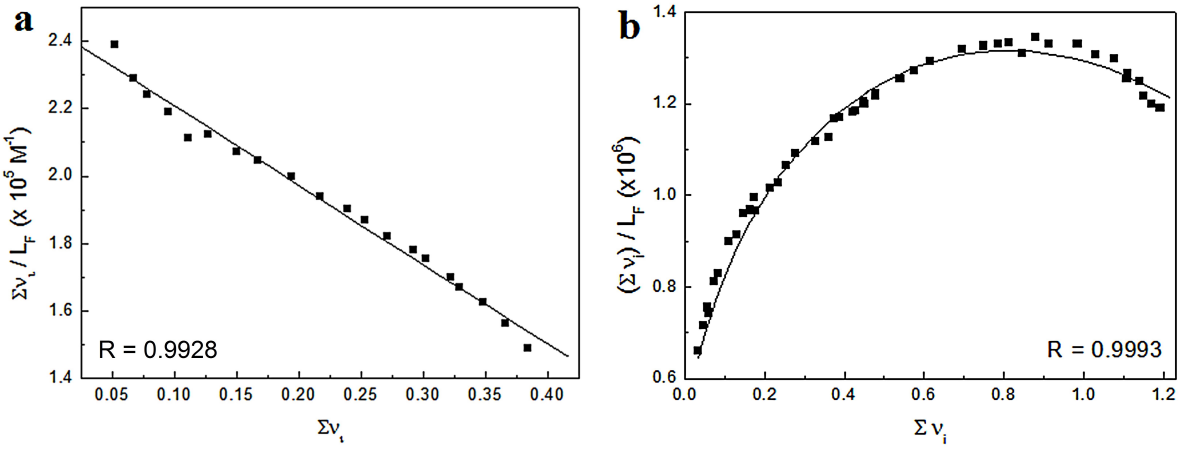

Figura 10: Gráficos de Scatchard para a interação entre a HSA e os flavonóides ISO (a) e 2PHE (b) gerados a partir do método BDF. A linha representa o ajuste teórico dos dados experimentais. R é o coeficiente de correlação.

O gráfico de Scatchard para o complexo HSA-Isovitexina apresenta um perfil linear característico de sistemas não cooperativos. No entanto, a análise de Scatchard para a interação HSA-2PHE mostrou uma curvatura descendente que indica a existência de cooperatividade positiva na formação do complexo. A cooperatividade positiva ocorre quando a ligação no primeiro sítio da proteína melhora a afinidade do ligante pelo segundo sítio [38].

Os dados experimentais do complexo HSA-ISO foram ajustados usando a equação de Scatchard para um sistema não cooperativo (Figura 10a) [38]:

$$\frac{\sum \nu_i}{L_F} = nK_a - K_a \sum \nu_i \tag{7}$$

sendo que K_a é a constante de associação e n o número de sítios de ligação. Os resultados obtidos a partir da análise de Scatchard (Equação 7) para K_a e n foram $2,35 \times 10^5 M^{-1}$

e $1,04$, respectivamente. Esses valores estão em acordo com os resultados obtidos pela análise de equilíbrio de ligação (seção 4.2).

Por outro lado, devido a complexidade do gráfico de Scatchard para o complexo HSA-2PHE, os dados experimentais adquiridos para essa interação foram ajustados utilizando um modelo de ligação global no qual a macromolécula (M) apresenta dois sítios de associação para o ligante (L). O mecanismo de reação para esse modelo de ligação global pode ser descrito como [38]:

$$M + L \rightleftharpoons ML;\ k_1 \tag{8}$$

$$ML + L \rightleftharpoons ML_2;\ k_2 \tag{9}$$

sendo que k_1 e k_2 são as constantes de associação do primeiro e segundo sítio, respectivamente, as quais podem ser obtidas a partir da seguinte equação:

$$\sum \nu_i = \frac{2k_1L_F + 2k_1k_2L_F^2}{1 + 2k_1L_F + 2k_1k_2L_F^2} \tag{10}$$

A análise dos dados utilizando a Equação 10 (Figura 10b) indicou que a estequiometria de ligação do complexo HSA-2PHE foi 1:2 e que os valores das constantes k_1 e k_2 foram $2,42{\times}10^5$ e $6,90{\times}10^6\ M^{-1}$, respectivamente. O valor de k_1 está em concordância com os resultados obtidos pela análise de equilíbrio de ligação (seção 4.2). A discrepância entre o número de sítios de ligação encontrada pelo método BDF e a análise de equilíbrio de ligação pode ser devido a restrições inerentes do último modelo (Equação 2). O coeficiente de Hill calculado utilizando $n_H = 2/(1+\sqrt{k_1/k_2})$ foi igual a $1,68$, indicando que a interação entre a HSA e a 2PHE exibe uma cooperatividade positiva, como mencionado anteriormente pela análise do perfil do gráfico [38].

4.5 Competição de sítio

A partir das análises de equilíbrio de ligação e Scatchard confirmou-se que a interação entre a HSA e a Isovitexina apresenta uma estequiometria de ligação $1:1$. Desse modo, o sítio 1 da HSA seria o mais provável para a ligação do flavonóide ISO, visto que, a sonda fluorescente (Trp214) utilizada para o experimento de fluorescência encontra-se

no interior desse sítio. Por outro lado, a análise dos dados para o complexo HSA-2PHE apresentou uma discrepância no número de sítios de ligação. Por esse motivo, experimentos de competição de sítio foram realizados com o objetivo de confirmar o número correto de sítios de ligação e também para identificar a localização deles na proteína. A competição de sítios de ligação foi realizada utilizando o deslocamento de marcadores específicos para o sítio 1 - varfarina (*warfarin*, WAR), sítio 2 - ibuprofeno (*ibuprofen*, IBU) e sítio 3 - laranja de metila (*methyl orange*, MTO) [21, 26].

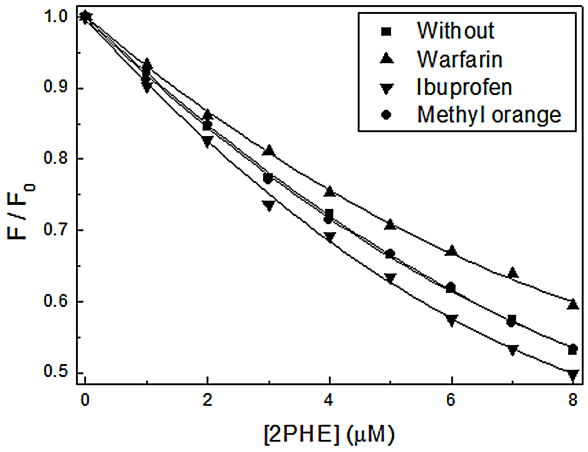

Figura 11: Taxas (F/F_0) de supressão de fluorescência da HSA pela 2PHE na ausência (*Without*) e presença de marcadores específicos de sítios: varfarina (sítio 1, *Warfarin*), ibuprofeno (sítio 2, *Ibuprofen*) ou laranja de metila (sítio 3, *Methyl orange*). $[HSA] = [marcador] = 4\ \mu M$ em tampão fosfato 50 μM com 150 mM de NaCl, pH 7,0 e 298K.

Para investigar os sítios de ligação da 2PHE na HSA, as taxas de supressão de fluorescência (F/F_0) na ausência e presença de marcadores específicos foram comparadas e são apresentadas na Figura 11. A taxa de supressão de fluorescência da HSA pela 2PHE diminui na presença de WAR (marcador do sítio 1), aumenta na presença de IBU (marcador do sítio 2) e permanece a mesma na presença de MTO (marcador do sítio 3), quando comparada com F/F_0 para 2PHE sem emprego de marcadores. Esses resultados indicam que a 2PHE se liga ao sítio 1 e 2 da HSA, os quais estão localizados no subdomínio IIA e IIIA, respectivamente. A identificação de dois sítios de ligação para a 2PHE na HSA corrobora com os resultados obtidos pela análise de Scatchard (seção 4.4).

4.6 Análise de estrutura secundária

A possível variação de estrutura secundária da HSA induzida pela interação com os flavonóides (ISO e 2PHE) foi investigada utilizando as técnicas de espectroscopia de FT-IR e far-UV CD. Inicialmente, a análise de estrutura secundária demonstrou que a proteína é composta majoritariamente por α-hélices (≈ 62 %), o que está de acordo com a literatura [25]. Com relação aos estudos de interação com os flavonóides Isovitexina e 2-Fenilcromona, a análise conformacional não indicou variações significativas de estrutura secundária da HSA, como pode ser observado pelos espectros de far-UV CD apresentados na Figura 12. Na mesma linha de raciocínio, os espectros de FT-IR demonstraram os mesmos resultados conformacionais indicados pelos espectros de dicroísmo circular (Figura 5, S6, S7 e S8 no Anexo I e II).

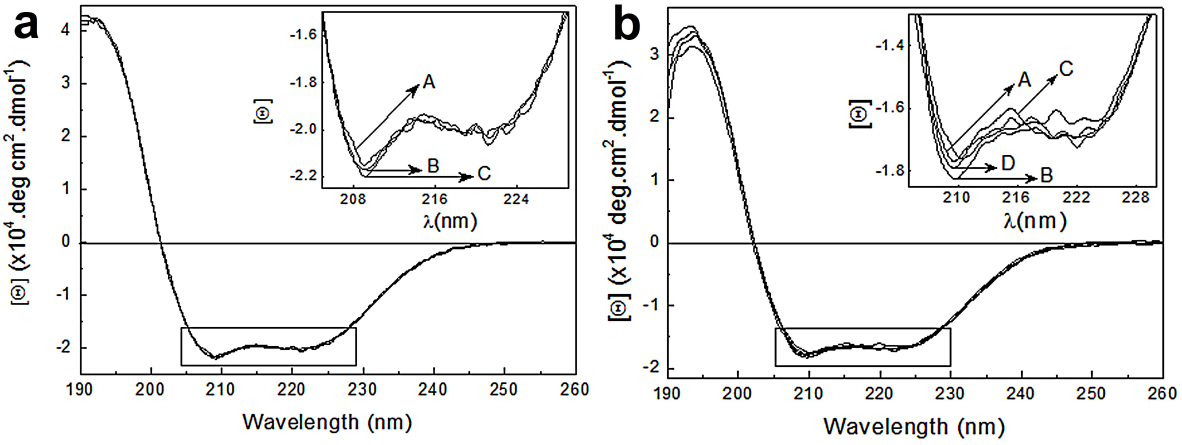

Figura 12: Espectros de dicroísmo circular da HSA na ausência e presença dos flavonóides Isovitexina (a) e 2-Fenilcromona (b) em temperatura ambiente (25 °C). O inserto corresponde ao detalhe dos picos em 209 e 222 nm. $[HSA] = 4\ \mu M$ em tampão fosfato 50 μM com 150 mM de NaCl, pH 7,0. Razões molares entre $[ISO]$ e $[HSA]$: 0:1 (A), 0,5:1 (B) e 1:1 (C). Razões molares entre $[2PHE]$ e $[HSA]$: 0:1 (A), 1:1 (B) e 2:1 (C). (D) mostra o espectro de CD da HSA na presença de etanol.

4.7 Abordagem computacional

A interação entre a HSA e os flavonóides também foi investigada utilizando ferramentas computacionais. Cálculos *ab initio* foram efetuados com a finalidade de obter

de forma sistemática as estruturas moleculares dos flavonóides. A otimização e análise vibracional das estruturas foram realizadas utilizando métodos de teoria do funcional de densidade (DFT). A verificação da consistência dessas estruturas foi feita comparando características de transições eletrônicas (absorção UV-Vis) teóricas e experimentais (Tabela S2 no Anexo II e IV). Depois de obter as estruturas otimizadas, cálculos de potencial eletrostático molecular (MEP) foram realizados para identificar as distribuições de cargas parciais nas estruturas moleculares dos flavonóides (Figura 13).

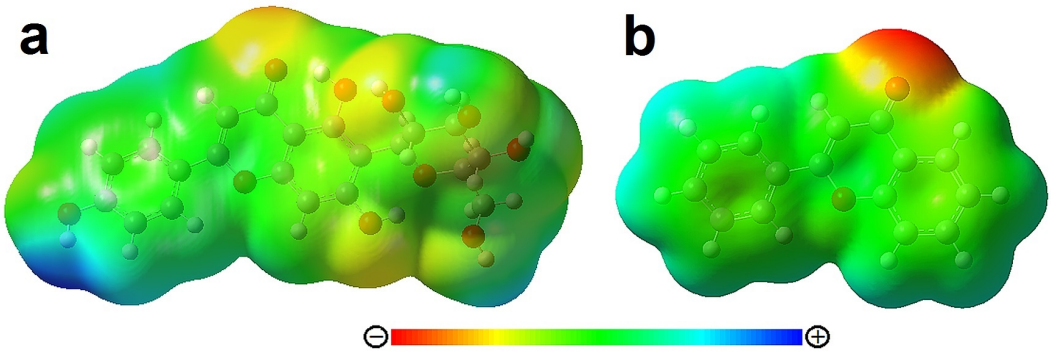

Figura 13: Potencial eletrostático molecular (MEP) do flavonóide Isovitexina (a) e 2-Fenilcromona (b), regiões com distribuição de cargas parciais positivas (azul), negativas (vermelho) e neutras (verde).

A partir da Figura 13, pode-se observar que tanto o MEP da Isovitexina quanto da 2-Fenilcromona revela uma majoritária distribuição de carga parciais neutras localizada ao longo das faces paralelas aos anéis benzenos das moléculas. Na estrutura do flavonóide ISO é possível verificar que a mais densa distribuição de cargas parciais positivas encontra-se ao redor do átomo de hidrogênio H4', enquanto que, significativas distribuições negativas ocorrem nas proximidades do átomo de oxigênio O4 e das hidroxilas (OH) da glicosilação. Na estrutura molecular da 2-Fenilcromona, observa-se que a mais densa distribuição de cargas parciais negativas localiza-se ao redor do átomo de oxigênio O4.

A avaliação das regiões de distribuições de cargas parciais positivas e negativas em ambos flavonóides reveladas pelos potenciais eletrostáticos moleculares sugerem que as interações eletrostáticas poderiam desempenhar um papel importante na complementaridade de cargas parciais e/ou formação de pontes de hidrogênio na estabilização dos complexos HSA-flavonóides. Ao passo que as amplas porções de distribuição de cargas

parciais neutras poderiam envolver-se em contatos hidrofóbicos.

As estruturas moleculares dos flavonóides obtidas pelos métodos de DFT foram usadas nos cálculos de modelagem molecular. A abordagem de modelagem molecular foi utilizada levando em consideração as informações obtidas dos resultados experimentais, tais como: número de sítios de ligação e localização dos sítios na HSA. Para o complexo HSA-ISO, as simulações de modelagem molecular foram realizadas com o flavonóide ISO situado no sítio 1 da HSA. Por outro lado, devido à complexidade da interação HSA-2PHE, simulações de dinâmica molecular da estrutura cristalina da HSA foram efetuadas em condições fisiológicas (150 mM de NaCl e pH 7,0). O intuíto dos cálculos de dinâmica molecular foi gerar conformações do receptor (HSA) que tornam os cálculos de modelagem molecular mais consistentes com os resultados experimentais. Essas conformações foram adquiridas a partir das trajetórias obtidas pela análise de *cluster* [39]. Essa análise gerou seis *clusters* e a conformação mais representativa de cada *cluster* foi utilizada nos cálculos de modelagem molecular para investigar a interação da 2PHE com o sítio 1 e 2 da HSA.

A menor energia de ligação teórica (ΔG_B^T) das simulações de modelagem molecular para o complexo HSA-ISO foi $-27,5\ kJmol^{-1}$, com uma correspondente constante de ligação teórica (K_B^T) de $6,7{\times}10^4\ M^{-1}$ em 298 K, determinada por $K_B^T = exp\ (-\Delta G_B/RT)$. Este resultado computacional está de acordo com os valores determinados pela análise de equilíbrio de ligação (seção 4.2) e pelo método BDF (seção 4.4). Para o complexo HSA-2PHE, as menores energias de ligação teóricas para o sítio 1 e 2 dos seis *clusters* da HSA foram calculadas, assim como as suas correspondentes constantes de ligação teóricas (Tabela S3 no Anexo IV). Dentre os seis *clusters* da HSA, o *cluster* 4 apresentou os valores das constantes de ligação teóricas ($k_1^T = 1,04{\times}10^5\ M^{-1}$ e $k_2^T = 1,55{\times}10^5\ M^{-1}$) em concordância com os resultados experimentais.

A Figura 14 apresenta o resultado de modelagem molecular para a menor energia de ligação do complexo HSA-ISO. A Figura 14a mostra que o flavonóide ISO se encontra na entrada do sítio 1 da HSA e próximo ao resíduo Trp214. A entrada do sítio 1 é uma região menos hidrofóbica do que o fundo do bolso do sítio (Figura S11 no Anexo II). Esse fato garante um microambiente de ligação adequado para a glicosilação da Isovitexina.

A Figura 14b apresenta detalhes do microambiente do sítio de ligação. O conjunto de resíduos de cadeia lateral apolar Ala191, Pro339, Val343, Pro447, Cys448 e Val455 contribui principalmente para as interações hidrofóbicas com a ISO. No entanto, cada átomo de oxigênio da cadeia principal da Ala191 e Pro339 realiza uma ponte de hidrogênio com o átomo de hidrogênio H4' e H4"da ISO, respectivamente. De acordo com o MEP da Isovitexina, o átomo de hidrogênio H4' apresenta a mais densa distribuição de cargas parciais positivas na estrutura do flavonóide (Figura 13). Os resíduos de cadeia lateral polar neutra Gln221, Asn295, Tyr341 e Tyr452 participam de interações eletrostáticas de complementariedade de cargas parciais, exceto o resíduo Tyr452 que encontra-se envolvido em interações hidrofóbicas com a face planar neutra do anel B da ISO (Figura 13a). O átomo de oxigênio da cadeia principal do resíduo Asn295 forma uma ponte de hidrogênio com o átomo de hidrogênio H6"da ISO. Os resíduos de cadeia lateral polar Lys195, Arg218, Asp451 e Lys436 estão envolvidos em interações eletrostáticas, exceto o resíduo Lys195 que apresenta os átomos apolares (carbonos) da cadeia lateral realizando contatos hidrofóbicos com a face planar do anel B da ISO, assim como Tyr452. Os resíduos de Arg218 e Asp451 estão envolvidos em interações eletrostáticas de complementariedade de cargas parciais com as hidroxilas da glicosilação do flavonóide. O grupo NH_3^+ da cadeia lateral do resíduo Lys436 realiza interações π-cátion com o anel B da ISO. A interação π-cátion é uma interação molecular não covalente que ocorre entre um cátion (íon positivo) e a face de um sistema rico de elétron π como o anel benzeno B da ISO. Tal interação não covalente tem energia de ligação comparável com energias de pontes de hidrogênio [40].

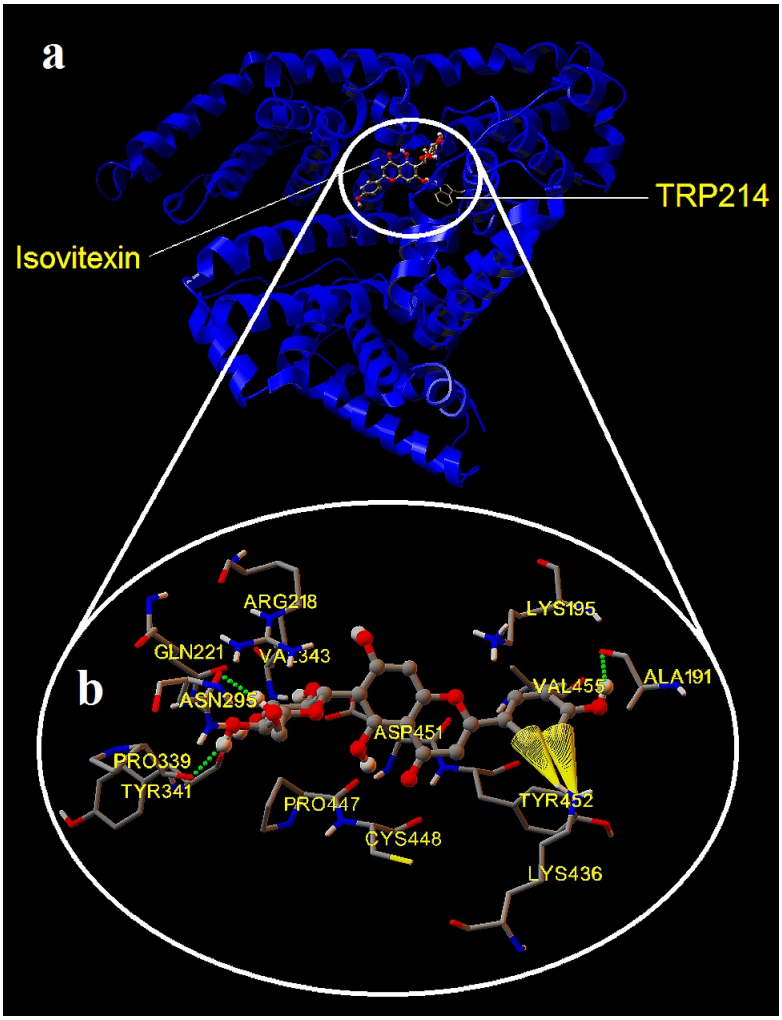

Figura 14: (a) Localização da molécula de Isovitexina próxima ao único resíduo de triptofano (Trp214) da HSA no subdomínio IIA (sítio 1). (b) Detalhe estrutural da interação entre a HSA-ISO obtido pelo método de modelagem molecular. A molécula ISO é representada utilizando o modelo *stick-balls*, os resíduos de aminoácidos são denotados usando o modelo *sticks* (C, cinza; O, vermelho; N, azul; S, amarelo; H, branco), as interações π-cátion são demonstradas como cones amarelos e as pontes de hidrogênio representadas por linhas tracejadas verdes.

A Figura 15 resume o resultado de modelagem molecular da interação entre a HSA e a 2-Fenilcromona em três perspectivas diferentes. No topo, a Figura 15a apresenta a estrutura tridimensional da proteína com o sítio 1 do lado esquerdo, o resíduo Trp214 ao meio e o sítio 2 do lado direito. No meio, as Figuras 15b e c mostram o microambiente molecular com os resíduos de aminoácidos mais próximos envolvidos nas interações da proteína com o ligante. Abaixo, as Figuras 15d e *e* apresentam em detalhes todas as interações não covalentes responsáveis pela formação e estabilização do complexo HSA-2PHE.

Os resultados apresentados na Figura 15 foram obtidos utilizando a conformação do quarto *cluster* da HSA (o mais representativo, Tabela S3 no Anexo IV), o qual corrobora os dados experimentais. Na Figura 15b, os resíduos mais próximos que interagem com a 2PHE são: Lys199, Leu(219, 234, 238 e 260), Ala291, Glu292, Arg257 e Tyr150. Na Figura 15c, os resíduos mais próximos envolvidos nas interações com a 2PHE são: Leu(387 e 453), Arg485, Phe488, Ser489, Tyr411 e Lys414.

A análise das interações envolvidas nos sítios 1 e 2 da HSA foi realizada utilizando o programa LigPlot [41]. No sítio 1 (Figura 15d), os resíduos Lys199, Leu(219, 234, 238 e 260), Ala291 e Glu292 estão envolvidos em interações hidrofóbicas com a 2PHE. Os resíduos de aminoácidos Arg257 e Tyr150 formam pontes de hidrogênio com o átomo de oxigênio O4 da molécula de 2-Fenilcromona, o qual apresenta a mais densa distribuição de cargas parciais negativas no MEP do flavonóide (Figura 13b). Os grupos NH e NH_2 da cadeia lateral da Arg257 formam pontes de hidrogênio com a 2PHE. O grupo OH da cadeia lateral da Tyr150 realiza uma ponte de hidrogênio com o flavonóide. No sítio 2 (Figura 15e), os resíduos Leu387, Tyr411, Leu453, Arg485 e Phe488 participam de interações hidrofóbicas com a 2-Fenilcromona. O grupo NH_3^+ da cadeia lateral da Lys414 realiza uma ponte de hidrogênio com o átomo O4 do flavonóide 2PHE. O grupo OH da cadeia lateral Ser489 estabelece uma ponte de hidrogênio com o átomo O1 da 2PHE.

Uma avaliação das interações não covalentes envolvidas nos sítios de ligação da HSA indica que no sítio 1 existe um maior conjunto de contatos hidrofóbicos com a 2-Fenilcromona do que no sítio 2.

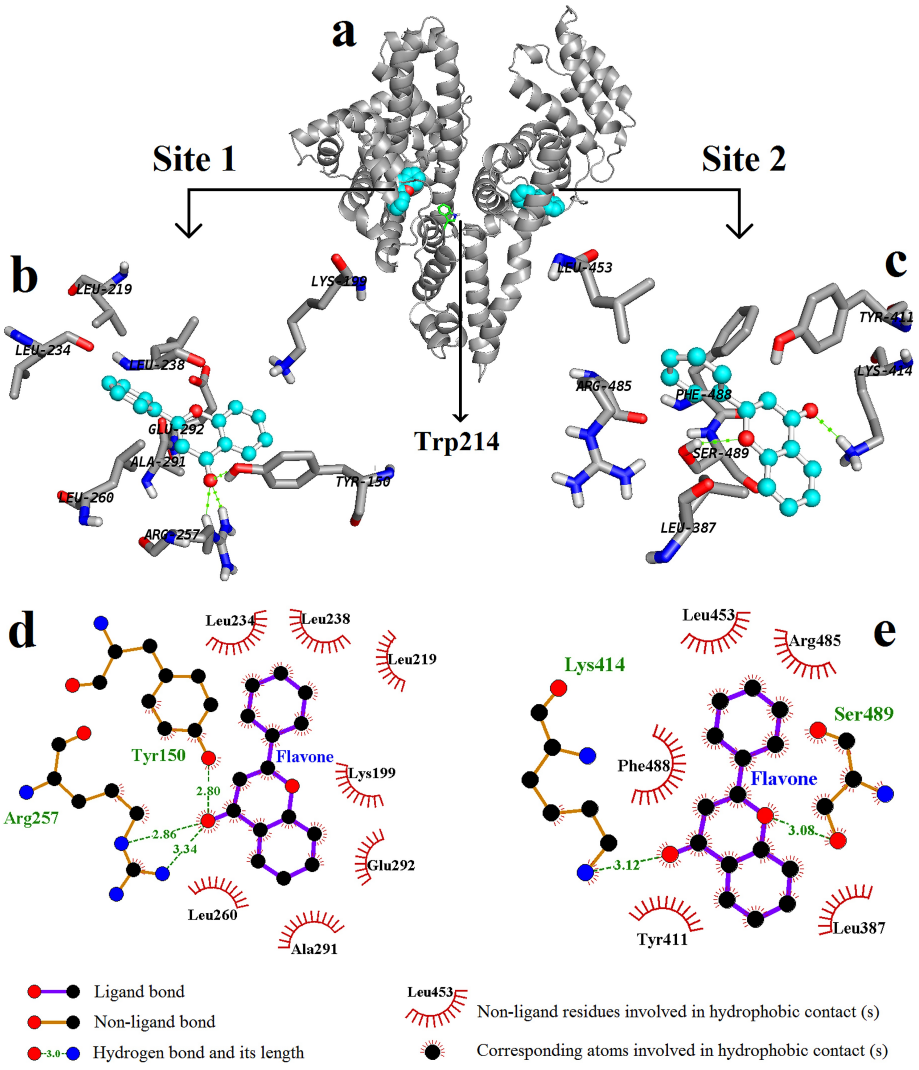

Figura 15: (a) Localização das moléculas de 2-Fenilcromona no subdomínio IIA (sítio 1) e IIIA (sítio 2) do quarto *cluster* da HSA, próximo ao único resíduo de triptofano (Trp214). A proteína é mostrada utilizando a representação de *cartoon* e as moléculas de 2-Fenilcromona com o modelo de *spheres*. Detalhe estrutural tridimensional do microambiente de interação da 2PHE com o sítio 1 (b) e sítio 2 (c) da HSA obtido pelos cálculos de modelagem molecular. As moléculas 2PHE são mostrada usando o modelo *stick-balls*, os resíduos de aminoácidos são denotados utilizando o modelo *sticks* (C, cinza; O, vermelho; N, azul; S, amarelo; H, branco) e as pontes de hidrogênio são indicadas por linhas tracejadas verdes. Representação bidimensional dos mapas de interação entre a 2PHE e os resíduos de aminoácidos do sítio 1 (d) e sítio 2 (e) da HSA. Esses mapas de interação foram obtidos usando o programa LigPlot.

Os resultados de modelagem molecular dos complexos HSA-flavonóides indicam que a interação hidrofóbica é a principal contribuição envolvida no microambiente de ligação dos flavonóides ISO e 2PHE com os sítios da HSA. Uma análise da área superficial de acessibilidade (ASA) ao solvente dos complexos formados também sugerem que a contribuição predominante para as interações nos sítios de ligação da HSA é a hidrofóbica (Tabela S3 e Tabela S4 no Anexo II e IV, respectivamente). No complexo HSA-ISO, a variação de ASA para átomos não polares e polares dos resíduos envolvidos no complexo é de 70 % e 30 %, respectivamente. No complexo HSA-2PHE, as variações de área superficial de acessibilidade para os átomos apolares e polares dos resíduos que participam da formação do complexo com a 2PHE são 70 % e 30 % no sítio 1, 50 % e 50 % no sítio 2, e 61 % e 39 % nos dois sítios em conjunto, respectivamente. No entanto, as análises computacionais também evidenciam que as interações eletrostáticas contribuem significativamente para a estabilização dos complexos HSA-flavonóides. Este conjunto de resultados computacionais está de acordo com os dados experimentais.

5 Conclusões

A interação dos flavonóides Isovitexina e 2-Fenilcromona com a Albumina do Soro Humano (HSA) foi investigada utilizando técnicas experimentais de espectroscopia de fluorescência, absorbância UV-Vis, dicroismo circular e infravermelho com transformada de Fourier, juntamente com métodos computacionais como cálculo *ab initio*, dinâmica molecular e modelagem molecular. Os resultados de espectroscopia de fluorescência e absorbância UV-Vis indicam que o processo de supressão de fluorescência da HSA pelos flavonóides pode ser descrito pelo mecanismo estático. O flavonóide 2-Fenilcromona é mais eficiente na supressão da emissão da HSA do que a flavona Isovitexina. Os resultados também indicam que a afinidade e estabilidade térmica da ligação HSA-2PHE são maiores comparadas com a interação HSA-ISO. No entanto, para ambos complexos HSA-flavonóides, os valores das constantes de ligação sugerem que a afinidade é do tipo moderada, ou seja, a ligação não é demasiadamente fraca para impedir a distribuição e não forte o bastante para evitar a diminuição da concentração no plasma sanguíneo. Esta afinidade moderada fornece a condição apropriada para uma distribuição uniforme e eficiente dos flavonóides, que é desempenhada pela HSA em todo o sistema circulatório sanguíneo possibilitando alcançar órgãos alvos. A análise termodinâmica sugere que a interação hidrofóbica é a principal contribuição evolvida no processo de formação dos complexos HSA-flavonóides. Entretanto, a interação eletrostática não deve ser negligenciada, pois é importante para a estabilização dos complexos formados. A análise de Scatchard obtida pela método BDF sugere que a interação HSA-ISO é não cooperativa e somente uma molécula de ISO se liga a HSA. Por outro lado, a interação entre a HSA e a 2PHE apresenta uma cooperatividade positiva e duas moléculas de 2PHE se ligam a proteína. A competição de sítio revelou que os sítios de ligação entre da 2-Fenilcromona na HSA são os sítios 1 e 2. Os cálculos da abordagem computacional corroboram com os resultados experimentais, fornecendo um detalhamento das interações hidrofóbicas e eletrostáticas nos microambientes de ligação dos flavonóides na HSA. A abordagem teórica evidenciou resíduos de aminoácidos importantes envolvidos nas interações, assim como átomos dos flavonóides que são cruciais para a interação com a proteína transportadora.

Referências

[1] I. P. Caruso, W. Vilegas, F. P. de Souza, M. A. Fossey, and M. L. Cornelio, "Binding of antioxidant flavone isovitexin to human serum albumin investigated by experimental and computational assays," *Journal of Pharmaceutical and Biomedical Analysis*, vol. 98, pp. 100–106, Sept. 2014.

[2] I. P. Caruso, J. M. B. Filho, A. S. de Araujo, F. P. de Souza, M. A. Fossey, and M. L. Cornelio, "An integrated approach with experimental and computational tools outlining the cooperative binding between 2-phenylchromone and human serum albumin," *Food Chemistry*, vol. 196, pp. 935–942, Apr. 2016.

[3] Bohm, B. A., *Introduction to Flavonoids: Chemistry and Biochemistry of Organic Natural Products*. CRC Press, Jan. 1999.

[4] E. Middleton, C. Kandaswami, and T. C. Theoharides, "The effects of plant flavonoids on mammalian cells: implications for inflammation, heart disease, and cancer," *Pharmacological Reviews*, vol. 52, pp. 673–751, Dec. 2000.

[5] E. Grotewold, ed., *The Science of Flavonoids*. New York, NY: Springer New York, 2006.

[6] O. M. Andersen and K. R. Markham, eds., *Flavonoids: Chemistry, Biochemistry and Applications*. Boca Raton, FL: CRC Press, 1 edition ed., Dec. 2005.

[7] J. H. de Vries, P. L. Janssen, P. C. Hollman, W. A. van Staveren, and M. B. Katan, "Consumption of quercetin and kaempferol in free-living subjects eating a variety of diets," *Cancer Letters*, vol. 114, pp. 141–144, Mar. 1997.

[8] N. C. Cook and S. Samman, "Flavonoids—Chemistry, metabolism, cardioprotective effects, and dietary sources," *The Journal of Nutritional Biochemistry*, vol. 7, pp. 66–76, Feb. 1996.

[9] B. H. Havsteen, "The biochemistry and medical significance of the flavonoids," *Pharmacology & Therapeutics*, vol. 96, pp. 67–202, Dec. 2002.

[10] L. R. Ferguson, "Role of plant polyphenols in genomic stability," *Mutation Research*, vol. 475, pp. 89–111, Apr. 2001.

[11] J. B. Harborne and C. A. Williams, "Advances in flavonoid research since 1992," *Phytochemistry*, vol. 55, pp. 481–504, Nov. 2000.

[12] J. A. Ross and C. M. Kasum, "Dietary flavonoids: bioavailability, metabolic effects, and safety," *Annual Review of Nutrition*, vol. 22, pp. 19–34, 2002.

[13] T. P. T. Cushnie and A. J. Lamb, "Antimicrobial activity of flavonoids," *International Journal of Antimicrobial Agents*, vol. 26, pp. 343–356, Nov. 2005.

[14] S.-T. Huang, C.-T. Chen, K.-T. Chieng, S.-H. Huang, B.-H. Chiang, L.-F. Wang, H.-S. Kuo, and C.-M. Lin, "Inhibitory effects of a rice hull constituent on tumor necrosis factor alpha, prostaglandin E2, and cyclooxygenase-2 production in lipopolysaccharide-activated mouse macrophages," *Annals of the New York Academy of Sciences*, vol. 1042, pp. 387–395, May 2005.

[15] R. G. Coelho, L. M. Batista, L. C. d. Santos, A. R. M. d. S. Brito, and W. Vilegas, "Phytochemical study and antiulcerogenic activity of Syngonanthus bisulcatus (Eriocaulaceae)," *Revista Brasileira de Ciências Farmacêuticas*, vol. 42, pp. 413–417, Sept. 2006.

[16] C. Yan, H. Liu, and L. Lin, "Simultaneous determination of vitexin and isovitexin in rat plasma after oral administration of Santalum album L. leaves extract by liquid chromatography tandem mass spectrometry," *Biomedical chromatography: BMC*, vol. 27, pp. 228–232, Feb. 2013.

[17] L. Bravo, "Polyphenols: chemistry, dietary sources, metabolism, and nutritional significance," *Nutrition Reviews*, vol. 56, pp. 317–333, Nov. 1998.

[18] J. Jung, K. Ishida, J.-i. Nishikawa, and T. Nishihara, "Inhibition of estrogen action by 2-phenylchromone as AhR agonist in MCF-7 cells," *Life Sciences*, vol. 81, pp. 1446–1451, Oct. 2007.

[19] Q. Najmus-Saqib, F. Alam, and M. Ahmad, "Antimicrobial and cytotoxicity activities of the medicinal plant Primula macrophylla," *Journal of Enzyme Inhibition and Medicinal Chemistry*, vol. 24, pp. 697–701, June 2009.

[20] "Scopus." Disponível online em `https://www.scopus.com/`, data de acesso 03.08.2016.

[21] T. Peters, *All About Albumin: Biochemistry, Genetics, and Medical Applications*. Academic Press, Dec. 1995.

[22] G. Sudlow, D. J. Birkett, and D. N. Wade, "The characterization of two specific drug binding sites on human serum albumin," *Molecular Pharmacology*, vol. 11, pp. 824–832, Nov. 1975.

[23] G. Sudlow, D. J. Birkett, and D. N. Wade, "Further characterization of specific drug binding sites on human serum albumin," *Molecular Pharmacology*, vol. 12, pp. 1052–1061, Nov. 1976.

[24] J. Ghuman, P. A. Zunszain, I. Petitpas, A. A. Bhattacharya, M. Otagiri, and S. Curry, "Structural basis of the drug-binding specificity of human serum albumin," *Journal of Molecular Biology*, vol. 353, pp. 38–52, Oct. 2005.

[25] S. Sugio, A. Kashima, S. Mochizuki, M. Noda, and K. Kobayashi, "Crystal structure of human serum albumin at 2.5 Å resolution," *Protein Engineering*, vol. 12, pp. 439–446, June 1999.

[26] F. Zsila, "Subdomain IB Is the Third Major Drug Binding Region of Human Serum Albumin: Toward the Three-Sites Model," *Molecular Pharmaceutics*, vol. 10, pp. 1668–1682, May 2013.

[27] C. Dufour and O. Dangles, "Flavonoid-serum albumin complexation: determination of binding constants and binding sites by fluorescence spectroscopy," *Biochimica Et Biophysica Acta*, vol. 1721, pp. 164–173, Jan. 2005.

[28] E.-H. Liu, L.-W. Qi, and P. Li, "Structural relationship and binding mechanisms of five flavonoids with bovine serum albumin," *Molecules (Basel, Switzerland)*, vol. 15, no. 12, pp. 9092–9103, 2010.

[29] I. P. Caruso, W. Vilegas, M. A. Fossey, and M. L. Cornelio, "Exploring the binding mechanism of Guaijaverin to human serum albumin: Fluorescence spectroscopy and computational approach," *Spectrochimica Acta Part A: Molecular and Biomolecular Spectroscopy*, vol. 97, pp. 449–455, Nov. 2012.

[30] J. R. Lakowicz, ed., *Principles of Fluorescence Spectroscopy*. Boston, MA: Springer US, 2006.

[31] S. Bi, L. Ding, Y. Tian, D. Song, X. Zhou, X. Liu, and H. Zhang, "Investigation of the interaction between flavonoids and human serum albumin," *Journal of Molecular Structure*, vol. 703, pp. 37–45, Oct. 2004.

[32] W. Kauzmann, "Some Factors in the Interpretation of Protein Denaturation1," in *Advances in Protein Chemistry* (M. L. A. C.B. Anfinsen, Kenneth Bailey and John T. Edsall, ed.), vol. 14, pp. 1–63, Academic Press, 1959.

[33] G. Némethy and H. A. Scheraga, "Structure of Water and Hydrophobic Bonding in Proteins. II. Model for the Thermodynamic Properties of Aqueous Solutions of Hydrocarbons," *The Journal of Chemical Physics*, vol. 36, pp. 3401–3417, June 1962.

[34] C. Tanford, *The Hydrophobic Effect: Formation of Micelles and Biological Membranes*. New York: Wiley, 2nd edition ed., Jan. 1980.

[35] M. Rotenberg, S. Cohen, and R. Margalit, "Thermodynamics of porphyrin binding to serum albumin: effects of temperature, of porphyrin species and of albumin-carried fatty acids," *Photochemistry and Photobiology*, vol. 46, pp. 689–693, Nov. 1987.

[36] P. D. Ross and S. Subramanian, "Thermodynamics of protein association reactions: forces contributing to stability," *Biochemistry*, vol. 20, pp. 3096–3102, May 1981.

[37] T. M. Lohman and W. Bujalowski, "Thermodynamic methods for model-independent determination of equilibrium binding isotherms for protein-DNA interactions: spectroscopic approaches to monitor binding," *Methods in Enzymology*, vol. 208, pp. 258–290, 1991.

[38] E. D. Cera, *Thermodynamic Theory of Site-Specific Binding Processes in Biological Macromolecules*. Cambridge, UK ; New York: Cambridge University Press, 1 edition ed., Feb. 2005.

[39] X. Daura, K. Gademann, B. Jaun, D. Seebach, W. F. van Gunsteren, and A. E. Mark, "Peptide Folding: When Simulation Meets Experiment," *Angewandte Chemie International Edition*, vol. 38, pp. 236–240, Jan. 1999.

[40] J. C. Ma and D. A. Dougherty, "The Cation−pi Interaction," *Chemical Reviews*, vol. 97, pp. 1303–1324, Aug. 1997.

[41] A. C. Wallace, R. A. Laskowski, and J. M. Thornton, "LIGPLOT: a program to generate schematic diagrams of protein-ligand interactions," *Protein Engineering*, vol. 8, pp. 127–134, Feb. 1995.

Anexo I - Artigo publicado na JPBA

Journal of Pharmaceutical and Biomedical Analysis 98 (2014) 100–106

Contents lists available at ScienceDirect

Journal of Pharmaceutical and Biomedical Analysis

journal homepage: www.elsevier.com/locate/jpba

Binding of antioxidant flavone isovitexin to human serum albumin investigated by experimental and computational assays

Ícaro Putinhon Caruso[a,b], Wagner Vilegas[c], Fátima Perreira de Souza[a,b], Marcelo Andrés Fossey[a,b], Marinônio Lopes Cornélio[a,b,*]

[a] Departamento de Física, Instituto de Biociências, Letras e Ciências Exatas (IBILCE), UNESP, Rua Cristovão Colombo 2265, CEP 15054-000, São José do Rio Preto, SP, Brazil
[b] Centro Multiusuário de Inovação Biomolecular (CMIB), Instituto de Biociências, Letras e Ciências Exatas (IBILCE), UNESP, Rua Cristovão Colombo 2265, CEP 15054-000, São José do Rio Preto, SP, Brazil
[c] Instituto de Química (IQ), UNESP, Rua Prof. Francisco Degni 55, CEP 14800-900, Araraquara, SP, Brazil

ARTICLE INFO

Article history:
Received 27 January 2014
Received in revised form 30 April 2014
Accepted 13 May 2014
Available online 22 May 2014

Keywords:
Isovitexin
Human serum albumin
Fluorescence spectroscopy
Binding density function
Molecular modeling

ABSTRACT

The flavonoids are a large class of polyphenolic compounds which occur naturally in plants where they are widely distributed. Isovitexin (ISO) is a glycosylated flavonoid that exhibits a potential antioxidant activity. Some recent studies have shown the pharmacokinetic activity of isovitexin in rat blood plasma, however, without detailing the molecular target that is linked and what physicochemical forces govern the interaction. In mammalians, the most abundant protein in blood plasma is the albumin and is not unlike with human, which human serum albumin (HSA) is the major extracellular protein and functions as a carrier of various drugs. The interaction between HSA and ISO was investigated using fluorescence, UV–vis absorbance, circular dichroism (CD), Fourier transform infrared spectroscopy (FT-IR) together with, computational methods like *ab initio* and molecular modeling calculation. Fluorescence quenching indicated that ISO location is within the hydrophobic pocket in subdomain IIA (site 1) of HSA, close to the Trp214 residue. The Stern–Volmer quenching constants determined at 288, 298 and 308 K and its dependence on temperature indicated that the quenching mechanism was static. From the analysis of binding equilibrium were determined; the binding site number and binding constants, with the correspondent thermodynamic parameters, ΔH, ΔG and ΔS for HSA–ISO complex. Also, a second binding analysis, binding density function (BDF) method, which is independent of any binding model pre-established obtained similar results. The fluorescence resonance energy transfer estimated the distance between the donor (HSA–Trp214) and acceptor (ISO), while FT-IR and CD spectroscopy measured possible changes of secondary structure at the formation of the HSA–ISO complex. The optimized geometry of isovitexin calculation performed with its ground state by using DFT/B3LYP/6-311+G(d,p) method. The HSA–ISO complex interactions determined by molecular modeling tool corroborated with the thermodynamic analysis from the experimental data.

1. Introduction

Flavonoids are a large class of naturally occurring polyphenolic compounds widely distributed in plants. The literature shows that flavonoids can present antioxidant, anticancer, antiviral, anti-inflammatory and heart disease protective activities [1]. Isovitexin (apigenin-6-C-β-D-glucopyranoside) is a glycoside flavonoid consisting of the flavone apigenin and the saccharide glucose, as shown in Fig. 1. Like many antioxidants present anti-inflammatory activity, ISO exhibits a potential antioxidant as well; studies have demonstrated that, in inflammatory processes induced by lipopolysaccharide (LPS) in mouse macrophage, this flavone is capable of inhibiting the production and, or release of tumor necrosis factor α (TNF-α) and prostaglandin E_2 (PG_2) [2]. Studies also have showed that isovitexin presents a possibly antiulcerogenic activity and it could help in peptic ulcer treatment [3]. ISO molecule is found, for example in rice hulls (*Oryza sativa* L.) [2], "*sempre-vivas chapadeira*" (*Syngonanthus bisulcatus* Rul.) [3] and tanxiang

* Corresponding author at: Departamento de Física, Instituto de Biociências, Letras e Ciências Exatas (IBILCE), UNESP, Rua Cristovão Colombo 2265, CEP 15054-000, São José do Rio Preto, SP, Brazil. Tel.: +55 17 32212246; fax: +55 17 32212247.
E-mail addresses: ykrocaruso@hotmail.com (Í.P. Caruso), vilegasw@gmail.com (W. Vilegas), fatima@ibilce.unesp.br (F.P. de Souza), marcelo@ibilce.unesp.br (M.A. Fossey), mario@ibilce.unesp.br, mariol.cornelio@gmail.com (M.L. Cornélio).

http://dx.doi.org/10.1016/j.jpba.2014.05.015
0731-7085/

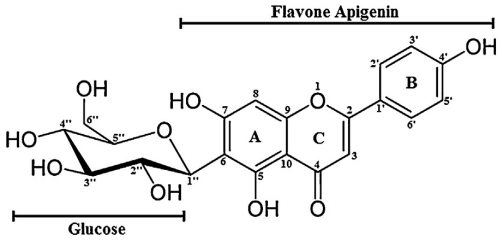

Fig. 1. (a) Chemical structure of isovitexin (apigenin-6-C-β-D-glucopyranoside).

(*Santalum album*) [4]. With such a promising profile as herbal medicine, pharmacokinetic studies were conducted in order to ascertain its presence in blood plasma after oral administration [4].

Human serum albumin (HSA) is the main extracellular protein, and it is present in high concentration, in blood plasma. HSA is a monomeric globular protein composed of three structurally similar domains (I, II and III), each containing two subdomains (A and B). Aromatic and heterocyclic ligands bind to HSA primarily within two hydrophobic pockets in subdomains IIA and IIIA, namely sites 1 and 2, respectively. Site 1 is the primary binding site for drugs like warfarin and phenylbutazone analogs, whereas diazepam and ibuprofen are bound primarily to site 2 [5]. The exceptional capacity of HSA to interact with several organic and inorganic molecules makes this protein an important regulator of intercellular fluxes and the main carrier for many drugs to different molecular targets. Therefore, more detailed studies of the microenvironment of binding sites of HSA are important for understanding the mechanism of HSA–drug interactions [5,6].

In this paper, a detailed study of the interaction between ISO and HSA was observed using spectroscopy methods including fluorescence spectroscopy, UV–vis absorbance, circular dichroism (CD), Fourier transform infrared spectroscopy (FT-IR), and computational methods like *ab initio* and molecular docking calculations. In particular, this work also made use of the binding density function (BDF) method for data analysis of fluorescence quenching that is very sparsely explored to study protein–ligand interaction. Such data set complements in great detail the information that is obtained in pharmacokinetic approaches of ISO, describing the non-covalent interactions that are responsible for the stability of the HSA–ISO complex.

2. Materials and methods

2.1. Materials and solutions

Human serum albumin fraction V was purchased from Sigma Chemical Co., and used as supplied. Isovitexin provided by Prof. Dr. Wagner Vilegas (UNESP, Brazil), which extraction and isolation were described previously [3]. All other chemicals were of analytical reagent grade and Milli-Q ultrapure water was used throughout the experiments. HSA was dissolved in aqueous and deuterated phosphate buffer solution of 50 mM at pH 7.0 (and pD 7.0) containing 0.15 M of NaCl. The stock solution of ISO was prepared in absolute ethanol. The aliquots of ISO applied in the following experiments were carefully evaluated to avoid aggregation of the flavonoid [7].

2.2. UV–vis absorbance spectroscopy

UV–vis absorption spectrum was recorded at room temperature on a Cary-3E spectrophotometer (Varian, Palo Alto, CA) equipped with 1.0 cm quartz cells of path length. UV–vis absorption spectra were recorded in the 250–500 nm range. Both concentrations of HSA and ISO were 4.0 μM. The final ethanol concentration in buffer was <1%.

2.3. Fluorescence spectroscopy

The fluorescence measurements were performed using an ISS PC1 steady-state spectrofluorimeter (Champaign, IL, USA) equipped with a Neslab RTE-221 thermostat bath. Both excitation and emission bandwidths were set at 8.0 nm. The excitation wavelength at 295 nm avoided the absorption of tyrosine residues, but excites the single tryptophan residue (Trp214) of HSA. The emission spectrum was collected in the range of 305–500 nm which was corrected for the background fluorescence of the buffer and for inner filter effects [8]. In the fluorescence quenching experiments, the titrations were performed by adding small aliquots from ISO stock solution to HSA solution (3.0 mL) at constant concentrations of 2.0, 4.0 and 8.0 μM. In experiments for Stern–Volmer and binding equilibria analysis, HSA concentration remained constant at 4.0 μM and ISO concentration varied from 0 to 4.8 μM with increment of 0.4 μM at 288, 298 and 308 K. For binding density function (BDF) method, the titration was performed at HSA constant concentrations of 2.0, 4.0 and 8.0 μM and ISO concentration varied from 0 to 3.4, 4.8 and 6.4 μM, respectively, at 298 K. The effect of ethanol as co-solvent was verified adding small aliquots to HSA solution (4.0 μM at 3.0 mL, 298 K) within the volume changes of the previous titrations. In all experiments, the final volume of ethanol in buffer was <1%.

2.4. Fourier transform infrared spectroscopy

The Fourier transform infrared (FT-IR) spectra obtained at room temperature utilized Nexus 670 FT-IR spectrometer (Nicolet, USA). All infrared spectra used the transmittance method in the range of 2200–1300 cm^{-1} with resolution of 4.0 cm^{-1} and 512 scans. The FT-IR experiments were performed with deuterated HSA solution of 20 mg/mL (0.3 mM) at pD 7.0. For the preparation of free ISO and HSA–ISO complex solutions, the solvent (ethanol) of ISO stock solution was evaporated and resuspended using the phosphate buffer and HSA solutions in D_2O, respectively, keeping the final concentration of ISO for the ligand–protein ratio of 0:1, 0.5:1 and 1:1. Subtraction, smoothing, baseline correction, second derivative, Fourier self-deconvolution and curve fitting are detailed in Supplementary material [9,10].

2.5. UV circular dichroism spectroscopy

All UV CD spectra recorded at room temperature at Jasco J-815 spectropolarimeter (Jasco, USA) and equipped with 0.01 cm quartz cell of path length. The range of UV CD spectra was from 190 to 260 nm with a scan rate of 20 nm/min, and total of 10 accumulations. The HSA concentration kept constant during all experiment at 4.0 μM while that the ISO to HSA ratios were of 0:1, 0.5:1 and 1:1. The final ethanol concentration in buffer was <1%. The equipment baseline correction and buffer spectrum was subtracted from free and complexed HSA. Secondary structures were estimated with CONTINLL software of CDPro package, using the reference set of proteins SMP56 [11].

2.6. Ab initio calculation

The Gaussian 09 program [12] provided by Núcleo de Computação Científica da Universidade Estadual Paulista (NCC/GridUNESP) was applied to the calculation of ISO structure. The optimized geometry calculated at the gas phase with ISO molecule isolated by using DFT/B3LYP/6-311+G(d,p) method. The next step, the vibrational frequency calculation, was performed to

check the optimized ISO molecule. TD-DFT/B3LYP/6-311+G(d,p) calculation was performed to the optimized ISO, taking into account some excited states. The solvent effect in ethanol was verified using the PCM calculation [13]. The molecular electrostatic potential (MEP) map was calculated to investigate the distribution of charge density on the molecular surface of ISO.

2.7. Molecular modeling calculation

The crystal structure of HSA (PDB ID: 1AO6) [14] downloaded from the Protein Data Bank. The 3D structure of ISO molecule was obtained from Gaussian 09 program [12]. AutoDockTools (ADT) [15] was used to prepare HSA and ISO. Grid maps were generated with 0.375 Å spacing and dimensions of 60 × 60 × 60 points by the AutoGrid 4.2 program [16], these maps were centered near the Trp 214 residue. The AutoDock 4.2 program [16] was employed to study the binding site between ISO and HSA by applying the Lamarckian Genetic Algorithm (LGA) for minimization. For each docking simulation, 100 different conformers were generated.

2.8. Accessible surface area calculations

The accessible surface area (ASA) of free or uncomplexed HSA and its docked complex with ISO was calculated using the NACCESS program [17]. The HSA–ISO complex structure was obtained from the best molecular modeling structure. Changes in absolute ASA for residue *i* were calculated using the following equation:

$$\Delta ASA^i = ASA^i_{uncomplexed} - ASA^i_{complexed} \quad (1)$$

where $ASA^i_{uncomplexed}$ and $ASA^i_{complexed}$ is the absolute accessible surface area for free and complexed HSA residues, respectively. If one residue loses more than 10 Å^2 of absolute ASA undergoing from the uncomplexed to the complexed state, it is considered involved in the interaction.

3. Results and discussion

3.1. Fluorescence quenching process of HSA by isovitexin

The fluorescence quenching process may be a result of several mechanisms as reactions with the excited state, molecular rearrangement, energy transfer, ground state complex formation and collisional quenching. These different mechanisms are usually classified as either dynamic or static depending on their dependence with temperature and viscosity, or preferably by measuring the fluorescence lifetime [18]. The fluorescence intensity of HSA decreased with increasing ISO concentration (Supplementary material, Fig. S1), indicating that ISO microenvironment is around the single tryptophan residue (Trp214) within the hydrophobic pocket of subdomain IIA, site 1 of HSA. The effect of ethanol on the fluorescence intensity of HSA can be considered negligible (Supplementary material, Fig. S2).

The data analysis regarding fluorescence quenching process was performed applying Stern–Volmer equation [18]:

$$\frac{F_0}{F} = 1 + K_q\tau_0[Q] = 1 + K_{SV}[Q] \quad (2)$$

where F_0 and F are the steady-state fluorescence intensities in the absence and presence of quencher (Q), respectively. K_q is the bimolecular quenching constant, τ_0 is the fluorophore lifetime in the absence of quencher which value for HSA is 10^{-8} s [18], [Q] is the quencher concentration and K_{SV} is the Stern–Volmer quenching constant. In the investigated concentration range, the results of fluorescence quenching at 288, 298 and 308 K are in accordance with the Stern–Volmer equation (Supplementary material, Fig. S3).

Table 1
Stern–Volmer quenching constant (K_{SV}), bimolecular quenching constant (K_q), binding constant (K_b), and binding site numbers (n) of the interaction between HSA and isovitexin at pH 7.0 and 288, 298 and 308 K.

T (K)	K_{SV} ($\times 10^4$ M^{-1})	K_q ($\times 10^{13}$ M^{-1} s^{-1})	K_b ($\times 10^5$ M^{-1})	n
288	7.20	7.20	1.05	1.16
298	5.91	5.91	0.83	1.09
308	4.67	4.67	0.58	1.01

The correlation coefficient is ≥0.995.

The results shown in Table 1 denote that the Stern–Volmer constant values (K_{SV}) are inversely correlated with temperature increment. The bimolecular quenching constant (K_q) values, which were calculated by using Eq. (2) are greater than 2.0×10^{10} M^{-1} s^{-1}, which represents the maximum diffusion collision rate at various quenchers with biopolymers [18]. In addition, the absorption spectrum of HSA presented changes in the presence of ISO (Supplementary material, Fig. S4). Therefore, the quenching mechanism of HSA–ISO in essence is the static process (ground state complex).

3.2. Analysis of binding equilibria

For static quenching mechanism, if it is assumed that the binding sites are the same and independent at the protein, the binding constant (K_b) and the number of binding sites (n) can be calculated using the following equation [19]:

$$\log\left(\frac{F_0 - F}{F}\right) = n \log K_b - n \log\left(\frac{1}{[D_0] - (F_0 - F)[P_0]/F}\right) \quad (3)$$

Fig. 2 shows the binding equilibrium plots for the fluorescence quenching of HSA by ISO at 288, 298 and 308 K. The dependence of $\log[(F_0 - F)/F]$ on the value of $\log(1/[D_0] - (F_0 - F)[P_0]/F)$ is linear, with a slope equal to the value of n and the value n log K_b fixed on the ordinate. For the HSA–ISO complex, K_b and n values at 288, 298 and 308 K are presented in Table 1. It was observed that the number of binding sites of the complex is approximately equal to 1.0. K_b value decreased in correlation with temperature rising, which is in agreement with trends of K_{SV}.

3.3. Thermodynamic analysis

The driven forces responsible for the interaction between HSA and ISO were calculated from the van't Hoff equation:

$$\ln K_b = -\frac{\Delta H^\circ}{RT} + \frac{\Delta S^\circ}{R} \quad (4)$$

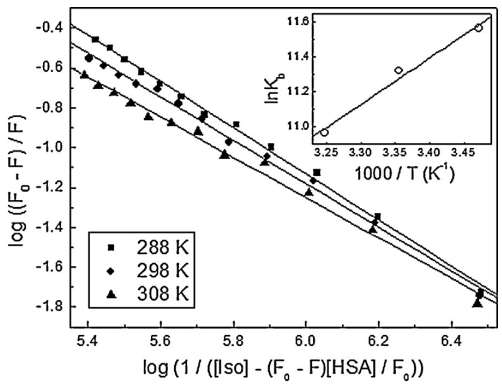

Fig. 2. Double-log plots for the fluorescence quenching of HSA by isovitexin at pH 7.0 and 288, 298 and 308 K. The insert corresponds to the van't Hoff plot for the interaction.

Table 2
Thermodynamic parameters of the HSA–ISO complex at pH 7.0 and 288, 298 and 308 K.

T (K)	ΔH° (kJ mol^{-1})	ΔG° (kJ mol^{-1})	ΔS° (J mol^{-1} K^{-1})	R
288		−27.7		
298	−22.1	−27.9	19.6	0.992
308		−28.1		

R is the correlation coefficient.

where ΔH° is the enthalpy changes, ΔS° is the entropy changes, R is the universal gas constant and K_b is the binding constant at the correspondent temperature (T). Table 2 shows ΔH° and ΔS° values obtained through the slope and the ordinate of van't Hoff relationship (insert Fig. 2), and lists the corresponding values of Gibbs free energy changes (ΔG°) as calculated from the relation:

$$\Delta G^\circ = \Delta H^\circ - T\Delta S^\circ \quad (5)$$

The values of $\Delta G^\circ < 0$ indicated that the process is spontaneous, and the comparison between ΔH° and ΔS° defines whether the hydrophobic and, or electrostatic contribution would play an important role on the stabilization of the complex. According to the literature [20], positive values for both ΔH° and ΔS° indicate hydrophobic interactions, whereas negative values connote the action of van der Waals force and hydrogen bonding. In general, values of $\Delta S^\circ > 0$ are considered as evidence due to hydrophobic interaction. Besides that the specific electrostatic interaction between ionic species in aqueous solution is characterized by $\Delta S^\circ > 0$ and $\Delta H^\circ \approx 0$. For the HSA–ISO complex, the results of thermodynamic analysis showed that $\Delta H^\circ < 0$ and $\Delta S^\circ > 0$. The negative enthalpic term provided the greatest contribution for ΔG°, characterizing an enthalpically driven exothermic reaction. The enthalpy–entropy magnitude balance indicated that the hydrophobic interaction offered the main contribution for the formation and stabilization of the HSA–ISO complex. However, signal values for enthalpy and entropy changes also indicated that the electrostatic interactions could play an important role in complex stabilization by forming interactions as van der Walls, hydrogen bonds and charge neutralization.

3.4. Binding density function method

The thermodynamic basis for the binding density function (BDF) method is that the distribution of ligands bound per macromolecule in i different states ($\sum \nu_i$) is strictly determined at equilibrium by the free ligand concentration (L_F). Thus, if L_F is the same for two (or more) solutions at different total macromolecule concentration (M_T), then $\sum \nu_i$ will also be the same in each solution. As a result, constant values of L_F and $\sum \nu_i$ will exist for a number of different combinations of L_T and M_T, that satisfy the mass conservation equation [21]:

$$L_T = L_F + \left(\sum \nu_i\right) M_T \quad (6)$$

Considering the general relationship between the concentration of each macromolecule species with i ligands bound and the experimentally observed signal (S_{obs}) from the macromolecule, the fractional signal molar changes (ΔS_{obs}) observed in the presence of L_T and M_T will be given by:

$$\Delta S_{obs} = \frac{S_{obs} - S_F M_T}{S_F M_T} \quad (7)$$

where $S_F M_T$ is the observed signal for free macromolecule in the absence of ligand (F_0, see Section 3.1). Then for the fluorescence quenching experiments have to be $\Delta S_{obs} = (F - F_0)/F_0$ [21]. A horizontal line was drawn intersecting the three titration curves in Fig. 3, defining one constant value of ΔS_{obs} and three sets of (L_{Tx}; M_{Tx}) (x = 1, 2 and 3) for which L_F and $\sum \nu_i$ were constants (see insert in Fig. 3).

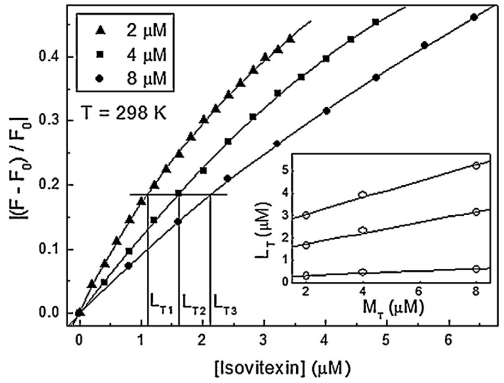

Fig. 3. Titrations of isovitexin in HSA solutions, as monitored by fluorescence quenching of the Trp214 residue of HSA for three different protein concentrations at pH 7.0 and 298 K. L_{T1}, L_{T2} and L_{T3} represent the ligand concentration for the constant fractional signal molar change value of three different protein concentration (M_{T1}, M_{T2} and M_{T3}). The insert corresponds to only three sets of concentration pairs (L_T; M_T) to exemplify the utilization of Eq. (9) obtaining $\sum \nu_i$ and L_F values.

From the L_F and $\sum \nu_i$ values obtained from Eq. (6), it can be build the Scatchard plot for the binding between HSA and ISO (Supplementary material, Fig. S5) without using any binding model *a priori*. Scatchard plot was built using the following equation:

$$\frac{\sum \nu_i}{L_F} = n K_a - K_a \left(\sum \nu_i\right) \quad (8)$$

where K_a is the association constant and n is binding site number. The obtained values for K_a and n from Scatchard plot were 2.35×10^5 M^{-1} and 1.04, respectively, which are in accordance with the results obtained from analysis of binding equilibria (Section 3.2).

3.5. Distance measurement between HSA–Trp214 and isovitexin

Fluorescence resonance energy transfer (FRET) is a method that can monitor the proximity and relative angular orientation of fluorophores. According to Förster non-radiative energy transfer theory. The energy transfer occurs under the following conditions. The donor produces fluorescent light, the emission spectrum of the donor and the absorbance spectrum of the acceptor have a partial overlap, and the distance between the donor and acceptor is less than 8.0 nm [18]. According to this theory, the average distance r in the binding between HSA–Trp214 (donor) and ISO (acceptor) can be calculated by the equation:

$$E = 1 - \frac{F}{F_0} = \frac{R_0^6}{R_0^6 + r^6} \quad (9)$$

where E is the efficiency of energy transfer and R_0 is the critical distance when the transfer efficiency is 50%.

$$R_0^6 = 8.79 \times 10^{-25} K^2 n^{-4} \phi J \quad (10)$$

In Eq. (10), K^2 is the orientation space factor, n is the refracted index of the medium, ϕ is the fluorescence quantum yield of the donor, J is the effect of the spectral overlap between the emission spectrum of the donor and the absorption spectrum of the acceptor (see Fig. 4), which may be calculated by the following equation:

$$J = \frac{\int_0^\infty F(\lambda)\varepsilon(\lambda)\lambda^4 d\lambda}{\int_0^\infty F(\lambda) d\lambda} \quad (11)$$

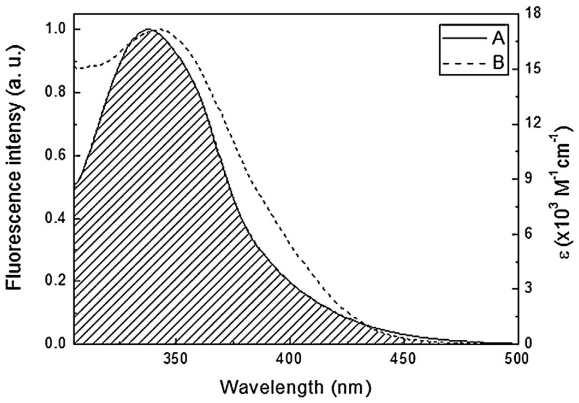

Fig. 4. Spectral overlaps of the HSA fluorescence (A) with isovitexin absorption (B) ([HSA] = [ISO] = 4.0 μM).

where $F(\lambda)$ is the corrected fluorescence intensity of the donor in the wavelength range from λ to $\lambda + \Delta\lambda$, and $\varepsilon(\lambda)$ is the extinction coefficient of the acceptor at λ.

In order to obtain the distance between HSA–Trp214 and ISO, the concentration of both was 4.0 μM. In this study, $K^2 = 2/3$, $n = 1.36$, and $\phi = 0.074$ [22]. According to Eqs. (9)–(11), it was calculated the values of $J = 1.982 \times 10^{-14}\ \mathrm{cm^3\,L\,mol^{-1}}$, $E = 0.187$, $R_0 = 2.512$ nm and $r = 3.209$ nm. The range distance between donor and acceptor fluorophore is from 2.0 to 8.0 nm [19], indicating that the energy transfer from HSA to ISO likely may occur.

3.6. HSA secondary structural analysis

The possible secondary structural changes of HSA induced by binding of ISO were investigated using FT-IR and UV CD spectroscopy analysis. The amide I′ band is in the region from 1600 to 1700 $\mathrm{cm^{-1}}$ and attributed to the stretching vibration of C=O of amide groups in the main chain of the protein. The amide I′ band of HSA presents centered at 1650 $\mathrm{cm^{-1}}$, which is characteristic for proteins with largest percentage of α-helix secondary structure. The increasing of ISO concentration provides the slight increasing of amide I′ absorbance, without any displacement of the band (Supplementary material, Fig. S6). The band assignments that form the amide I′ for HSA was characterized from the second derivative spectra according to the literature (see more details in Supplementary material) [23].

Fig. 5 shows the curve fitting for the ISO to HSA ratios of 0:1 and 1:1. The ISO/HSA ratio of 0.5:1 presents identical result to 0:1 ratio (Supplementary material, Fig. S8). The spectrum of free HSA in D_2O contains as major component of α-helix secondary structure (61%), which is in agreement with previous results for HSA [14]. The curve fitting results showed in Fig. 5 demonstrate that the interaction of HSA with ISO do not cause significant changes in its secondary structure.

The principle of circular dichroism technique consists of different absorption of right or left circularly polarized light that some molecules present. The CD spectra present two negative bands in the ultraviolet region 209 and 221 nm, which is characteristic of the α-helix structure of protein (Supplementary material, Fig. S9) [24]. The CD spectra of HSA did not present significant changes with the addition of the ISO–ethanol (Fig. S9). The structural analysis calculated by CONTINLL software [11] showed that the secondary structural of HSA did not present conformational changes with the addition of ISO aliquots, maintaining 63% of α-helix structure. The results obtained from CD spectra corroborated with FT-IR analysis.

3.7. Ab initio calculation

The optimization and vibrational calculation performed for ISO by using the DFT/B3LYP/6-311+G(d,p) method found that the optimized structure is stable (global minimum on the potential energy surface) since no imaginary frequency is verified. Some calculated bond distances, bond angles, and dihedral angles presented in Table S1 of Supplementary material. The results of TD-DFT calculation were in agreement with the experimental UV–vis absorbance data (Supplementary material, Table S2), since the maximum experimental UV–vis absorbance corresponds to the vertical transition according to the Franck–Condon principle. Therefore, the results of *ab initio* calculations for ISO are consistent with experimental data.

From the MEP of ISO (Supplementary material, Fig. S10) was possible to observe the existence of a neutral charge distribution at the planar face between the rings B and C. It can also be seen a dense distribution of positive charge near the H4′ hydrogen atom. On the other hand, a negative electrostatic potential is localized near the O4 oxygen atom, and other regions of the molecule comparatively less dense near of the O5, O7 and O2″ atoms, practically surrounding ring A, of the flavone.

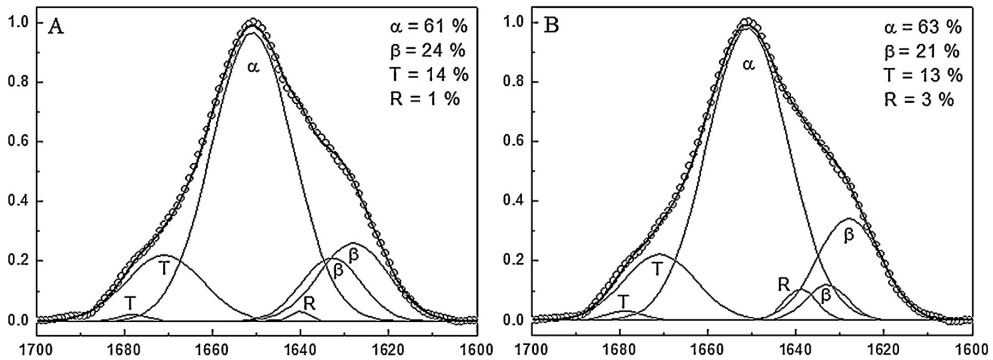

Fig. 5. Gaussians curve fitting of the deconvoluted amide I′ band of HSA in absence and presence of isovitexin at room temperature and pH 7.0. Fourier self-deconvoluted spectra were performed using FWHH = 20 $\mathrm{cm^{-1}}$ and $K = 2$. Gaussians adjustment curves of the deconvoluted amide I′ band for isovitexin to HSA ratios: (A) 0:1 and (B) 1:1, with HSA constant concentration of 20 mg/mL (0.3 mM). Gaussians adjustment curves are shown with thin lines (α-helix, α; β-sheet, β; random structure, R; turn, T), summed up Gaussians curves shown with thick line and deconvoluted spectra shown with open circles (○). The correlation coefficient (R) and qui-squared (χ^2) for the adjustments were: (A) 0.999 and 5.0×10^{-5} and (B) 0.999 and 2.0×10^{-5} respectively.

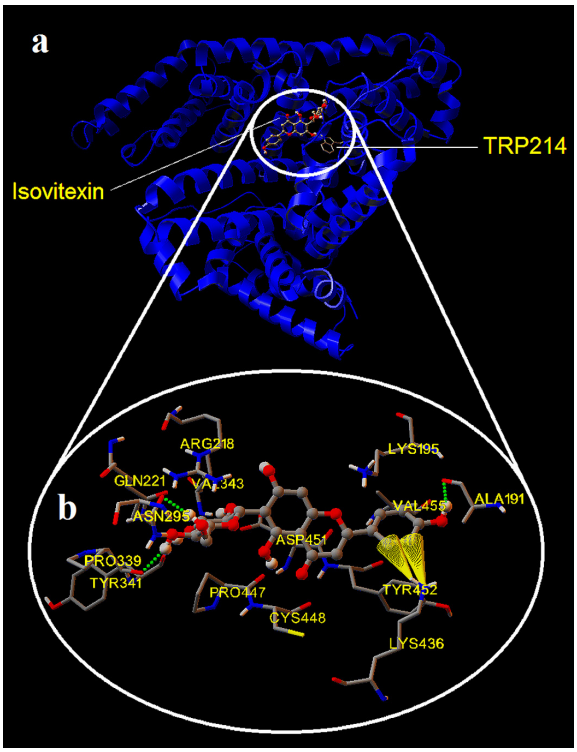

Fig. 6. (a) Location of isovitexin molecule near the single tryptophan residue (Trp 214) of the HSA in the subdomain IIA (site 1). (b) Structural details of the interaction between HSA and isovitexin obtained by molecular modeling method. Isovitexin molecule is shown as sticks and balls model, the amino acid residues are denoted as sticks model (C, gray; O, red; N, blue; S, yellow; H, white), the π–cation interactions are shown as yellow cones, and the hydrogen bonds depicted by green dotted line. (For interpretation of the references to color in this figure legend, the reader is referred to the web version of this article.)

3.8. Molecular modeling calculations

Fig. 6 shows the result of the best binding energy among the molecular modeling simulations. The best binding energy for the HSA–ISO complex is $-27.5\,kJ\,mol^{-1}$, with a corresponding theoretical binding constant of $6.7 \times 10^4\,M^{-1}$ at 298 K, which is in agreement with the values determined by analysis of binding equilibria (K_b, Section 3.2) and binding density function method (K_a, Section 3.4).

Fig. 6a shows that ISO is at the entrance of the site 1 of HSA and closes to the Trp214 residue. The entrance of the site 1 of HSA is lesser hydrophobic region than the pocket bottom, as shown at the hydrophobic surface generated for HSA–ISO complex by Chimera 1.8 software [25] (Supplementary material, Fig. S11). Fig. 6b presents in more details the binding site environment. A set of nonpolar side chain residues like Ala191, Pro339, Val343, Pro447, Cys448 and Val455 mostly contributes to the hydrophobic interactions with ISO. However, Ala191 and Pro339 residues form hydrogen bonds with ISO, presenting formation distances of 1.989 and 2.036 Å, respectively. The oxygen atom of Ala191 main chain makes up a hydrogen bond with the H4′ hydrogen atom of ISO, this hydrogen atom presents the densest positive charge distribution shown at the MEP of the flavonoid (Fig. S10). The oxygen atom of Pro339 main chain forms a hydrogen bond with the H4″ hydrogen atom of ISO. The neutral polar side chain residues like Gln221, Asn295, Tyr341 and Tyr452 are mainly taking part in electrostatic interactions (charge neutralization), except the Tyr452 residue which is involved in hydrophobic interactions with the neutral charge distribution at the planar face of ring B of ISO (Fig. S10). Asn295 side chain makes up a hydrogen bond with ISO, exhibiting a formation distance of 2.015 Å. The oxygen atom of Asn295 main chain forms a hydrogen bond with the H6″ hydrogen atom of ISO. The polar side chain residues like Lys195, Arg218, Asp451 and Lys436 participate in electrostatic interactions, except the Lys195 residue whose (carbons) nonpolar atoms of the side chain perform hydrophobic interactions with the planar face of the ring B of ISO, as well as Tyr452 residue. Arg218 and Asp451 residues are involved in electrostatic interactions of charge neutralization with the flavonoid glycosylation. A special case occurs with Lys436 residue, it performs electrostatic interactions of the cation–π type with the ring B of ISO (see Fig. 6). The cation–π interaction is a noncovalent molecular interaction that occurs between a cation (positive anion) and the face of an electron-rich π system as the B benzene ring of ISO. Such noncovalent interaction has bonding energies comparable with hydrogen bond energies [26].

3.9. Accessible superficial area calculation

The average area lost by HSA residues in the complexation with ISO was approximately 25 $Å^2$. Arg218, Lys195 and Tyr452 were the residues with highest loss of ASA in the complex formation (Supplementary material, Table S3). ASA changes for nonpolar and polar atoms of the residues involved in HSA–ISO complexation was of 70% and 30%, respectively. Although, Lys195, Asp451 and Tyr452 are polar residues their largest change in ASA occurred in their nonpolar atoms, demonstrating that these residues participate of hydrophobic interactions in the complexation. ASA results suggest that the hydrophobic interactions are the main interactions involved in the HSA–ISO complex formation even though the electrostatic interaction should not be neglected, which is in accordance with the thermodynamic analysis (Section 3.3).

4. Conclusion

The interaction between flavone isovitexin and HSA investigated using a pool of spectroscopic techniques that in combination with *ab initio* and molecular modeling calculations observed and described in more depth the complex formation. The main physicochemical observable element was the fluorescence signal of the Trp214 residue which was quenched with the addition of ISO aliquots, revealing that ISO molecule is in the vicinity of the Trp214 microenvironment. The validation of the procedure through two different methodologies, Stern–Volmer binding equilibrium and binding density function analysis, both reached similar values of binding constant, number of sites and the energetic of the interaction. These approaches are different with respect to other analytical techniques such as HPLC-UV and HPLC–MS commonly used in pharmacokinetic measurements that rely on some internal standard. The comparison between these two groups of analytical techniques unveils that while HPLC-UV and HPLC–MS can verify the presence of the analyte in the blood plasma. This specific condition could complicate the analysis herewith because is not possible to distinguish the protein in which the observable is (Trp, in our case). Nevertheless, if the protein of interest is purified from the blood plasma and performed analyses with HPLC-UV and HPLC–MS, such techniques could not give details as we demonstrated in the present investigation.

Regarding the complex formation the assays with temperature suggested that the quenching mechanism was static, and the same results were also determined carefully by means of UV–vis absorption difference spectra of HSA. The analysis of binding equilibria

demonstrated that only one ISO molecule binds to HSA, and from the binding constant (K_b) we calculated the thermodynamic parameters for the formation of the HSA–ISO complex. The negative ΔG values indicated that the binding reaction was spontaneous, and the values of the enthalpy and entropy changes suggested that the hydrophobic interactions played an important role at the formation and stabilization of the HSA–ISO complex. The observation was essentially phenomenological, so that it did not reveal the nature of the hydrophobic forces which results came from the dispersion forces. These forces alone could not explain the complex formation, and this led to the conclusion that the complex assembly was a result of the behavior of the system itself. Those considerations could also be applied to the electrostatic interactions (van der Waals interactions, hydrogen bonds, charge neutralization, cation–π interaction). The data obtained from binding density function (BDF) method matched with binding equilibrium analysis; it was an important result since BDF method is independent of any binding model. The distance between donor (HSA–Trp214) and acceptor (ISO) calculated by FRET was 3.209 nm, suggesting that the energy transfer occurred. From FT-IR and CD spectroscopy analysis, no significant change of secondary structure due to the formation of the HSA–ISO complex was observed. The molecular modeling calculations indicated that the ligand as a whole matches its molecular architecture (MEP) with the binding pocket of subdomain IIA of HSA. The results indicated that the interaction of isovitexin with HSA had a contribution balance between electrostatic (hydrogen bonds, charge neutralization and cation–π interaction) and hydrophobic interactions, which was also in agreement with the thermodynamic analysis, describing a detailed view of the microenvironment of the binding site.

Acknowledgments

The author IPC gratefully acknowledges a CAPES scholarship and financial support received from FAPESP. IPC also recognizes GridUNESP by availability of Gaussian 09 quantum chemical program, Prof. Dr. Alexandre Suman de Araújo by feasibility of computational time for AutoDock program in Calix cluster, Prof. Dr. João Ruggiero Neto by availability of spectropolarimeter, and Prof. Dr. Márcio Francisco Colombo by feasibility of UV–vis spectrometer.

Appendix A. Supplementary data

Supplementary data associated with this article can be found, in the online version, at http://dx.doi.org/10.1016/j.jpba.2014.05.015.

References

[1] E. Grotewold, The Science of Flavonoids, Springer, New York, 2006.
[2] S.T. Huang, C.T. Chen, K.T. Chieng, S.H. Huang, B.H. Chiang, L.F. Wang, H.S. Kuo, C.M. Lin, Inhibitory effects of a rice hull constituent on tumor necrosis factor α, prostaglandin E2, and cyclooxygenase-2 production in lipopolysaccharide-activated mouse, Ann. N. Y. Acad. Sci. 1042 (2005) 387–395.
[3] R.G. Coelho, L.M. Batista, L.C. Santos, A.R.M.S. Brito, W. Vilegas, Phytochemical study and antiulcerogenic activity of *Syngonanthus bisulcatus* (Eriocaulaceae) Braz, J. Pharm. Sci. 42 (2006) 413–417.
[4] C. Yan, H. Liu, L. Lin, Simultaneous determination of vitexin and isovitexin in rat plasma after oral administration of *Santalum album* L. leaves extract by liquid chromatography tandem mass spectrometry, Biomed. Chromatogr. 27 (2013) 228–232.
[5] T. Peters, All About Albumin. Biochemistry, Genetics and Medical Application, Academic Press, San Diego, CA, 1996.
[6] I.P. Caruso, W. Vilegas, M.A. Fossey, M.L. Cornélio, Exploring the binding mechanism of Guaijaverin to human serum albumin: fluorescence spectroscopy and computational approach, Spectrochim. Acta A 97 (2012) 449–455.
[7] L. Pohjala, P. Tammela, Aggregating behavior of phenolic compounds – a source of false bioassay results? Molecules 17 (2012) 10774–10790.
[8] I.E. Borissevitch, More about the inner filter effect: corrections of Stern–Volmer fluorescence quenching constants are necessary at very low optical absorption of the quencher, J. Lumin. 81 (1999) 219–224.
[9] Y.N. Chirgadze, O.V. Fedorov, N.P. Trushina, Estimation of amino acid residue side-chain absorption in the infrared spectra of protein solutions in heavy water, Biopolymers 14 (1975) 679–694.
[10] D.M. Byler, H. Susi, Examination of the secondary structure of protein by deconvolved FTIR spectra, Biopolymers 25 (1986) 469–487.
[11] N. Sreerama, R.W. Woody, A self-consistent method for the analysis of protein secondary structure from circular dichroism, Anal. Biochem. 282 (2000) 252–260.
[12] M.J. Frisch, G.W. Trucks, H.B. Schlegel, G.E. Scuseria, M.A. Robb, J.R. Cheeseman, G. Scalmani, V. Barone, B. Mennucci, G.A. Petersson, H. Nakatsuji, M. Caricato, X. Li, H.P. Hratchian, A.F. Izmaylov, J. Bloino, G. Zheng, J.L. Sonnenberg, M. Hada, M. Ehara, K. Toyota, R. Fukuda, J. Hasegawa, M. Ishida, T. Nakajima, Y. Honda, O. Kitao, H. Nakai, T. Vreven, J.A. Montgomery Jr., J.E. Peralta, F. Ogliaro, M. Bearpark, J.J. Heyd, E. Brothers, K.N. Kudin, V.N. Staroverov, R. Kobayashi, J. Normand, K. Raghavachari, A. Rendell, J.C. Burant, S.S. Iyengar, J. Tomasi, M. Cossi, N. Rega, J.M. Millam, M. Klene, J.E. Knox, J.B. Cross, V. Bakken, C. Adamo, J. Jaramillo, R. Gomperts, R.E. Stratmann, O. Yazyev, A.J. Austin, R. Cammi, C. Pomelli, J.W. Ochterski, R.L. Martin, K. Morokuma, V.G. Zakrzewski, G.A. Voth, P. Salvador, J.J. Dannenberg, S. Dapprich, A.D. Daniels, O. Farkas, J.B. Foresman, J.V. Ortiz, J. Cioslowski, D.J. Fox, Gaussian 09, Revision A.02, Gaussian, Inc., Wallingford, CT, 2009.
[13] E. Cances, B. Mennucci, J. Tomasi, Evaluation of solvent effects in isotropic and anisotropic dielectrics, and in ionic solutions with a unified integral equation method: theoretical bases, computational implementation and numerical applications, J. Chem. Phys. 107 (1997) 3032–3041.
[14] S. Sugio, A. Kashima, S. Mochikuzi, M. Noda, K. Kobayashi, Crystal structure of human serum albumin at 2.5 Å resolution, Protein Eng. 12 (1999) 439–446.
[15] M.F. Sanner, Python: a programming language for software integration and development, J. Mol. Graphics Modell. 17 (1999) 57–61.
[16] G.M. Morris, D.S. Goodsell, R.S. Halliday, R. Huey, W.E. Hart, R.K. Belew, A.J. Olson, Automated docking using a Larmarckian genetic algorithm and an empirical binding free energy function, J. Comput. Chem. 19 (1998) 1639–1662.
[17] S.J. Hubbard, J.M. Thornton, NACCESS; Computer Program, Department of Biochemistry and Molecular Biology, University College, London, 1993.
[18] J.R. Lakowicz, Principles of Fluorescence Spectroscopy, 2nd ed., Kluwer Academic Publishers/Plenum Press, New York, 1999.
[19] S. Bi, L. Ding, Y. Tian, D. Song, X. Zhou, X. Liu, H. Zhang, Investigation of the interaction between flavonoids and human serum albumin, J. Mol. Struct. 703 (2004) 37–45.
[20] P.D. Ross, S. Subramanian, Thermodynamics of protein association reactions: forces contributing to stability, Biochemistry 20 (1981) 3096–3102.
[21] T.M. Lohman, W. Bujalowski, Thermodynamics methods for model-independent determination of equilibrium binding isotherms for protein–DNA interactions: spectroscopic approaches to monitor binding, Methods Enzymol. 208 (1991) 158–290.
[22] Y.J. Hu, Y. Liu, J.B. Wang, X.H. Xiao, S.S. Qu, Study of the interaction between monoammonium glycyrrhizinate and bovine serum albumin, J. Pharm. Biomed. Anal. 36 (2004) 915–919.
[23] A. Barth, Infrared spectroscopy of proteins, Biochim. Biophys. Acta 1767 (2007) 1073–1101.
[24] M.G. Gore, Spectrophotometry and Spectrofluorimetry: A Practical Approach, Oxford University Press, New York, 2000, pp. 123–125.
[25] E.F. Pettersen, T.D. Goddard, C.C. Huang, G.S. Couch, D.M. Greenblatt, E.C. Meng, T.E. Ferrin, UCSF Chimera – a visualization system for exploratory research and analysis, J. Comput. Chem. 25 (2004) 1605–1612.
[26] J.C. Ma, D.A. Dougherty, The cation–π interaction, Chem. Rev. 97 (1997) 1303–1324.

Anexo II - Material suplementar do Anexo I

Supplementary material – Binding of antioxidant flavone isovitexin to human serum albumin investigated by experimental and computational assays

Ícaro Putinhon Caruso[a,b] , Wagner Vilegas[c], Fátima Pereira de Souza[a,b], Marcelo Andrés Fossey[a,b], Marinônio Lopes Cornélio[a,b,*]

[a] Departamento de Física, Instituto de Biociências, Letras e Ciências Exatas (IBILCE), UNESP, Rua Cristovão Colombo 2265, CEP 15054-000, São José do Rio Preto, SP, Brasil;

[b] Centro Multiusuário de Inovação Biomolecular (CMIB), Instituto de Biociências, Letras e Ciências Exatas (IBILCE), UNESP, Rua Cristovão Colombo 2265, CEP 15054-000, São José do Rio Preto, SP, Brasil;

[c] Instituto de Química (IQ), UNESP, Rua Prof. Francisco Degni 55, CEP 14800-900, Araraquara, SP, Brasil.

* Corresponding author e-mail address: mario@ibilce.unesp.br

Analysis methodology for FT-IR spectra

The free HSA spectrum (ligand-protein ratio 0:1) was obtained subtracting the buffer solution absorbance from the deuterated HSA solution spectrum ([HSA] = 20 mg/mL). The HSA spectra complexed with Isovitexin were acquired subtracting the ISO solution absorbance from the solution spectra of the HSA with ISO, for ligand-protein ratios of 0.5:1 and 1:1. A planar and inexpressive absorbance in the range of 2200 – 1800 cm^{-1} is a criterion for obtaining a subtracted spectrum. The contribution of the side chain of the amino acid residues of HSA simulated in the range 1800 – 1500 cm^{-1} according to the literature for buffer solution in D_2O [1]. The simulation of the side chain spectrum was performed using a program written in MATLAB platform (MathWorks, MA, USA). The contribution of the side chain spectrum was removed from the subtracted spectra of the free and complexed HSA, observing the disappearance of the tyrosine ring vibration band at 1515 cm^{-1}. The HSA spectra without contribution of side chain were smoothed using a fifteen-point Savitsky-Golay smoothing function to reduce noise. In addition, a linear baseline correction between 1600 and 1700 cm^{-1} (amide I' band) was performed. The subtractions, smoothing and baseline corrections, were performed using the GRAMS/32 software (Galactic Industries Corporation, USA). From the OMNIC E.S.P. 5.1 software (Nicolet Instrument Corp., USA), the second derivatives, Fourier self-deconvolution (full width at half height FWHH = 20 cm^{-1} and enhancement factor K = 2.0) obtained the corrected spectra, in order to estimate the number and positions of the component bands of the amide I'. Based on these parameters, the Gaussian curve fitting was employed to the deconvoluted spectra in the range 1700 – 1600 cm^{-1}, using the software ORIGIN (OriginLab Corporation, USA). Following the methods described by Byler & Susi, for the curve fitting to amide I' band [2]. After identifying the individual bands with their representative second structures, the percentage of each second structure of HSA (free and complexed) was calculated by the area its band with respect to the total area of the amide I' band.

Band assignments for amide I' band

The band assignments that form the amide I' for HSA was characterized as follows: 1638 – 1615 cm^{-1} for β-sheet, 1654 – 1639 cm^{-1} for random structure, 1660 – 1642 cm^{-1} for α-helices and 1691 – 1653 cm^{-1} for turns in D_2O solution. According to the second derivative analysis of the amide I' band (see Fig. S7), for the ratios of 0:1 and 0.5:1 to ISO:HAS. The following secondary structures: 1628 and 1633 cm^{-1} for β-sheet, 1640 cm^{-1} for random, 1651 cm^{-1} for α-helix and 1671 and 1678 cm^{-1} for turns were assigned. For ratio of 1:1, the assignments were: 1628 and 1633 cm^{-1} for β-sheet, 1639 cm^{-1} for random, 1651 cm^{-1} for α-helix and 1671 and 1679 cm^{-1} for turns.

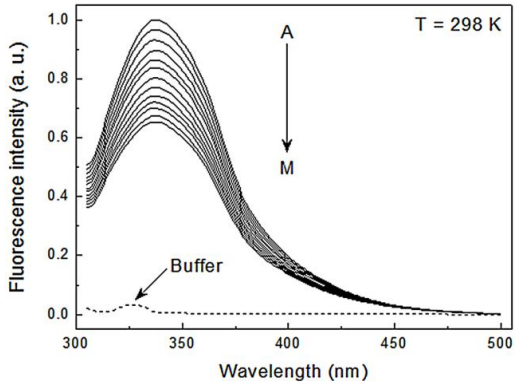

Fig. S1. Emission spectra of HSA obtained with the increments of the ISO concentration (pH 7.0, T = 298 K, λ_{ex} = 295 nm). [HSA] = 4.0 μM; [ISO] (μM), A – M: from 0 to 4.8 with the increments of 0.4. The dotted line corresponds to the buffer emission spectrum.

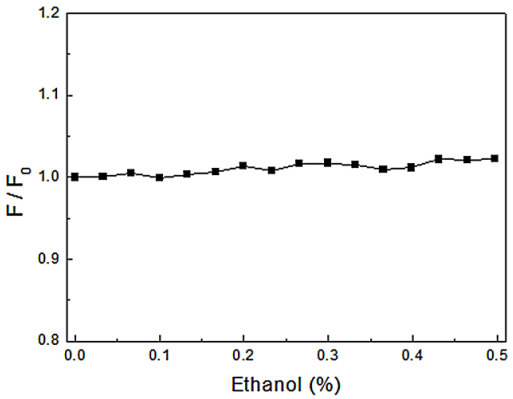

Fig. S2. Effect of ethanol on the fluorescence intensity of HSA (4.0 μM, pH 7.0, T = 298 K, λ_{ex} = 295 nm). Percentage of the ethanol volume in HSA solution varied from 0 to 0.5 with the increment of 3.33×10^{-2} %.

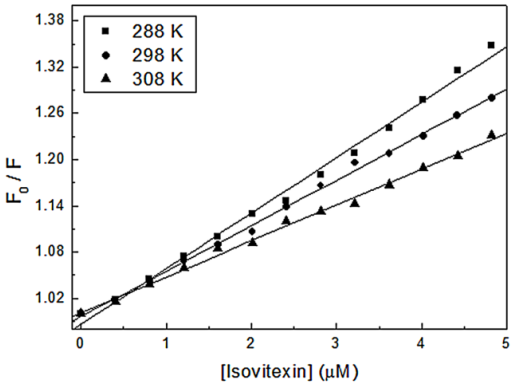

Fig. S3. Stern-Volmer plots for the fluorescence quenching of the HSA by Isovitexin at pH 7.0 and 288, 298 and 308 K.

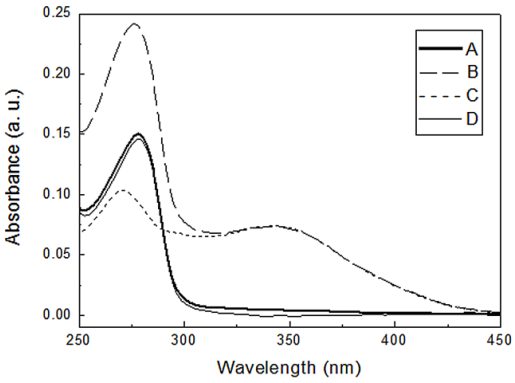

Fig. S4. UV-Vis absorption spectrum of free HSA (A), HSA-ISO complex (B), free ISO (C) and spectral subtraction between HSA-ISO complex and free ISO (D) at room temperature and pH 7.0. [HSA] = [ISO] = 4.0 μM.

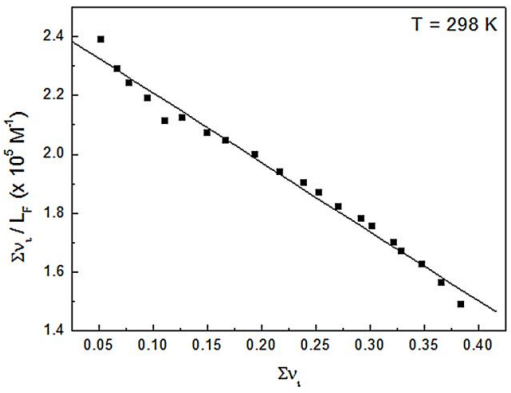

Fig. S5. Scatchard plot for the binding between Isovitexin and HSA generated from BDF method (pH 7.0 and 298 K).

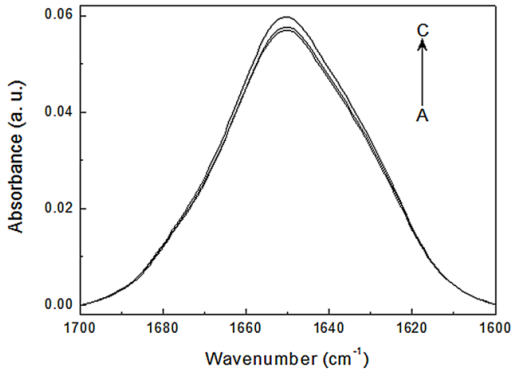

Fig. S6. FT-IR spectra of the amide I' band of HSA, in the absence and presence of ISO concentrations at pH 7.0 and room temperature. [HSA] = 20 mg/mL (0.3 mM); Isovitexin to HSA ratios: (A) 0:1, (B) 0.5:1 and (C) 1:1.

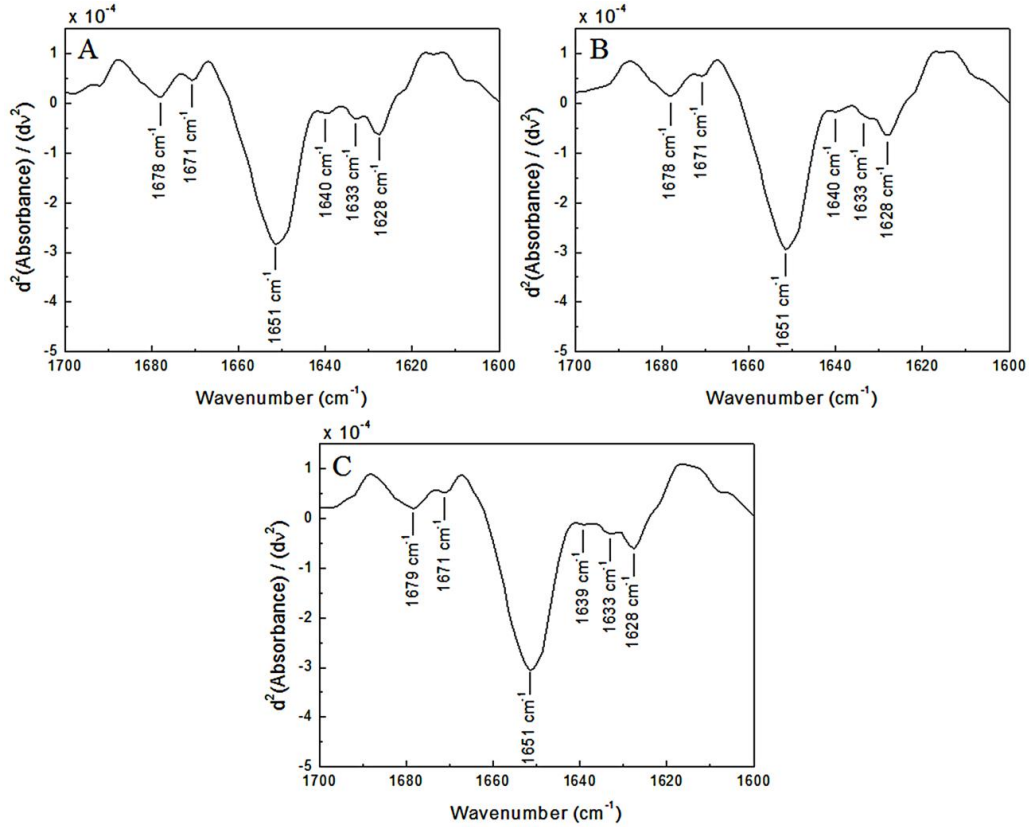

Fig. S7. Second derivate of amide I' band. Infrared spectra of the free HSA (A) and ISO/HSA molar ratios of 0.5:1 (B) and 1:1 (C) (pH 7.0 and room temperature).

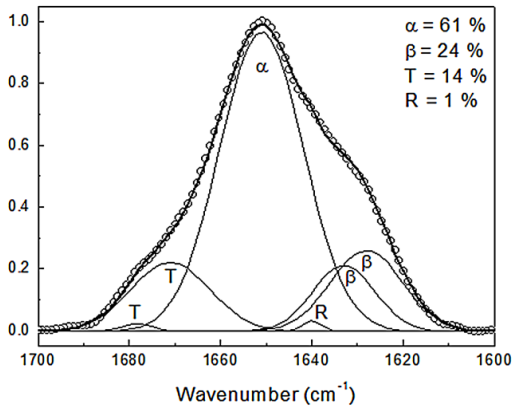

Fig. S8. Gaussians adjustment curves of the deconvoluted amide I' band for ISO to HSA ratios of 0.5:1, [HSA] = 20 mg/mL (0.3 mM). Gaussians adjustment curves are shown with thin lines (——) (α-helix, α; β-sheet, β; random structure, R; turn, T), summed up Gaussians curves shown with the thick line (——) and deconvoluted spectra shown with open circles (○). The correlation coefficient (R) and qui-squared (χ^2) for the adjustment were 0.999 and 4.0×10^{-5}, respectively.

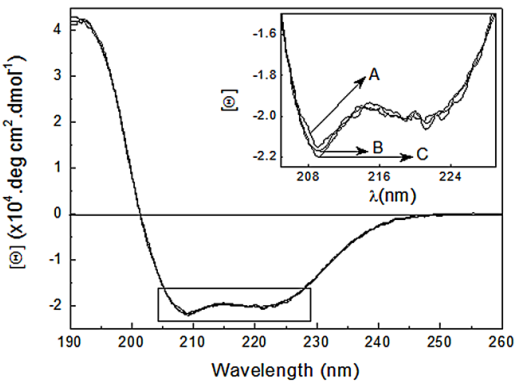

Fig. S9. CD spectra of HSA in the absence and presence of the flavonoid Isovitexin at pH 7.0, and room temperature. The insert corresponds to the detail of the peaks at 209 and 221 nm. [HSA] = 4.0 μM; Isovitexin to HSA ratios: (A) 0:1, (B) 0.5:1 and (C) 1:1.

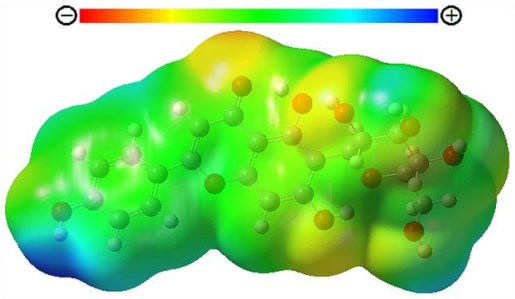

Fig. S10. Molecular electrostatic potential (MEP) map of Isovitexin molecule calculated using the DFT/B3LYP/6-311+G(d,p) method.

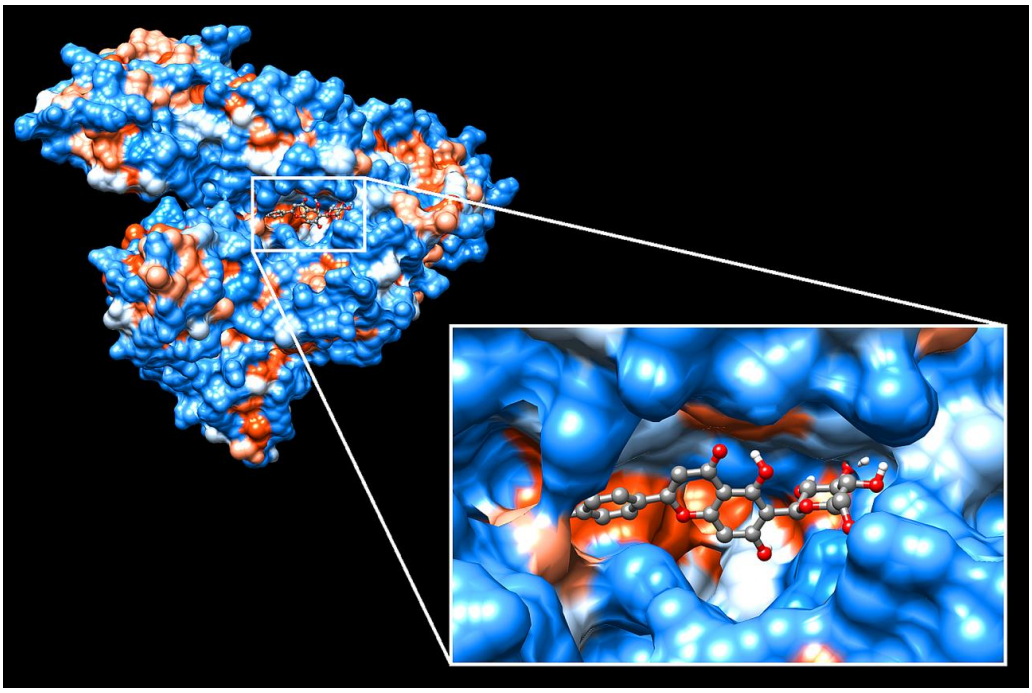

Fig. S11. Hydrophobicity surface of the HSA-ISO complex generated using Chimera 1.8 software. The blue color represents hydrophilic residue regions and the orange color, hydrophobic residue regions. In details the hydrophobic pocket region in subdomain IIA (site 1) of HSA. Isovitexin molecule is shown as sticks and balls model (C, gray; O, red; H, white).

Table S1
Some structure details of the optimized structure of Isovitexin at the DFT/B3LYP/6-311+G(d,p) method.

Bond distance (Å)	
O1 – C2	1.361
C2 – C3	1.360
C2 – C1’	1.469
C1’ – C2’	1.403
C5’’ – O5’’	1.434
C1’’ – C2’’	1.544
Bond angles (^{o})	
C2 – C1’ – C2’	120.691
C7 – C6 – C1’’	123.810
C5 – C6 – C1’’	118.198
C6 – C1’’ – O	108.296
Dihedral angles (^{o})	
O1 – C2 – C1’– C2’	16.087
C3 – C2 – C1’ – C2’	–163.297
C7 – C6 – C1’’ – O	28.599
C5 – C6 – C1’’ – O	– 153.014

Table S2
Experimental and theoretical absorbance wavelength $\lambda(nm)$, excitation energy $E(eV)$, absorbance $Abs(u.a.)$ and oscillator strength $f(u.a.)$ of Isovitexin in ethanol.

Experimental		TD-DFT/B3LYP/6-311+G(d,p)		
Ethanol		Ethanol (24.85)		
$\lambda(nm)$	$Abs(u.a.)$	$\lambda(nm)$	$E(eV)$	$f(u.a.)$
272	0.448	251	4.941	0.068
		255	4.865	0.002
		261	4.759	0.151
		264	4.696	0.175
		274	4.527	0.005
		291	4.257	0.009
		294	4.218	0.115
335	0.424	320	3.876	0.359
		346	3.585	0.456

Table S3

Change in accessible surface area (ΔASA in Å^2) of the residues involved in HSA-ISO complexation; ΔASA_{total} for all atoms, $\Delta ASA_{nonpolar}$ for all nonpolar atoms and ΔASA_{polar} for all polar atoms.

Residue	[a] ΔASA_{total}	$\Delta ASA_{nonpolar}$	ΔASA_{polar}
Ala191	17.92	14.99	2.93
Lys195	40.88	34.75	6.13
Trp214	15.09	15.07	0.02
Arg218	41.88	12.90	28.98
Asn295	23.28	1.14	22.15
Lys436	16.91	4.51	12.40
Pro447	24.53	22.75	1.75
Cys448	24.08	20.72	3.36
Asp451	25.84	21.87	3.97
Tyr452	30.09	29.64	0.45
Val455	15.90	15.90	0

[a] Only values > 10 Å^2 are reported.

References

[1] Y. N. Chirgadze, O. V. Fedorov, N. P. Trushina, Estimation of Amino Acid Residue Side-Chain Absorption in the Infared Spectra of Protein Solutions in Heavy Water, Biopolymers 14 (1975) 679-694.

[2] D. M. Byler, H. Susi, Examination of the Secondary Structure of Protein by Deconvolved FTIR Spectra, Biopolymers 25 (1986) 469-487.

Anexo III - Artigo publicado na *Food Chemistry*

Food Chemistry 196 (2016) 935–942

Contents lists available at ScienceDirect

Food Chemistry

journal homepage: www.elsevier.com/locate/foodchem

An integrated approach with experimental and computational tools outlining the cooperative binding between 2-phenylchromone and human serum albumin

Ícaro Putinhon Caruso [a,b], José Maria Barbosa Filho [c], Alexandre Suman de Araújo [b], Fátima Pereira de Souza [a,b], Marcelo Andrés Fossey [a,b], Marinônio Lopes Cornélio [a,b,*]

[a] Departamento de Física, Instituto de Biociências, Letras e Ciências Exatas (IBILCE), UNESP, Rua Cristovão Colombo 2265, CEP 15054-000 São José do Rio Preto, SP, Brazil
[b] Centro Multiusuário de Inovação Biomolecular (CMIB), Instituto de Biociências, Letras e Ciências Exatas (IBILCE), UNESP, Rua Cristovão Colombo 2265, CEP 15054-000 São José do Rio Preto, SP, Brazil
[c] Laboratório de Tecnologia Famacêutica (LTF), UFPB, Cidade Universitária, CEP 58051-900 João Pessoa, PB, Brazil

ARTICLE INFO

Article history:
Received 17 April 2015
Received in revised form 1 September 2015
Accepted 7 October 2015
Available online 9 October 2015

Keywords:
2-Phenylchromone
Human serum albumin
Fluorescence spectroscopy
Binding density function
Cooperative binding
Computational methods

ABSTRACT

2-Phenylchromone (2PHE) is a flavone, found in cereals and herbs, indispensable in the human diet. Its chemical structure is the basis of all flavonoids present in black and green tea, soybean, red fruits and so on. Although offering such nutritional value, it still requires a molecular approach to understand its interactions with a specific target. The combination of experimental and computational techniques makes it possible to describe the interaction between 2PHE and human serum albumin (HSA). Fluorescence spectroscopy results show that the quenching mechanism is static, and thermodynamic analysis points to an entropically driven complex. The binding density function method provides information about a positive cooperative interaction, while drug displacement experiments indicate Sites 1 and 2 of HSA as the most probable binding sites. From the molecular dynamic study, it appears that the molecular docking is in agreement with experimental data and thus more realistic.

1. Introduction

Flavonoids are polyphenolic secondary metabolites that are widely distributed in higher plants and are ingested by humans in their food (Bravo, 1998). They have attracted considerable attention in the scientific community, owing to a biological and physiological interest. The literature shows that flavonoids can present antioxidant, anticancer, antiviral, anti-inflammatory and heart disease protective activities (Grotewold, 2006). Flavones are one of the major classes of flavonoids, and are mainly found in cereals and herbs (Bravo, 1998). 2-Phenylchromone (2PHE) is a flavone which has the basic structure of all flavonoids, as shown in Fig. 1a. In addition to its antioxidant activity, 2PHE also exhibits the inhibitory property of estrogen without binding to the estrogen receptor, but acting as a competitive agonist for the aryl hydrocarbon receptor, which means that it is anti-estrogenic flavonoid (Jung, Ishida, Nishikawa, & Nishihara, 2007). 2PHE present in *Primula macrophylla* (Primulaceae) is the major compound responsible for the antileishmanial activity of the plant (Najmus-Saqib, Alam, & Ahmad, 2009).

Human serum albumin (HSA) is the main extracellular protein, and is highly concentrated, in blood plasma. HSA is a monomeric globular protein composed of three structurally similar domains (I, II and III), each containing two subdomains (A and B). Aromatic and heterocyclic ligands bind to HSA primarily within two hydrophobic pockets in subdomains IIA and IIIA, namely Sites 1 and 2, respectively. Site 1 is the primary binding site for drugs like warfarin and phenylbutazone analogs, whereas diazepam and ibuprofen are bound primarily to Site 2 (Peters, 1996). Studies have indicated that the subdomain IB can also be a binding site for compounds such as bilirubin, hemin and methyl orange. Subdomain IB has been called Site 3 (Zsila, 2013). The exceptional capacity of HSA to interact with several organic and inorganic molecules turns this protein into an important regulator of intercellular fluxes and the main carrier for many drugs to different molecular targets. Up until now most of the studies with several kinds of flavonoids (Caruso, Vilegas, Fossey, & Cornélio, 2012; Caruso, Vilegas, Souza, Fossey,

* Corresponding author at: Departamento de Física, Instituto de Biociências, Letras e Ciências Exatas (IBILCE), UNESP, Rua Cristovão Colombo 2265, CEP 15054-000 São José do Rio Preto, SP, Brazil.
E-mail addresses: ykrocaruso@hotmail.com (Í.P Caruso), jbarbosa@ltf.ufpb.br (J.M.B. Filho), asaraujo@ibilce.unesp.br (A.S. de Araújo), fatima@ibilce.unesp.br (F.P. de Souza), marcelo@ibilce.unesp.br (M.A. Fossey), mario@ibilce.unesp.br (M.L. Cornélio).

http://dx.doi.org/10.1016/j.foodchem.2015.10.027
0308-8146/

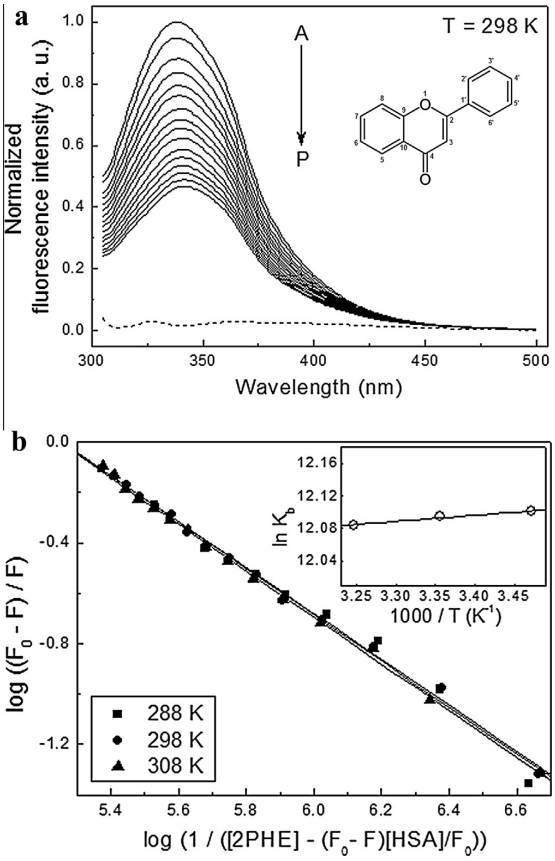

Fig. 1. (a) Emission spectra of HSA obtained with the increments of the 2PHE concentration (pH 7.0, T = 298 K, λ_{ex} = 295 nm). [HSA] = 4.0 μM; [2PHE] (μM), A–P: from 0 to 6.0 with the increments of 0.4. The dotted line corresponds to the emission spectrum of 2PHE in phosphate buffer (6.0 μM). The insert corresponds to the chemical structure of 2-phenylchromone. (b) Double-log plots for the fluorescence quenching of HSA by 2PHE at pH 7.0 and 288, 298 and 308 K. The insert corresponds to the van't Hoff plot for the HSA–2PHE complex.

& Cornélio, 2014; Peters, 1996; Sinisi, Forzato, Cefarin, Navarini, & Berti, 2015; Wu, Yan, Wang, Wang, & Li, 2015) investigating the mechanism of interaction have identified a single binding site. Therefore, a more detailed study of the microenvironment of the binding sites of HSA is important in order to achieve a better comprehension of this mechanism.

This paper presents a broad and detailed study on the interaction between the polyphenolic compound considered to be the basic structure of flavonoids (2PHE) and the principal carrier protein in human blood plasma (HSA). The formation of the HSA–2PHE complex was investigated using spectroscopy methods including fluorescence spectroscopy, UV–Vis absorbance, circular dichroism (CD), and computational methods like *ab initio*, molecular dynamic and docking calculations. In particular, this work also made use of the binding density function (BDF) method for data analysis of fluorescence quenching, which is very sparsely explored in the study of protein–ligand interactions. This data set may contribute scientifically to a better understanding of the interaction mechanisms involved in the formation of the protein–flavonoid complex, and the distribution and transportation of flavonoids, which is an important research field in food chemistry.

2. Materials and methods

2.1. Materials and solutions

Human serum albumin fraction V, 2-phenylchromone, warfarin, ibuprofen, methyl orange, dibasic sodium phosphate, citric acid, ethanol and sodium chloride (NaCl) were purchased from Sigma Chemical Co. All other chemicals were of analytical reagent grade and Milli-Q ultrapure water was used throughout the experiments. HSA was dissolved in a phosphate buffer solution of 50 mM at pH 7.0, and adjusted with citric acid, containing 0.15 M of NaCl. The stock solution of 2PHE was prepared in absolute ethanol. The concentrations of the stock solutions of HSA and 2PHE were determined spectroscopically using the molar extinction coefficient of 36,500 and 25,100 $M^{-1}cm^{-1}$ at 280 and 294 nm, respectively. Aliquots of 2PHE applied in the following experiments were carefully evaluated to avoid aggregation of the flavonoid (Pohjala & Tammela, 2012).

2.2. UV–Vis absorbance spectroscopy

UV–Vis absorption spectrum was recorded at room temperature (298 K), controlled by air conditioning and monitored by a thermometer, on a Cary-3E spectrophotometer (Varian, Palo Alto, CA) equipped with a quartz cell with 1.0 cm optical path length. UV–Vis absorption spectra were recorded in the 250–500 nm range, with an integration time of 0.333 s and a spectral bandwidth of 2.0 nm.

2.3. Fluorescence spectroscopy

The fluorescence measurements were performed using an ISS PC1 steady-state spectrofluorimeter (Champaign, IL, USA) equipped with a quartz cell with 1.0 cm optical path length and a Neslab RTE-221 thermostat bath. Both excitation and emission bandwidths were set at 8.0 nm. The excitation wavelength of 295 nm was chosen since it provides no excitation of tyrosine residues, but excites the single tryptophan residue (Trp214) of HSA (Lakowicz, 1999). The emission spectrum was collected in the range of 305–500 nm with increments of 1.0 nm, which was corrected for the background fluorescence of the buffer and for inner filter effects (Borissevitch, 1999). Each point in the emission spectrum is the average of 10 accumulations. In the fluorescence quenching experiments, titrations were performed by adding small aliquots from the 2PHE stock solution to the HSA solution (3.0 ml) at constant concentrations of 1.0, 2.0 and 4.0 μM. In experiments for Stern–Volmer and binding equilibria analysis, the HSA concentration remained constant at 4.0 μM, and the 2PHE concentration varied from 0 to 6.0 μM with increments of 0.4 μM at 288, 298 and 308 K. For the binding density function (BDF) method, the titration was performed at HSA constant concentrations of 1.0, 2.0 and 4.0 μM, and the 2PHE concentration varied from 0 to 2.8, 3.6 and 6.0 μM, respectively, at 298 K. The effect of ethanol as a co-solvent was verified by adding small aliquots to the HSA solution (4.0 μM at 3.0 ml, 298 K) within the volume changes of the previous titrations. In all experiments, the final volume of ethanol in the buffer was <1%.

2.4. Drug displacement experiment

Site-specific marker displacement experiments were carried out by titrating complexes of HSA (4.0 μM at 298 K) with warfarin, ibuprofen and methyl orange at molar ratios of 1:0 and 1:1, with the 2PHE concentration increasing from 0 to 8.0 μM in increments of 1.0 μM. Warfarin, ibuprofen and methyl orange are site-specific

markers that bind to HSA at subdomain IIA (Site 1), IIIA (Site 2) and IB (Site 3), respectively (Peters, 1996; Zsila, 2013). The fluorescence quenching experiments of HSA by 2PHE in the absence and presence of site-specific markers were performed using the same method in the previous section (Section 2.3).

2.5. UV circular dichroism spectroscopy

UV CD spectra were recorded at room temperature on a Jasco J-710 spectropolarimeter equipped with a demountable quartz cell with a 0.01 cm optical path length, model DRC-H (Jasco, USA). The UV CD spectra were recorded in the 190–260 nm range with a scan rate 20 nm/min and a spectral resolution of 0.1 nm. For each spectrum 10 accumulations were performed. The HSA concentration remained constant throughout the experiment at 4.0 μM, while the 2PHE to HSA ratios were 0:1, 1:1 and 2:1. The contribution of the CD spectrum to the buffer and the 2PHE was subtracted from free and complexed HSA. All CD spectra were taken as millidegrees (θ) and subsequently expressed in terms of mean residue ellipticity (MRE or [Θ]) in deg cm^2 dmol^{-1} using the following equation:

$$[\Theta] = \theta(m\,\mathrm{deg})/(10\,[P]\,l\,n) \quad (1)$$

where [P] is the molar concentration of the protein (HSA), n is the quantity of amino acid residues (585), and l is the optical path length (cm). Secondary structures were estimated with CONTINLL software from the CDPro package, using the reference set of proteins SMP56 (Sreerama & Woody, 2000). The effect of ethanol as a co-solvent was verified by adding an aliquot to the HSA solution (4.0 μM at 3.0 ml, 298 K) within the volume change of the last titration. In all experiments, the final volume of ethanol in the buffer was <1%.

2.6. Ab initio calculation

The Gaussian 09 program (Frisch et al., 2009) provided by the Núcleo de Computação Científica da Universidade Estadual Paulista (NCC/GridUNESP) was applied to the calculation of the 2PHE structure. The optimized geometry calculated at the gas phase with the 2PHE molecule isolated by the DFT/B3LYP/6-311++G(2d,p) method. The next step, the vibrational frequency calculation, was performed to check the optimized 2PHE molecule. The TD-DFT/B3LYP/6-311+G(d,p) calculation was performed with the optimized 2PHE, taking into account all excitations from the 9 highest occupied molecular orbitals (HOMOs) to the 9 lowest unoccupied molecular orbitals (LUMOs). The solvent effect in ethanol was verified using the PCM calculation (Mennucci, Cancès, & Tomasi, 1997). The molecular electrostatic potential (MEP) map was calculated to investigate the distribution of charge density on the molecular surface of 2PHE.

2.7. Molecular dynamic calculation

All the molecular dynamic (MD) simulations were performed with the NAMD 2.9 program (Phillips et al., 2005). The molecular system was modeled with the CHARMM36 force field (Best et al., 2012) and TIP3P water model (Jorgensen, Chandrasekhar, Madura, Impey, & Klein, 1983). The crystal structure of HSA at a 2.5 Å resolution (PDB-ID: 1AO6) (Sugio, Kashima, Mochikuzi, Noda, & Kobayashi, 1999) was placed in the center of a 100 Å cubic box solvated by a solution of 0.15 M of NaCl in water, and the protonation state of ionizable residues was set considering a neutral pH (pH = 7.0). Periodic boundary conditions were used and all simulations were performed in NPT ensemble. The temperature was kept constant at 298 K using Langevin dynamics with a damping coefficient of 1 ps^{-1}. The pressure was maintained at 1 atm by a Nose–Hoover Langevin piston, with a piston period of 200 fs, a damping time scale of 100 fs and a barostat noise temperature of 298 K. The cutoff for small-range interactions was set to 12 Å, with a switch distance of 10 Å and a pair list distance of 14 Å. The long-range electrostatic interactions were calculated using the particle mesh Ewald (PME) algorithm. In every MD simulation a time step of 2 fs was used and all covalent bonds involving hydrogen atoms were constrained to their equilibrium distance. A conjugate gradient minimization algorithm was utilized to relax the superposition of atoms generated in the box construction process. A subsequent 2 ns equilibration MD simulation was performed, where the protein backbone atoms were restrained with 10 kcal/mol Å^2. Finally, a 50 ns MD simulation was performed for data acquisition. Following the simulations, the tool *g_cluster* from the GROMACS package (Pronk et al., 2013) was used to perform a cluster analysis in 2500 conformations of albumin, taken at intervals of 20 ps from the 50 ns trajectory. The gromos algorithm (Daura et al., 1999), using a cutoff of 2 Å, was used to generate the clusters. The RMSD was calculated between all the structures and superimposed considering only non-hydrogen atoms.

2.8. Molecular modeling calculation

The HSA structures used in the molecular modeling calculations were obtained from the cluster analysis performed by the molecular dynamic simulations. The three-dimensional structure of the 2PHE molecule was obtained from the Gaussian 09 program (Frisch et al., 2009). AutoDockTools (ADT) (Sanner, 1999) was used to prepare the HSA and 2PHE by merging non-polar hydrogen atoms, adding partial charges and atom types. The ligand rigid root was generated automatically, setting all possible rotatable bonds defined as active by torsions (2PHE has 1 torsion). Grid maps were generated with 0.375 Å spacing and the dimensions of 60 × 60 × 60 points by the AutoGrid 4.2 program (Morris et al., 1998). These maps were centered on Sites 1 and 2 of the HSA structures. The AutoDock 4.2 program (Morris et al., 1998) was employed to study the binding site between 2PHE and HSA by applying the Lamarckian Genetic Algorithm (LGA) for minimization where the number of energy evaluations was 2.5 million, population size was 150 and root-square-mean deviation (RMSD) tolerance for cluster analysis was 2.0 Å. Random starting positions on the entire protein surface and random orientations were used for the ligand (2PHE). For each docking simulation, 100 different conformers were generated. The structural representation was prepared using PyMOL (Delano, 2002) and the map of interaction was calculated using LigPlot (Wallace, Laskowski, & Thomton, 1995).

2.9. Accessible surface area calculations

The accessible surface area (ASA) of uncomplexed HSA and its docked complexes with 2PHE were calculated using the NACCESS program (Hubbard & Thornton, 1993). The HSA–2PHE complex structures were obtained from the best molecular modeling structure and changes in absolute ASA for residue i were calculated using the following equation:

$$\Delta\mathrm{ASA}^i = \mathrm{ASA}^i_{\mathrm{uncomplexed}} - \mathrm{ASA}^i_{\mathrm{complexed}} \quad (2)$$

where $\mathrm{ASA}^i_{\mathrm{uncomplexed}}$ and $\mathrm{ASA}^i_{\mathrm{complexed}}$ is the absolute accessible surface area for free and complexed HSA residues, respectively. If one residue loses more than 10 Å^2 of absolute ASA going from the uncomplexed to the complexed state, it is considered to be involved in the interaction.

3. Results and discussions

3.1. Fluorescence quenching process of HSA by 2-phenylchromone

The fluorescence quenching process can occur when the intensity of the fluorescence signal decreases. Various molecular interactions may result in quenching, among them reactions with the excited state, molecular rearrangement, energy transfer, ground state complex formation and collisional quenching. These different mechanisms are usually classified as either dynamic or static. In addition, quenching mechanisms can be distinguished by their dependence on temperature and viscosity, or preferably by measuring the fluorescence lifetime. Higher temperatures result in faster diffusion and therefore a larger extension of collisional quenching. But higher temperatures also imply a dissociation of the weakly bound complex, leading to a less static quenching process (Lakowicz, 1999). The fluorescence intensity of the HSA decreased with an increasing 2PHE concentration (Fig. 1a), indicating that the microenvironment of the single tryptophan residue (Trp214) of the HSA is affected by the presence of the 2PHE. The effect of ethanol on the fluorescence intensity of HSA is negligible (Supplementary material, Fig. S1).

Data analysis regarding the fluorescence quenching process was performed by applying the Stern–Volmer equation (Lakowicz, 1999):

$$F_0/F = 1 + K_q\tau_0[Q] = 1 + K_{SV}[Q] \quad (3)$$

where F_0 and F are the steady-state fluorescence intensities in the absence and presence of a quencher (Q), respectively. K_q is the bimolecular quenching constant, τ_0 is the fluorophore lifetime in the absence of quencher, whose value for HSA is 10^{-8} s (Lakowicz, 1999), [Q] is the quencher concentration and K_{SV} is the Stern–Volmer quenching constant. In the investigated concentration range, the results of fluorescence quenching at 288, 298 and 308 K are in accordance with the Stern–Volmer equation (Supplementary material, Fig. S2).

The results in Table 1 show that the Stern–Volmer constant values are very close ($1.3 \times 10^5\ M^{-1}$) even with the temperature increment, such that the K_{SV} constants were temperature independent. Thus, evaluations of the K_q constants and the absorption spectrum of the fluorophore were performed to elucidate the quenching mechanism involved in the HSA–2PHE interaction. The bimolecular quenching constant values that were calculated by Eq. (3) are greater than $2.0 \times 10^{10}\ M^{-1}\ s^{-1}$, which represents the maximum diffusion collision rate for various quenchers with biopolymers. In addition, the absorption spectrum of the HSA presented changes in the presence of 2PHE (Supplementary material, Fig. S3). Consequently, the quenching mechanism of the HSA–2PHE interaction should follow the static process (ground state complex) (Lakowicz, 1999).

3.2. Analysis of binding equilibria

For the static quenching mechanism, the binding constant (K_b) and the number of binding sites (n) can be calculated using the following equation (Bi et al., 2004):

$$\log(F_0 - F)/F = n \log K_b - n \log(1/([D_0] - (F_0 - F)[P_0]/F)) \quad (4)$$

where $[D_0]$ and $[P_0]$ are the drug (2PHE) and protein (HSA) total concentration, respectively.

Fig. 1b shows the binding equilibrium plots for the fluorescence quenching of HSA by 2PHE at 288, 298 and 308 K. The dependence of $\log[(F_0 - F)/F]$ on the value of $\log(1/([D_0] - (F_0 - F)[P_0]/F))$ is linear, with a slope equal to the value of n and the value $n \log K_b$ fixed on the ordinate. For the HSA–2PHE complex, and n values at 288, 298 and 308 K are shown in Table 1. It was observed that the number of binding sites of the complex is approximately equal to 1.0. Neither K_b values nor values had relevant changes with increasing temperature.

Table 1
Stern–Volmer quenching constant (K_{SV}), bimolecular quenching constant (K_q), binding constant (K_b), and binding site numbers (n) of the interaction between HSA and 2PHE at pH 7.0 and 288, 298 and 308 K.

T (K)	K_{SV} ($\times 10^5\ M^{-1}$)	K_q ($\times 10^{14}\ M^{-1}\ s^{-1}$)	K_b ($\times 10^5\ M^{-1}$)	n
288	1.29	1.29	1.80	0.92
298	1.31	1.31	1.79	0.91
308	1.31	1.31	1.77	0.93

The correlation coefficient is $\geqslant 0.995$.

3.3. Thermodynamic analysis

The driving forces responsible for the interaction between HSA and 2PHE were calculated using the van't Hoff equation:

$$\ln K_b = -\frac{\Delta H^\circ}{RT} + \frac{\Delta S^\circ}{R} \quad (5)$$

where ΔH° is the enthalpy change, ΔS° is the entropy change, R is the universal gas constant and is the binding constant at the correspondent temperature (T). Table 2 shows ΔH° and ΔS° values obtained through the slope and the ordinate of the van't Hoff relationship (insert Fig. 1b), with the respective values of Gibbs free energy changes (ΔG°) as calculated with the Eqs. (5) and (6) in the temperature range of 288–308 K:

$$\Delta G^\circ = \Delta H^\circ - T\Delta S^\circ \quad (6)$$

The values of $\Delta G^\circ < 0$ indicated that the interaction process is spontaneous. For the HSA–2PHE complex, the results of thermodynamic analysis showed that ΔH° is very small and $\Delta S^\circ > 0$. The favorable entropic term ($-T\Delta S^\circ$) provided the major contribution for ΔG°, characterizing an entropically driven reaction. The present results therefore indicate that the forces which motivate the binding can be classified as a classical hydrophobic interaction (Kauzmann, 1959; Nemethy & Scheraga, 1962; Tanford, 1973), verified elsewhere for the interaction between HSA and porphyrins (Rotenberg, Cohen, & Margalit, 1987). The hydrophobic contribution may be a keystone in the interaction between HSA and 2PHE. In the meantime, it is not the only intermolecular interaction which contributes to complex stability, and it is also necessary to consider the electrostatic contribution (Ross & Subramanian, 1981).

3.4. Binding density function method

The thermodynamic basis for the binding density function (BDF) method is that the distribution of bound ligands per macromolecule in i different states (Σv_i) is strictly determined at equilibrium by the free ligand concentrations (L_F). Thus, if L_F is the same for two (or more) solutions at different total macromolecule concentrations (M_T), then Σv_i will also be the same in each solution. As a result, constant values of L_F and Σv_i will exist for a number

Table 2
Thermodynamic parameters of the HSA–2PHE complex at pH 7.0 and 288, 298 and 308 K.

T (K)	ΔH° (kJ mol^{-1})	ΔG° (kJ mol^{-1})	ΔS° (J mol^{-1} K^{-1})	R
288	−0.6	−28.9	98.4	
298		−29.9		0.978
308		−30.9		

R is the correlation coefficient.

of different combinations of total ligand (L_T) and total macromolecule (M_T) concentrations, which satisfy the mass conservation equation (Lohman & Bujalowski, 1991):

$$L_T = L_F + (\Sigma \nu_i) M_T \quad (7)$$

Considering the general relationship between the concentration of each macromolecule species with i bound ligands and the experimentally observed signal (S_{obs}) from the macromolecule, the fractional signal molar changes (ΔS_{obs}) observed in the presence of L_T and M_T will be given by:

$$\Delta S_{obs} = (S_{obs} - S_F M_T)/S_F M_T \quad (8)$$

where $S_F M_T$ is the observed signal for a free macromolecule in the absence of a ligand (F_0, see Section 3.1). Thus, for fluorescence quenching, experiments have to be $\Delta S_{obs} = (F - F_0)/F_0$ (Lohman & Bujalowski, 1991). A horizontal line was drawn intersecting the three titration curves in Fig. 2a, defining a constant value of ΔS_{obs} and three sets of (L_{Tx}; M_{Tx}) (x = 1, 2 and 3) for which L_F and $\Sigma \nu_i$ were constants (see insert in Fig. 2a).

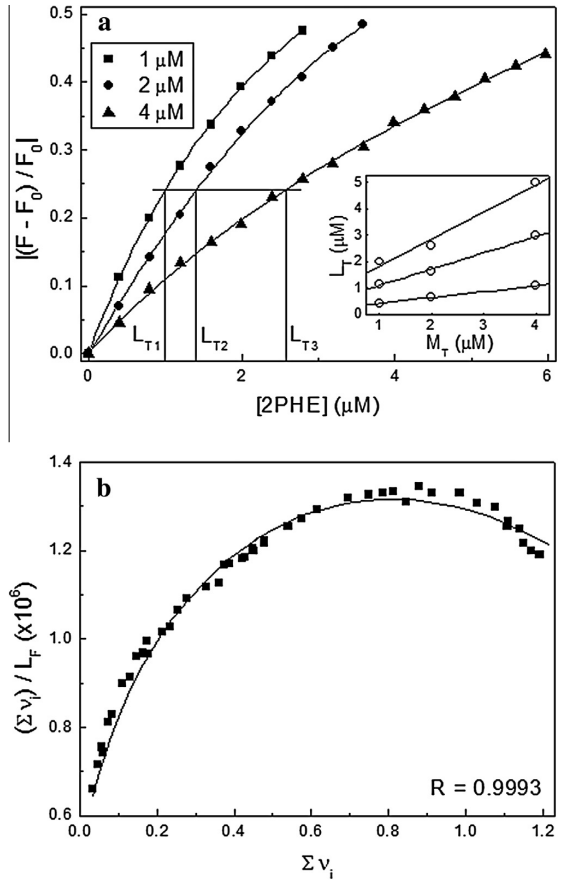

Fig. 2. (a) Titrations of 2PHE in HSA solutions, as monitored by fluorescence quenching of the Trp214 residue in HSA for three different protein concentrations at pH 7.0 and 298 K. L_{T1}, L_{T2} and L_{T3} represent the total ligand concentrations for the constant fractional signal molar change value of three different total protein concentrations (M_{T1}, M_{T2} and M_{T3}). The insert corresponds to only three sets of concentration pairs (L_T; M_T) to exemplify the utilization of Eq. (7) obtaining $\Sigma \nu_i$ and L_F values. (b) Scatchard plot for the binding between 2PHE and HSA generated from BDF method. The solid line shows fit of the experimental data using Eq. (11) and R is the correlation coefficient.

From the L_F and $\Sigma \nu_i$ values obtained from Eq. (7), the Scatchard plot for the binding between HSA and 2PHE can be built without the use of any binding model *a priori*. The Scatchard plot showed a downward curvature (Fig. 2b), indicating that the HSA–2PHE complex presents a positive cooperativity, which means that the binding at the first site enhances the affinity of the second one. The interaction between HSA and 2PHE was fitted using a global binding model in which the macromolecule contains two binding sites for a ligand. The reaction mechanism for this binding model can be described as follows (Di Cera, 1995):

$$M + L \overset{k_1}{\Longleftrightarrow} ML \quad (9)$$

$$ML + L \overset{k_2}{\Longleftrightarrow} ML_2 \quad (10)$$

where k_1 and k_2 are stepwise binding constants, which can be obtained from the following equation:

$$\sum \nu_i = \left(2k_1 L_F + 2k_1 k_2 L_F^2\right) / \left(1 + 2k_1 L_F + k_1 k_2 L_F^2\right) \quad (11)$$

The obtained values for k_1 and k_2 were 2.42×10^5 and $6.90 \times 10^6\ M^{-1}$, respectively. The k_1 value is in accordance with the results obtained from the analysis of binding equilibria (Section 3.2). The discrepancy between the number of binding sites found by BDF and binding equilibria analysis may be due to inherent constraints in the last model, according to Eq. (4). The Hill coefficient calculated using $n_H = 2/(1 + \sqrt{k_1/k_2})$ was 1.68, indicating that the interaction between HSA and 2PHE exhibits a positive cooperative as previously mentioned. The maximum binding capacity curve of HSA presented a corresponding 2PHE concentration of 0.76 μM (Supplementary material, Fig. S4).

3.5. Identification of the binding sites of 2-phenylchromone on HSA by drug displacement

The determination of the binding site location of 2PHE on HSA was performed using the competitive binding assay between 2PHE and specific site markers, namely, warfarin (WAR), ibuprofen (IBU) and methyl orange (MTO) for Sites 1, 2 and 3, respectively (Peters, 1996; Zsila, 2013). To probe the binding site of 2PHE on HSA, the fluorescence quenching rate (F/F_0) in the absence and presence of markers was compared, and are presented in Fig. 3. The quenching rate for 2PHE decreased in the presence of WAR (Site 1 marker), increased in the presence of IBU (Site 2 marker)

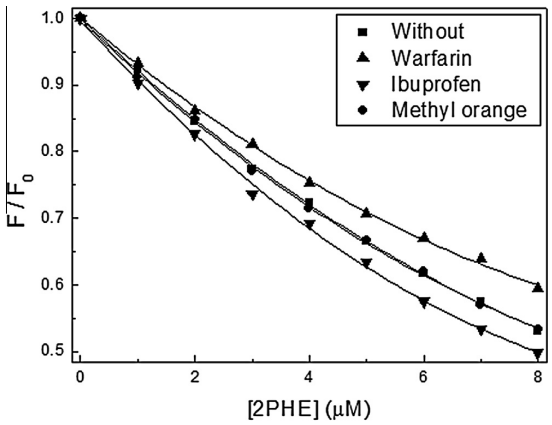

Fig. 3. Fluorescence quenching rates of HSA by 2PHE in the absence and presence of specific site markers (warfarin, ibuprofen or methyl orange). [HSA] = [Marker] = 4.0 μM, pH 7.0, T = 298 K, and λ_{ex} = 295 nm.

and remained the same in the presence of MTO (Site 3 marker), when compared with the quenching rate for 2PHE with no marker. The results suggest that 2PHE binds to Site 1 and Site 2 of HSA, which are located in subdomain IIA and IIIA, respectively. The identification of the two binding sites for 2PHE on HSA corroborates the result obtained by the BDF method (Section 3.4).

3.6. Ab initio calculation

The optimization and vibrational calculation performed for the 2PHE with the DFT/B3LYP/6-311++G(2d,p) method showed that the optimized structure is stable (global minimum on the potential energy surface) since no imaginary frequency was obtained. Some calculated bond distances, bond angles, and dihedral angles are presented in Table S1 of Supplementary material. The results of the TD-DFT calculation were in agreement with the experimental UV–Vis absorbance data (Supplementary material, Table S2), since the maximum experimental UV–Vis absorbance corresponds to the vertical transition according to the Franck–Condon principle. The results of *ab initio* calculations for 2PHE were therefore consistent with the experimental data.

From the MEP of 2PHE (Supplementary material, Fig. S7) it was possible to detect the existence of a neutral charge distribution on the planar faces of the rings of the molecule. A dense distribution of negative charges can also be seen near the O4 oxygen atom, while a slightly positive electrostatic potential is localized close to all the hydrogen atoms in the flavonoid.

3.7. Molecular dynamic and molecular modeling calculations

Molecular modeling results are highly modulated by the receptor structure used because, typically, this structure is kept rigid

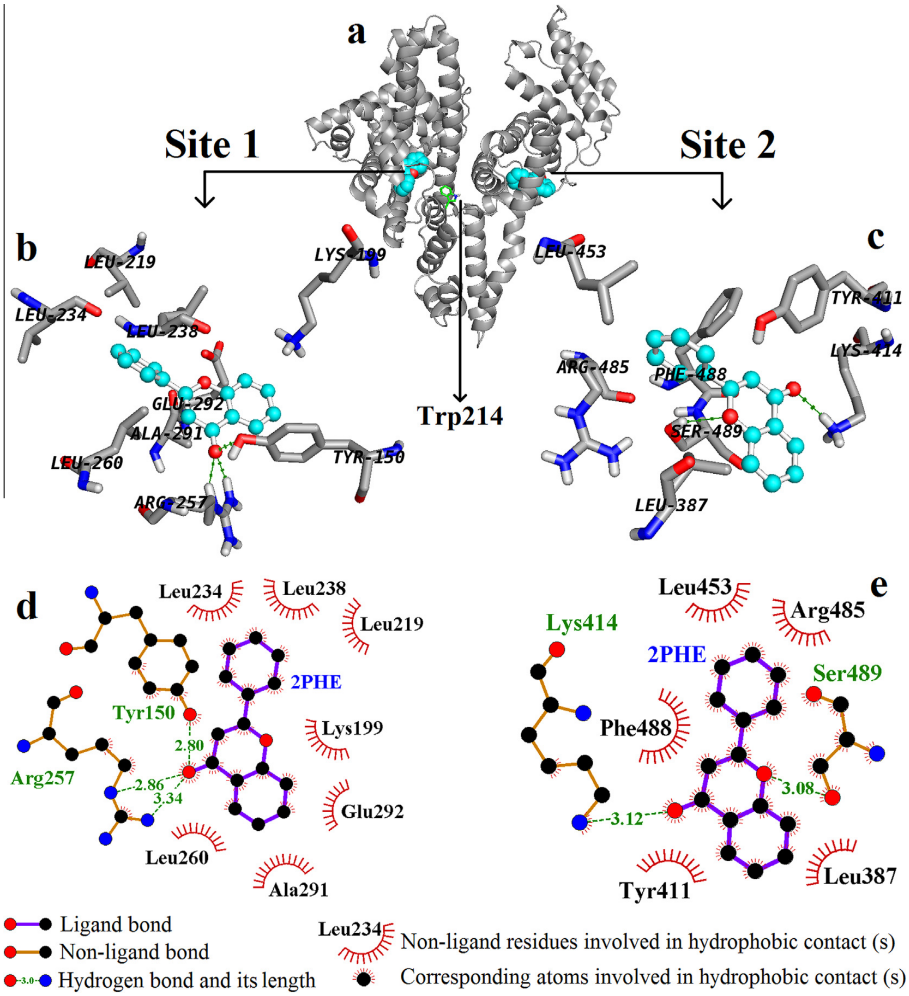

Fig. 4. (a) Location of the 2PHE molecules in the subdomain IIA (Site 1) and IIIA (Site 2) of the fourth cluster of HSA, close to the single tryptophan residue (Trp214). The protein is shown as a cartoon and 2PHE molecules as spheres. Three-dimensional structural detail of the microenvironment interaction of 2PHE with (b) Site 1 and (c) Site 2 of HSA obtained by molecular modeling calculations. 2PHE molecules are shown as stick and ball models, the amino acid residues are denoted as stick models (C, gray; O, red; N, blue; H, white), and the hydrogen bonds depicted by green dotted line. Two-dimensional representation of the interaction maps between 2PHE and residues of (d) Site 1 and (e) Site 2 of HSA. The structural representation was prepared using PyMOL (Delano, 2002) and the map of interactions was calculated using LigPlot (Wallace et al., 1995). (For interpretation of the references to color in this figure legend, the reader is referred to the web version of this article.)

during the calculations. Thus, the direct use of crystallographic structures in these calculations can generate spurious results since the solid state chemical environment does not match the physiological one, and this reflects in the protein structure, particularly on the conformation of the side-chains. To avoid these, molecular dynamic simulations of crystallographic HSA structure in an aqueous solution with physiological ionic strength (NaCl 150 mM) and pH = 7.0, were performed to generate the receptor conformations to be used in the molecular docking calculations. These structures were acquired from the obtained trajectory by cluster analysis. This procedure generated six clusters, and the most representative conformation of each was used in molecular docking calculations to study the interaction of the 2PHE with Sites 1 and 2 of HSA, based upon the drug displacement experiments (Section 3.5.). The best theoretical binding energies (ΔG_B) for the Sites 1 and 2 of the six HSA clusters were calculated, as well as their corresponding theoretical binding constants (K_B), determined by $K_B = \exp(-\Delta G_B/RT)$ (Supplementary material, Table S3). Among the six HSA clusters, the fourth cluster presented a theoretical binding energy and constant values (Table S3) in agreement with the binding equilibria analysis (K_b, Section 3.2.) and binding density function method (K_a, Section 3.4.).

Fig. 4 summarizes the interaction between human serum albumin and 2PHE from three different perspectives. At the top, Fig. 4a shows the tertiary structure of the protein with Site 1 on the left side, the Trp214 residue roughly positioned in between, and Site 2 on the right side. In the middle, Fig. 4b and c show the molecular microenvironment with the closest amino acid participants of the complex. At the bottom, Fig. 4d and e show in detail all the non covalent interactions responsible for stabilizing the complex. These results were obtained based on the fourth most representative cluster, which fits energetically with the experimental data. On the left branch (Fig. 4b) the closest residues interacting with 2PHE are: Lys119, Leu (219, 234, 238 and 260), Ala291, Glu292, Arg257 and Tyr150. While, on the right branch (Fig. 4c), the closest residues taking part in the interactions with 2PHE are: Leu (387 and 453), Arg485, Phe488, Ser489, Tyr411 and Lys414. Finally, using the LigPlot program (Wallace et al., 1995), it was possible to underline the residues which are crucial in stabilizing the complex. At Site 1 (Fig. 4d), Lys199, Leu (219, 234, 238 and 260), Ala291, and Glu292 are residues involved in the hydrophobic interactions with 2PHE. The residues Arg257 and Tyr150 formed hydrogen bonds with the O4 oxygen atom from the 2PHE molecule. It should be noted that the oxygen atom is positioned at the densest negative charge distribution, as can be seen at the MEP of the flavonoids (Fig. S7). The NH_2 and NH groups of the Arg257 side chain built two hydrogen bonds with 2PHE, at distances of 3.34 and 2.86 Å, respectively. The OH group of the Tyr150 side chain forms a hydrogen bond with 2PHE, with a length of 2.80 Å. At Site 2 (Fig. 4e) residues Leu387, Tyr411, Leu453, Arg485 and Phe488 performed hydrophobic interactions with the 2PHE. The Lys414 and Ser489 residues form hydrogen bonds with 2PHE, presenting formation distances of 3.12 and 3.08 Å, respectively. The group NH_2 of Lys side chain makes up a hydrogen bond with the O4 oxygen atom of 2PHE (the most electronegative atom of the flavonoid, see Fig. S7). The OH group of Ser489 side chain set up a hydrogen bond with the O1 oxygen atom of 2PHE.

The molecular dynamic and docking results indicate that the hydrophobic contribution is the major interaction involved in the binding microenvironment of the Sites 1 and 2 of HSA with 2PHE. In addition, the electrostatic interactions also contribute to the complex formation, stabilizing the binding with hydrogen bonds. This set of results is in agreement with the thermodynamic analysis (Section 3.3.).

3.8. Accessible superficial area calculation

The average area lost by HSA residues in the complex formation with 2PHE was approximately 21 and 22 $Å^2$ at Sites 1 and 2, respectively. Ala291 and Ser489 were the residues with the greatest loss of ASA in Sites 1 and 2, respectively (Supplementary material, Table S4). ASA changes for nonpolar and polar atoms of the residues involved in the HSA–2PHE complex formation were 70 and 30% at Site 1, 50 and 50% at Site 2, and 61 and 39% at both of the two sites together, respectively. ASA analysis suggests that hydrophobic interactions are a major contribution in the binding of 2PHE with HSA; however, electrostatic interactions also have a considerable contribution. This result is in accordance with the experimental data.

4. Conclusion

The interaction between 2-phenylchromone and HSA was investigated using fluorescence, UV–Visible and circular dichroism spectroscopy, along with computational methods, such as *ab initio*, molecular dynamic and molecular modeling calculations. Fluorescence and UV–Visible data analysis indicated that the main quenching mechanism is static. The analysis of binding equilibria demonstrated that the binding constant for 2PHE with HSA has a moderate affinity, having a balanced behavior not so low as to avoid dispensation and not too high to prevent the decrement of the blood plasma concentration. This moderate affinity provides an appropriate condition for uniformly efficient distribution of 2PHE by HSA in the blood circulatory system to reach target organs. The $\Delta G^\circ < 0$ value indicates that the binding process is spontaneous, and ΔH° very close to zero and the $\Delta S^\circ > 0$ values suggest that the hydrophobic interaction is the main contribution involved in the HSA–2PHE complex formation. Although the electrostatic interaction at first glance would be neglected it is still important in stabilizing the binding complex. The Scatchard plot obtained by the BDF method showed a downward curvature, indicating that the HSA–2PHE complex presents positive cooperativity. The fit of this binding isothermal suggests that two molecules of 2PHE bind to HSA, which was confirmed by the drug displacement experiments, showing that the subdomain IIA (Site 1) and IIIA (Site 2) were the most probable binding sites in HSA. The distance between donor (HSA-Trp214) and acceptor (2PHE) calculated by FRET was 1.982 nm, suggesting that a transfer of energy may possibly occur between them. From CD spectroscopy analysis, no significant change in secondary structure due to the complex formation was observed (Supplementary material). The molecular dynamic and modeling calculations indicated that the 2PHE as a whole matches its molecular architecture (MEP) with Sites 1 and 2 of HSA. The computational results indicated that hydrophobic interactions are the principal contribution in the HSA–2PHE complex formation and the electrostatic interactions (hydrogen bond) are important in the stabilization of the binding complex, which is in agreement with the experimental results.

Acknowledgments

The author I.P.C. gratefully acknowledges a CAPES scholarship and financial support received from FAPESP. I.P.C. also recognizes GridUNESP for the availability of Gaussian 09 quantum chemical program, and Prof. Dr. Márcio Francisco Colombo for the use of the UV–Vis spectrometer.

The author ASdA thanks for the grant #2010/18169-3 (FAPESP) and CENAPAD-SP (Centro Nacional de Processamento de Alto Desempenho em São Paulo).

Appendix A. Supplementary data

Supplementary data associated with this article can be found, in the online version, at http://dx.doi.org/10.1016/j.foodchem.2015.10.027.

References

Best, R. B., Zhu, X., Shim, J., Lopes, P. E. M., Mittal, J., Feig, M., & MacKerell, A. D. Jr., (2012). Optimization of the additive CHARMM all-atom protein force field targeting improved sampling of the backbone ϕ, ψ and side-chain $\chi 1$ and $\chi 2$ dihedral angles. *Journal of Chemical Theory and Computation, 8*, 3257–3273.

Bi, S., Ding, L., Tian, Y., Song, D., Zhou, X., Liu, X., & Zhang, H. (2004). Investigation of the interaction between flavonoids and human serum albumin. *Journal of Molecular Structure, 703*, 37–45.

Borissevitch, I. E. (1999). More about the inner filter effect: corrections of Stern–Volmer fluorescence quenching constants are necessary at very low optical absorption of the quencher. *Journal of Luminescence, 81*, 219–224.

Bravo, L. (1998). Polyphenols: Chemistry, dietary sources, metabolism, and nutritional significance. *Nutrition Reviews, 56*, 317–333.

Caruso, I. P., Vilegas, W., Fossey, M. A., & Cornélio, M. L. (2012). Exploring the binding mechanism of Guaijaverin to human serum albumin: Fluorescence spectroscopy and computational approach. *Spectrochimica Acta Part A: Molecular and Biomolecular Spectroscopy, 97*, 449–455.

Caruso, I. P., Vilegas, W., Souza, F. P., Fossey, M. A., & Cornélio, M. L. (2014). Binding of antioxidant flavone isovitexin to human serum albumin investigated by experimental and computational assays. *Journal of Pharmaceutical and Biomedical Analysis, 98*, 100–106.

Daura, X., Gademann, K., Jaun, B., Seebach, D., van Gunsteren, W. F., & Mark, A. E. (1999). Peptide folding: When simulation meets experiment. *Angewandte Chemie International Edition, 38*, 236–240.

Delano, W. L. (2002). *The PyMOL molecular graphics system*. San Carlos, CA,USA: DeLano Scientific.

Di Cera, E. (1995). *Thermodynamic theory of site-specific binding processes biological macromolecules*. Cambridge: Cambridge University Press.

Frisch, M. J., Trucks, G. W., Schlegel, H. B., Scuseria, G. E., Robb, M. A., Cheeseman, J. R., ... Fox, D. J. (2009). *Gaussian 09, revision A.02*. Wallingford, CT: Gaussian Inc.

Grotewold, E. (2006). *The science of flavonoids*. New York: Springer.

Hubbard, S. J., & Thornton, J. M. (1993). *NACCESS*. London: Computer Program, Department of Biochemistry and Molecular Biology, University College.

Jorgensen, W. L., Chandrasekhar, J., Madura, J. D., Impey, R. W., & Klein, M. L. (1983). Comparison of simple potential functions for simulating liquid water. *Journal of Chemical Physics, 79*, 926–935.

Jung, J., Ishida, K., Nishikawa, J., & Nishihara, T. (2007). Inhibition of estrogen action by 2-phenylchromone as AhR agonist in MCF-7cells. *Life Sciences, 81*, 1446–1451.

Kauzmann, W. (1959). Factor in interpretation of protein denaturation. *Advances in Protein Chemistry, 14*, 1–63.

Lakowicz, J. R. (1999). *Principles of fluorescence spectroscopy* (2nd ed.). New York: Kluwer Academic Publishers/Plenum Press.

Lohman, T. M., & Bujalowski, W. (1991). Thermodynamic methods for model-independent determination of equilibrium binding isotherms for protein–DNA interactions: Spectroscopic approaches to monitor binding. *Methods in Enzimology, 208*, 158–290.

Mennucci, B., Cancès, E., & Tomasi, J. (1997). Evaluation of solvent effects in isotropic and anisotropic dielectrics, and in ionic solutions with a unified integral equation method: Theoretical bases, computational implementation and numerical applications. *Journal of Physical Chemistry B, 101*, 10506–105017.

Morris, G. M., Goodsell, D. S., Halliday, R. S., Huey, R., Hart, W. E., Belew, R. K., & Olson, A. J. (1998). Automated docking using a Larmarckian genetic algorithm and an empirical binding free energy function. *Journal of Computational Chemistry, 19*, 1639–1662.

Najmus-Saqib, Q., Alam, F., & Ahmad, M. (2009). Antimicrobial and cytotoxicity activities of the medicinal plant *Primula macrophylla*. *Journal of Enzyme Inhibition and Medicinal Chemistry, 24*, 697–701.

Nemethy, G., & Scheraga, H. A. (1962). Structure of water and hydrophobic binding in proteins. II. Model for the thermodynamic properties of aqueous solutions of hydrocarbons. *Journal of Chemical Physics, 36*, 3401–3417.

Peters, T. (1996). All about albumin. *Biochemistry, genetics and medical application*. Academic Press: San Diego.

Phillips, J., Braun, R., Wang, W., Gumbart, J., Tajkhorshid, E., Villa, E., ... Schulten, K. (2005). Scalable molecular dynamics with NAMD. *Journal of Computational Chemistry, 26*, 1781–1802.

Pohjala, L., & Tammela, P. (2012). Aggregating behavior of phenolic compounds – A source of false bioassay results? *Molecules, 17*, 10774–10790.

Pronk, S., Páll, S., Schulz, R., Larsson, P., Bjelkmar, P., Apostolov, R., ... Lindahl, E. (2013). GROMACS 4.5: A high-throughput and highly parallel open source molecular simulation toolkit. *Bioinformatics, 29*, 845–854.

Ross, P. D., & Subramanian, S. (1981). Thermodynamics of protein association reactions: Forces contributing to stability. *Biochemistry, 20*, 3096–3102.

Rotenberg, M., Cohen, S., & Margalit, R. (1987). Thermodynamics of porphyrin binding to serum albumin: Effects of temperature, of porphyrin species and of albumin-carried fatty acids. *Photochemistry and Photobiology, 46*, 689–693.

Sanner, M. F. (1999). Python: A programming language for software integration and development. *Journal of Molecular Graphics and Modelling, 17*, 57–61.

Sinisi, V., Forzato, C., Cefarin, N., Navarini, L., & Berti, F. (2015). Interaction of chlorogenic acids and quinides from coffee with human serum albumin. *Food Chemistry, 168*, 332–340.

Sreerama, N., & Woody, R. W. (2000). A self-consistent method for the analysis of protein secondary structure from circular dichroism. *Analytical Biochemistry, 282*, 252–260.

Sugio, S., Kashima, A., Mochikuzi, S., Noda, M., & Kobayashi, K. (1999). Crystal structure of human serum albumin at 2.5 Å resolution. *Protein Engineering, 12*, 439–446.

Tanford, J. (1973). *The theory of the hydrophobic effect*. New York: Wiley.

Wallace, A. C., Laskowski, R. A., & Thomton, J. M. (1995). LIGPLOT: A program to generate schematic diagrams of protein-ligand interaction. *Protein Engineering, 8*, 127–134.

Wu, D., Yan, J., Wang, J., Wang, Q., & Li, H. (2015). Characterization of interaction between food colourant allura red AC and human serum albumin: Multispectroscopic analyses and docking simulations. *Food Chemistry, 170*, 423–429.

Zsila, F. (2013). Subdomain IB is the third major drug binding region of human serum albumin: Toward the three-sites model. *Molecular Pharmaceutics, 10*, 1668–1682.

Anexo IV - Material suplementar do Anexo III

Supplementary material – An integrated approach with experimental and computational tools outlining the cooperative binding between 2-phenylchromone and human serum albumin

Ícaro Putinhon Caruso[a,b] , José Maria Barbosa Filho[c], Alexandre Suman de Araújo[b], Fátima Pereira de Souza[a,b], Marcelo Andrés Fossey[a,b], Marinônio Lopes Cornélio[a,b,*]

[a] Departamento de Física, Instituto de Biociências, Letras e Ciências Exatas (IBILCE), UNESP, Rua Cristovão Colombo 2265, CEP 15054-000, São José do Rio Preto, SP, Brasil;

[b] Centro Multiusuário de Inovação Biomolecular (CMIB), Instituto de Biociências, Letras e Ciências Exatas (IBILCE), UNESP, Rua Cristovão Colombo 2265, CEP 15054-000, São José do Rio Preto, SP, Brasil;

[c]Laboratório de Tecnologia Famacêutica (LTF), UFPB, Cidade Universitária, CEP 58051-900, João Pessoa, PB, Brasil.

* Corresponding author e-mail address: mario@ibilce.unesp.br

The workflow summarizes all the experimental and computational methods and how they are cross validated.

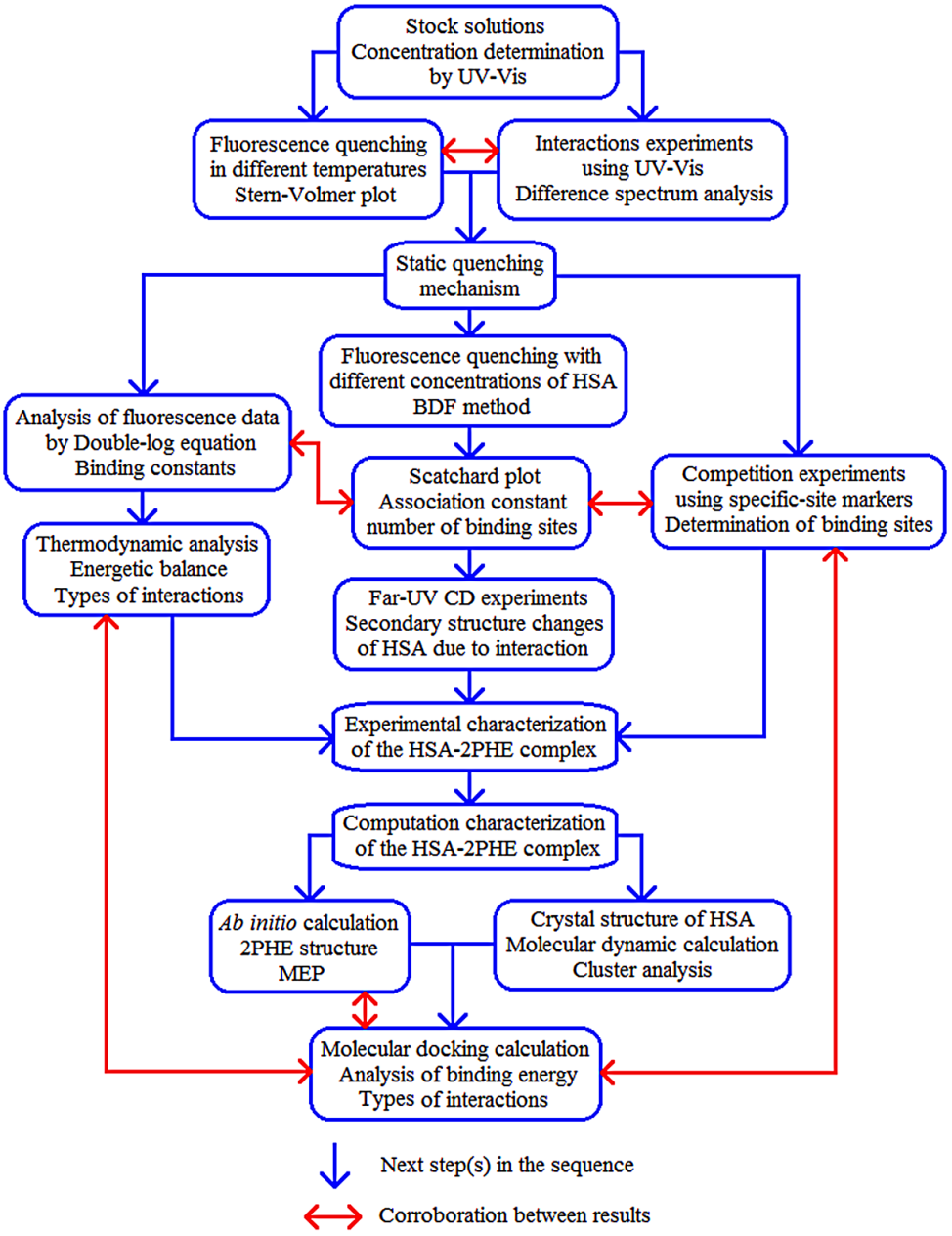

Distance Measurement between HSA-Trp214 and 2PHE

Fluorescence resonance energy transfer (FRET) is a spectroscopic method that can monitor the proximity and relative angular orientation of fluorophores. According to Förster non-radiative energy transfer theory, the energy transfer will occur under the following conditions: when the donor produces fluorescent light; when the emission spectrum of the donor and the absorbance spectrum of the acceptor have a partial overlap; when there is an orientation of the transition dipole of the donor and acceptor; and when the distance between the donor and acceptor is less than 8.0 nm (Lakowicz, 1999). According to this theory, the average distance r in the binding between HSA-Trp214 (donor) and 2PHE (acceptor) can be calculated by the equation:

$$E = 1 - F/F_0 = R_0^6/\left(R_0^6 + r^6\right) \tag{12}$$

where E is the efficiency of energy transfer and R_0 is the critical distance when the transfer efficiency is 50%.

$$R_0^6 = 8.79\times10^{-25} K^2 n^{-4} \phi\ J \tag{13}$$

In Eq. (13), K^2 is the orientation space factor, n is the refracted index of the medium, ϕ is the fluorescence quantum yield of the donor, and J is the effect of the spectral overlap between the emission spectrum of the donor and the absorption spectrum of the acceptor (Supplementary material, Fig. S5), which can be calculated by the following equation:

$$J = \int_0^\infty F(\lambda)\varepsilon(\lambda)\lambda^4 d\lambda \Big/ \int_0^\infty F(\lambda) d\lambda \tag{14}$$

where $F(\lambda)$ is the corrected fluorescence intensity of the donor in the wavelength range from λ to $\lambda + \Delta\lambda$, and $\varepsilon(\lambda)$ is the extinction coefficient of the acceptor at λ.

In this study, $K^2 = 2/3$, $n = 1.36$, and $\phi = 0.074$ (Caruso et al., 2012). According to Eqs. (9) – (11), values were calculated as follows: $J = 3.776\times10^{-15}$ cm^3·L·mol^{-1}, $E = 0.441$, $R_0 = 1.905$ nm and $r = 1.982$ nm. The average distance between donor and acceptor fluorophore is in the range

$0.5\,R_0 < r < 1.5\,R_0$ (Lakowicz, 1999), indicating that an energy transfer from HSA to 2PHE is likely to occur.

HSA secondary structural analysis

The secondary structural change analysis of HSA by binding 2PHE was investigated using far-UV CD spectroscopy. The principle of the circular dichroism technique is based on the different absorption of right or left circularly polarized light that some molecules present. The CD spectra present two negative bands in the ultraviolet region 209 and 222 nm, which is characteristic of the α-helix structure of protein (Supplementary material, Fig. S6) (Gore, 2000). Titration with the flavonoid did not result in significant changes in HSA secondary motifs (Fig. S6). The structural analysis calculated by CONTINLL software (Sreerama & Woody, 2000) showed that the content of the secondary structure of the α-helix motif remained at 60 % along the increment of 2PHE aliquots. In Fig. S6 it can be seen that the effect of ethanol on the CD spectrum of the HSA is negligible.

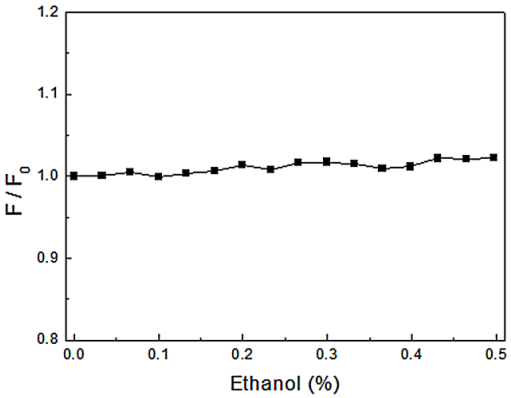

Fig. S1. Effect of ethanol on the fluorescence intensity of HSA (4.0 μM, pH 7.0, T = 298 K, λ_{ex} = 295 nm). Percentage of the ethanol volume in HSA solution varied from 0 to 0.5 with the increment of 0.0333 %.

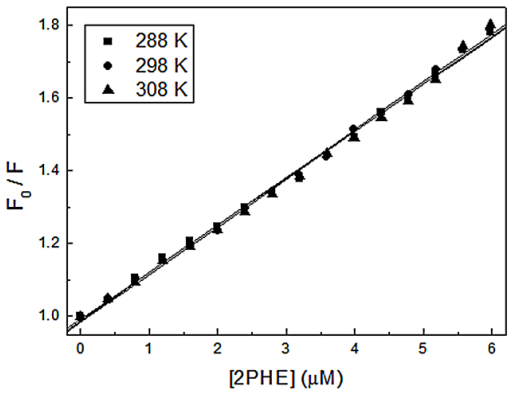

Fig. S2. Stern-Volmer plots for the fluorescence quenching of the HSA by 2PHE at pH 7.0 and 288, 298 and 308 K.

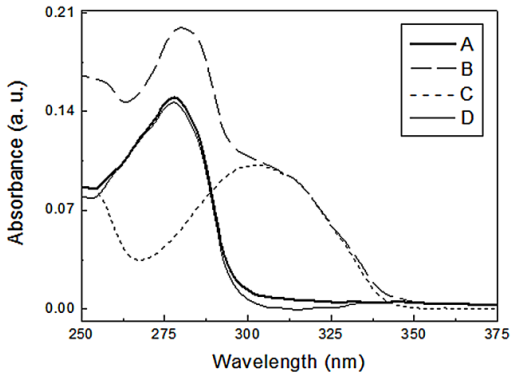

Fig. S3. UV-Vis absorption spectrum of free HSA (A), HSA-2PHE complex (B), free 2PHE (C) and spectral subtraction between HSA-2PHE complex and free 2PHE (D) at room temperature and pH 7.0. [HSA] = [2PHE] = 4.0 μM.

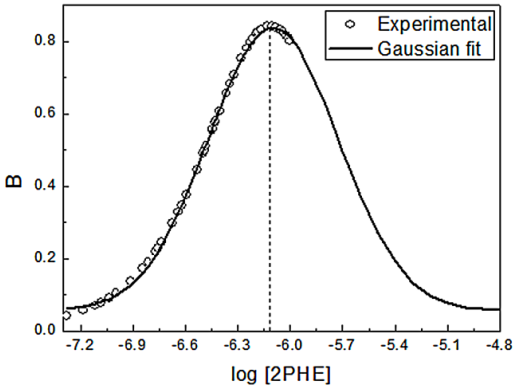

Fig. S4. 2PHE binding capacity of HSA (pH 7.0 and 298 K). Experimental curve was obtained using the values of k_1 and k_2 in the following equation (Di Cera, 1995):

$$B = \left(2k_1 L_F + 4k_1 k_2 L_F^2 + 2k_1^2 k_2 L_F^3\right) \Big/ \left(1 + 2k_1 L_F + k_1 k_2 L_F^2\right).$$

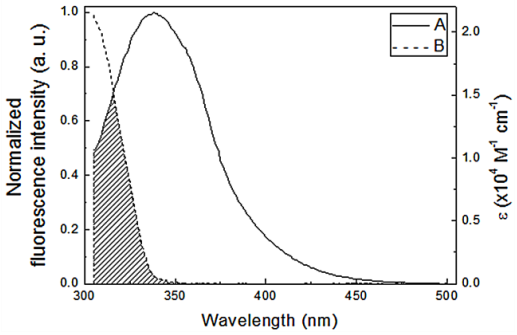

Fig. S5. Spectral overlap of the HSA fluorescence (A) with 2PHE absorption (B).

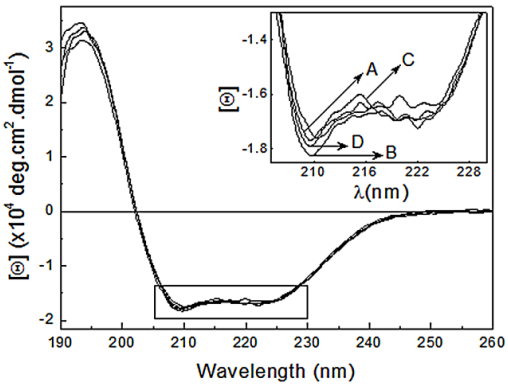

Fig. S6. CD spectra of HSA in absence and presence of 2PHE at pH 7.0 and room temperature. The insert corresponds to the detail of the peaks at 209 and 222 nm. [HSA] = 4.0 μM; 2PHE to HSA ratios: (A) 0:1, (B) 1:1 and (C) 2:1. (D) It shows the CD spectrum of HSA in presence of ethanol.

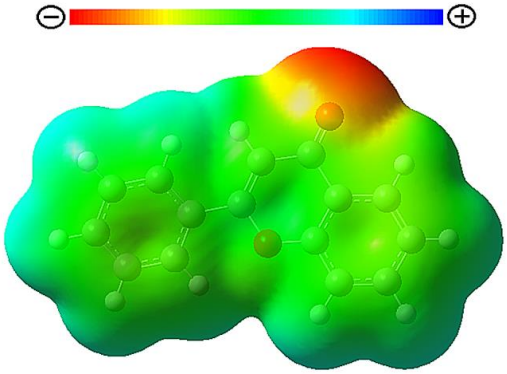

Fig. S7. Molecular electrostatic potential (MEP) map of 2PHE molecule calculated using the DFT/B3LYP/6-311++G(2d,p) method.

Table S1

Some structure details of the optimized structure of 2PHE at the DFT/B3LYP/6-311++G(2d,p) method.

Bond distance (Å)	
O1 – C2	1.360
C2 – C3	1.353
C2 – C1'	1.474
O1 – C9	1.370
C8 – C9	1.394
C1' – C2'	1.400
Bond angles (°)	
O1 – C2 – C3	121.905
O1 – C2 – C1'	112.282
C2 – O1 – C9	119.980
C7 – C8 – C9	118.830
Dihedral angles (°)	
O1 – C2 – C1' – C2'	– 20.926
C3 – C2 – C1' – C2'	158.212
C7 – C8 – C9 – O1	– 179.839
C5 – C10 – C4 – O4	– 0.161

Table S2

Experimental and theoretical UV-Vis absorbance wavelengths $\lambda(nm)$, excitation energy $E(eV)$, molar coefficient extinction $\varepsilon(M^{-1}cm^{-1})$ and oscillator strength $f(u.a.)$ of 2PHE in ethanol.

Experimental		TD-DFT/B3LYP/6-311+G(d,p)		
Ethanol		Ethanol (24.85)		
$\lambda(nm)$	$\varepsilon(M^{-1}cm^{-1})$	$\lambda(nm)$	$E(eV)$	$f(u.a.)$
251	20,800	235	5.283	0.025
		240	5.158	0.141
		250	4.964	0.015
		253	4.893	0.084
		265	4.686	0.051
		276	4.490	0.023
		293	4.231	0.392
294	25,100	305	4.059	0.346
		331	3.740	0.004

Table S3

Theoretical binding energy (ΔG_B) and constant (K_B) values determined by molecular dynamic and modeling calculations.

Cluster	Site 1		Site 2	
	ΔG_B ($kJmol^{-1}$)	K_B [b] (M^{-1})	ΔG_B ($kJmol^{-1}$)	K_B [b] (M^{-1})
1	–29.2	1.32×10^5	–22.2	7.82×10^3
2	–30.9	2.62×10^5	–23.4	1.27×10^4
3	–29.5	1.49×10^5	–23.8	1.49×10^4
4[a]	–28.6	1.04×10^5	–29.6	1.55×10^5
5	–32.2	4.44×10^5	–23.2	1.17×10^4
6	–28.9	1.17×10^5	–28.3	9.19×10^4

[a] The results for this cluster are in agreement with the experimental data.
[b] The theoretical binding constants were calculated using T = 298 K.

Table S4

Change in accessible surface area (ΔASA in $Å^2$) of the residues of site 1 and 2 involved in the HSA-2PHE complex; ΔASA_t for all atoms, ΔASA_{np} for all nonpolar atoms and ΔASA_p for all polar atoms.

Site 1				Site 2			
Residue	[a] ΔASA_t	ΔASA_{np}	ΔASA_p	Residue	[a] ΔASA_t	ΔASA_{np}	ΔASA_p
Tyr150	24.22	18	6.22	Leu387	30.71	30.71	0
Glu153	11.51	11.51	0	Asn391	10.24	0	10.24
Lys199	27.96	0	27.96	Arg410	24.28	8.5	15.78
Leu238	19.86	19.86	0	Tyr411	25.48	9.55	15.93
His242	14.26	12.33	1.93	Lys414	19.44	2.96	16.48
Leu260	18.16	18.16	0	Leu453	15.64	15.64	0
Ile264	11.53	11.53	0	Phe488	18.58	12.8	5.78
Ala291	31.8	21.69	10.11	Ser489	34	9.8	24.2
Glu292	26.96	18.1	8.86				

[a] Only values > 10 $Å^2$ are reported.

References

Caruso, I. P., Vilegas, W., Fossey, M. A., Cornélio, M. L. (2012). Exploring the binding mechanism of Guaijaverin to human serum albumin: Fluorescence spectroscopy and computational approach. *Spectrochimica Acta Part A: Molecular and Biomolecular Spectroscopy*, 97, 449-455.

Di Cera, E. (1995). Thermodynamic theory of site-specific binding processes biological macrolecules. Cambridge: Cambridge University Press.

Gore, M. G. (2000). Spectrophotometry and Spectrofluorimetry: A Practical Approach. New York: Oxford University Press, 123-125.

Lakowicz, J. R. (1999). Principles of Fluorescence Spectroscopy, 2nd ed., New York: Kluwer Academic Publishers/Plenum Press.

Anexo V - Artigos publicados em colaboração

International Journal of Biological Macromolecules 83 (2016) 178–184

Contents lists available at ScienceDirect

International Journal of Biological Macromolecules

journal homepage: www.elsevier.com/locate/ijbiomac

Functional expression, monodispersity and conformational changes in the SBMV virus viral VPg on binding TFE

R.B. Mariutti[a], I.P. Caruso[b], A. Ullah[a], F.R. De Morais[b], D. Rehders[c], R.K. Arni[a,b,*]

[a] Multiuser Center for Biomolecular Innovation, IBILCE/UNESP, Brazil
[b] Department of Physics, IBILCE/UNESP, Brazil
[c] Laboratory for Structural Biology of Infection and Inflammation, Hamburg University, Germany

ARTICLE INFO

Article history:
Received 14 July 2015
Received in revised form 8 November 2015
Accepted 10 November 2015
Available online 22 November 2015

Keywords:
VPg
Viral genome-linked protein
Expression
Purification

ABSTRACT

Southern bean mosaic virus (SBMV) RNA purified from infected plants was used for cloning the viral genome-linked protein (VPg) and was subsequently expressed in *Escherichia coli*. Circular dichroism (CD), dynamic light scattering (DLS) and saturation transfer difference (STD) by nuclear magnetic resonance (NMR) measurements were employed to determine the degree of monodispersity and to investigate the conformational changes in the absence and presence of trifluoroethanol (TFE) which indicated increased helical content with increasing concentration of TFE. 8-Anilino-1-naphthalenesulfonic acid (ANS) was used as a probe to compare the unfolding regions of the protein before and after addition of TFE. The results indicated that although the TFE concentration influences VPg folding, it does not play a role in nucleotide binding and that the local solvent hydrophobicity causes significant conformational changes.

1. Introduction

Genome-linked viral proteins (VPgs) are involved in a number of processes ranging from replication to viral protein synthesis [1,2]. VPgs are small proteins that are covalently linked to the 5′ end of viral RNA via a phosphodiester bond formed between the hydroxyl groups of amino acid residues and the 5′ phosphate groups of RNA [3,4]. Often encountered in viruses with single-stranded positive-sense RNA (ssRNA) genomes, VPgs from fungal viruses, plant viruses and animal viruses with double or positive single strand (ssRNA) have been characterized [5,6]. VPgs from plant and animal viruses share many features, for example, they are products of polyprotein processing and are uridylated by their cognate RNA-dependent RNA polymerase (RdRP) [7–9] enabling VPgs to operate as primers during viral RNA synthesis. VPgs also share the presence of high percentages of basic amino acids (mostly lysine, glycine, threonine and arginine) contributing to the interaction with the negatively charged RNA [10]. The covalent binding of VPgs to RNAs exhibits some differences; picornaviruses, potyviruses and caliciviruses use the hydroxyl group of a tyrosine residue whereas comoviruses and nepovirus are reported to use a serine residue [6]. Threonine also contains a hydroxyl group, but the only evidence that it is used for RNA binding was reported by [11] when investigating VPg from SBMV covalently attached to genomic RNAs. VPg from sobemovirus is a cleavage product of its precursor polyprotein (VPg-proteinase-polymerase) [12] and the residue for RNA binding is not conserved within its genre [13]. All positive-sense ssRNA viruses that infect mammalian, insect or plant cells replicate in association with host endomembrane [14] and different host factors may influence the process [15,16]. Some phytoviral (*Sesbania mosaic virus*; *Potato virus A*, *Potato virus Y*, *Lettuce mosaic virus*, and *Rice yellow mottle virus*) VPgs were shown to be natively unfolded proteins [17–20] and hence recalcitrant for crystallization. Therefore, to date, not a single crystal structure of these proteins has been determined. Nevertheless, the crystal structures of synthetic peptides corresponding to *Picornaviridae* VPgs (<3 kDa) (PDB: 2D7S, 4IKA, 3CDW) complexed with their cognate RdRP indicate that the peptides are almost completely random coiled without any alpha helix or beta strand. More recently, the solution structure of recombinant VPg from *Caliciviridae* (PDB: 2MXD) has been elucidated [21].

In the present study, VPg from SBMV was expressed in *Escherichia coli* and purified. Circular dichroism (CD) was employed to assess the VPg secondary structure conformational content and its variation in the presence of increasing concentrations of reagents that mimic membrane environments

* Corresponding author at: Multiuser Center for Biomolecular Innovation, Universidade Estadual Paulista (UNESP), São Jose do Rio Preto, 15054-000 SP, Brazil.
E-mail address: arni@sjrp.unesp.br (R.K. Arni).

http://dx.doi.org/10.1016/j.ijbiomac.2015.11.026
0141-8130/

International Journal of Biological Macromolecules 85 (2016) 40–47

Contents lists available at ScienceDirect

International Journal of Biological Macromolecules

journal homepage: www.elsevier.com/locate/ijbiomac

Experimental evidence and molecular modeling of the interaction between hRSV-NS1 and quercetin

Deriane Elias Gomes[a,b], Ícaro Putinhon Caruso[a,b], Gabriela Campos de Araujo[a,b], Isabella Otenio de Lourenço[a,b], Fernando Alves de Melo[a,b], Marinônio Lopes Cornélio[a,b], Marcelo Andrés Fossey[a,b], Fátima Pereira de Souza[a,b,*]

[a] Departamento de Física—Instituto de Biociências, Letras e Ciências Exatas (IBILCE) Universidade Estadual Paulista "Júlio de Mesquita Filho" (UNESP)—Campus de São José do Rio Preto—SP. Rua Cristóvão Colombo, 2265, Jardim Nazareth, Cep: 15054-000 São José do Rio Preto, SP, Brazil
[b] Centro Multiusuário de Inovação Biomolecular (CMIB)—Instituto de Biociências, Letras e Ciências Exatas (IBILCE) Universidade Estadual Paulista "Júlio de Mesquita Filho" (UNESP)—Campus de São José do Rio Preto—SP. Rua Cristóvão Colombo, 2265, Jardim Nazareth, Cep: 15054-000 São José do Rio Preto, SP, Brazil

ARTICLE INFO

Article history:
Received 14 November 2014
Received in revised form
29 November 2015
Accepted 14 December 2015
Available online 21 December 2015

Keywords:
Non structural protein 1
Flavonoids
Quercetin
Fluorescence spectroscopy
Molecular modeling
Human syncytial respiratory virus

ABSTRACT

Human Respiratory Syncytial Virus is one of the major causes of acute respiratory infections in children, causing bronchiolitis and pneumonia. Non-Structural Protein 1 (NS1) is involved in immune system evasion, a process that contributes to the success of hRSV replication. This protein can act by inhibiting or neutralizing several steps of interferon pathway, as well as by silencing the hRSV ribonucleoproteic complex. There is evidence that quercetin can reduce the infection and/or replication of several viruses, including RSV. The aims of this study include the expression and purification of the NS1 protein besides experimental and computational assays of the NS1-quercetin interaction. CD analysis showed that NS1 secondary structure composition is 30% alpha-helix, 21% beta-sheet, 23% turn and 26% random coils. The melting temperature obtained through DSC analysis was around 56 °C. FRET analysis showed a distance of approximately 19 Å between the NS1 and quercetin. Fluorescence titration results showed that the dissociation constant of the NS1-quercetin interaction was around 10^{-6} M. In thermodynamic analysis, the enthalpy and entropy balanced forces indicated that the NS1-quercetin interaction presented both hydrophobic and electrostatic contributions. The computational results from the molecular modeling for NS1 structure and molecular docking regarding its interaction with quercetin corroborate the experimental data.

1. Introduction

The participation of Human Respiratory Syncytial Virus (hRSV) in respiratory diseases during childhood can be life-threatening, with severe consequences like pneumonia and bronchiolitis. The major strategy that contributes to the success of hRSV replication is its immune system evasion efficacy, a process provided by Non-Structural Proteins (NS1 and NS2). NS1 is a small protein that has 139 amino acids [1] with 15 kDa. Extensive studies have shown that NS1 plays an important role in the modulation of the host response to infection, antagonizing the interferon-mediated antiviral state [2].

It has been reported that NS1 (1) co-localizes with the mitochondrial signaling protein (MAVS), inhibiting MAVS-RIG-I interaction and decreasing protein levels of members of the IFN induction pathway, such as TRAF3 and IKKe [3,4]; (2) interacts with microtubule-associated protein 1B (MAP1B), which may be important for surface recognition of these proteins with other host structures [5]; and (3) interacts with M protein and the *C*-terminus of P protein [6].

Flavonoids have gained world interest due to their nutraceutical and therapeutic importance, exhibiting several biological activities such as antioxidant, anti-inflammatory, cardioprotective, antibacterial, antitumor, hepatoprotective, and antiviral activities [7]. Thus, because quercetin is the most studied flavonoid and it has antiviral properties [8–11], we decided to investigate how

* Corresponding author.
E-mail addresses: derianegomes1@gmail.com (D.E. Gomes), ykrocaruso@hotmail.com (Í.P. Caruso), bicamposaraujo@hotmail.com (G.C.d. Araujo), isabella_o.lourenco@hotmail.com (I.O.d. Lourenço), fernanmello@gmail.com (F.A.d. Melo), mario@ibilce.com.br (M.L. Cornélio), marcelo@ibilce.unesp.br (M.A. Fossey), fatyssouza@gmail.com, fatyssouza@yahoo.com.br (F.P.d. Souza).

http://dx.doi.org/10.1016/j.ijbiomac.2015.12.051
0141-8130/

International Journal of Sciences
Research Article Volume 5 – February 2016 (02)

Investigation of the Interaction between Coumarins and Its Derivatives with Human Serum Albumin: STD-NMR, Fluorescence and Docking Molecular Studies

Fernanda Paulin Benzatti[1], Ícaro P. Caruso[1], Thiago Salem Pançonato Teixeira[2], Fábio Rogério Moraes[1], Fernando Alves de Melo[1], Luiz Claudio Di Stasi[3], Marinônio Lopes Cornélio[1], Fatima Pereira de Souza[4], Marcelo Andres Fossey[1]

[1]CMIB/Physics Departament, IBILCE, UNESP
[2]CMIB-IBILCE, UNESP
[3]Pharmacology Departament, IBB, UNESP
[4]Fátima Pereira de Souza, Instituto de Biociências, Letras e CiênciasExatas – IBILCE/UNESP. RuaCristóvão Colombo, 2265. São José do Rio Preto, SP, Brazil. CEP15054-000

Abstract: In this paper, binding interaction of Coumarin, including 4-Methylesculetin, Esculetin and Esculin, with human serum albumin (HSA) was investigated by using STD-NMR, fluorescence spectroscopy and molecular docking method. STD-NMR investigations indicated that the binding affinity sequence for HSA-ligands interaction was: 4-Methyllesculetin >Esculetin>Coumarin>Esculinbeingin accordance with the fluorescence studies. The molecular docking resultssuggested that coumarins and its derivatives were binding to HSA at subdomain IIA, nearby the Trp214 residue, which are consistent with the results of fluorescence quenching results. Overall, the experimental and theoretical data corroborate with each other and they are complementary.

Keywords: Coumarins and their derivatives, Human Serum Albumin, STD-NMR, fluorescence quenching, docking molecular.

Introduction

Coumarins comprise a very large class of compounds that occur naturally in plants [1]. Thesecompounds are lactones of o-hydroxy-cinnamic acid with typical benzopyrone framework. Coumarin and their derivatives have roles as anti-inflammatory, anti-coagulant, anti-retroviral, anti-arthritic, anti-asthmatic [2,3], antioxidant and intestinal anti-inflammatory activities [4,5]they can also cause significant changes in the regulation of the immune response, cell growth, and differentiation [6]. The mode and strength of coumarin activity usually could be modified by the number and type of small substituent, namely hydroxy or methoxy groups [1]. Coumarins have recently attracted much attention due to their broad pharmacological activities as precursor molecules for the synthesis of number of synthetic anticoagulant drugs [7]. The structural studies of complexes formed by simple coumarins with diverse proteins indicated that the nature of ligand-protein binding is a combination of hydrophobic, electrostatic and/or hydrogen bonding interactions [8]. Several coumarins derivatives are bound to serum proteins, especially human serum albumin (HSA). HSA, the most abundant and the major transport protein in the blood, is used as a carrier in the transport of various endogenous and exogenous compounds throughout the body until their target organs[9]. It greatly influences drug distribution and can play a major role in affecting drug absorption, distribution, metabolism, and excretion [10]. It is a globular protein synthesized and secreted from liver cells and contains 585 aminoacid residues with a total molar mass of 66 kDa. It has three homologous helical domains (I-III), each divided into A and B

Published at: http://www.ijsciences.com/pub/issue/2016-02/
DOI: 10.18483/ijSci.777; Online ISSN: 2305-3925; Print ISSN: 2410-4477

Fatima Pereira de Souza(Correspondence)
liujunchang@vip.sina.com
+55 17 32212463, Fax: +55 17 32212247

Biochimica et Biophysica Acta 1861 (2016) 970–979

Contents lists available at ScienceDirect

Biochimica et Biophysica Acta

journal homepage: www.elsevier.com/locate/bbalip

Active site mapping of *Loxosceles* phospholipases D: Biochemical and biological features

L. Vuitika [a], D. Chaves-Moreira [a], I. Caruso [b], M.A. Lima [c], F.H. Matsubara [a], M.T. Murakami [d], H.K. Takahashi [c], M.S. Toledo [c], M.A. Coronado [b], H.B. Nader [c], A. Senff-Ribeiro [a], O.M. Chaim [a], R.K. Arni [b], S.S. Veiga [a,*]

[a] Department of Cell Biology, Federal University of Paraná (UFPR), Curitiba, PR, Brazil
[b] Multiuser Center for Biomolecular Innovation, Department of Physics, São Paulo State University (UNESP), São José do Rio Preto, SP, Brazil
[c] Department of Biochemistry, Federal University of São Paulo (UNIFESP), São Paulo, SP, Brazil
[d] Brazilian Biosciences National Laboratory (LNBio), National Center for Research in Energy and Materials (CNPEM), Campinas, SP, Brazil

ARTICLE INFO

Article history:
Received 8 December 2015
Received in revised form 20 May 2016
Accepted 23 May 2016
Available online 24 May 2016

Keywords:
Brown spider venom
Phospholipase D
Site-directed mutagenesis
Activity modulation

ABSTRACT

Brown spider phospholipases D from *Loxosceles* venoms are among the most widely studied toxins since they induce dermonecrosis, triggering inflammatory responses, increase vascular permeability, cause hemolysis, and renal failure. The catalytic (H12 and H47) and metal-ion binding (E32 and D34) residues in *Loxosceles intermedia* phospholipase D (LiRecDT1) were mutated to understand their roles in the observed activities. All mutants were identified using whole venom serum antibodies and a specific antibody to wild-type LiRecDT1, they were also analyzed by circular dichroism (CD) and differential scanning calorimetry (DSC). The phospholipase D activities of H12A, H47A, H12A-H47A, E32, D34 and E32A-D34A, such as vascular permeability, dermonecrosis, and hemolytic effects were inhibited. The mutant Y228A was equally detrimental to biochemical and biological effects of phospholipase D, suggesting an essential role of this residue in substrate recognition and binding. On the other hand, the mutant C53A-C201A reduced the enzyme's ability to hydrolyze phospholipids and promote dermonecrosis, hemolytic, and vascular effects. These results provide the basis understanding the importance of specific residues in the observed activities and contribute to the design of synthetic and specific inhibitors for Brown spider venom phospholipases D.

1. Introduction

Accidental bites from the genus *Loxosceles* (brown spiders, also known as violin spiders) have been reported to induce several clinical signs, such as necrotic skin lesions with gravitational spreading (the hallmark of *Loxosceles* envenomation), hematological disturbances (thrombocytopenia and hemolytic anemia), and renal failure [1–4]. Brown spiders have a cosmopolitan distribution and the variation of species is reflected by their geographical prevalence. Accidents involving brown spiders have been reported in America, Europe, Asia, Africa, and Oceania [1–4].

Molecular biological technologies such as, the construction of a cDNA library from venom glands, cloning procedures, transcriptome analysis, heterologous recombinant toxin expression, and proteomics studies have revealed the complex composition of brown spider venoms. They contain at least three major classes of molecules: (1) phospholipases D (also known as *Loxosceles intermedia* Recombinant Dermonecrotic Toxins [LiRecDTs], based on their involvement in dermonecrosis following accidents); (2) metalloproteinases (which are members of the *Loxosceles* Astacin-like Proteinase [LALP] family) [5,6]; and (3) low molecular mass molecules, putatively classified as insecticidal toxins (Cystine Knot peptides [ICK]) [7,8]. The venom of Brown spiders also contains toxins with low levels of expression, such as hyaluronidases, translationally controlled tumor protein (TCTP), serine proteinases, serine proteinase inhibitors, and venom allergens [9–12].

Previous reports have proposed the existence of a family of phospholipase D toxins in *Loxosceles* spider venoms. Kalapothakis and colleagues classified the phospholipases D from *Loxosceles* spider venoms as the LoxTox family, which was further extended to include the phospholipase D homologs identified in Sicariid spiders, which are referred to as SicTox [13,14]. Wood et al. compiled the ArachnoServer database of toxins from spider venoms, which includes several toxins characterized as homologs of phospholipases D derived from *Loxosceles* species [15]. The existence of an intra-species family of antigenically and structurally related members has also been supported by experimental approaches, including the immunodetection of multiple homologs of phospholipase D in the venom of *Loxosceles* species [15,16].

Among the venoms of Brown spiders, the phospholipase D family and its homologs are the most widely studied. Members of this family of

* Corresponding author at: Department of Cell Biology, Federal University of Paraná, Jardim das Américas, 81531-990, Curitiba, Paraná, Brazil.
E-mail address: veigass@ufpr.br (S.S. Veiga).

http://dx.doi.org/10.1016/j.bbalip.2016.05.009
1388-1981/

Biochimica et Biophysica Acta 1850 (2015) 393–400

Contents lists available at ScienceDirect

Biochimica et Biophysica Acta

journal homepage: www.elsevier.com/locate/bbagen

Chemical and thermal influence of the $[4Fe–4S]^{2+}$ cluster of A/G-specific adenine glycosylase from *Corynebacterium pseudotuberculosis*

Raphael J. Eberle [a], Monika A. Coronado [a], Icaro P. Caruso [a], Débora O. Lopes [b], Anderson Miyoshi [c], Vasco Azevedo [c], Raghuvir K. Arni [a,*]

[a] Multiuser Center for Biomolecular Innovation, Departament of Physics, Universidade Estadual Paulista (UNESP), São Jose do Rio Preto, SP 15054-000, Brazil
[b] Laboratory of Molecular Biology, Federal University of São João Del-Rei (CCO), Av. Sebastião Gonçalves Coelho, 400, Divinópolis, MG 35501-296, Brazil
[c] Laboratório de Genética Celular e Molecular, Instituto de Ciências Biológicas, Universidade Federal de Minas Gerais, Av. Antônio Carlos, 6627-Pampulha, CP 486, CEP 31, Belo Horizonte, MG 270-901, Brazil

ARTICLE INFO

Article history:
Received 18 August 2014
Received in revised form 28 October 2014
Accepted 14 November 2014
Available online 20 November 2014

Keywords:
C. pseudotuberculosis
MutY
$[4Fe–4S]^{2+}$ cluster
DNA repair
Spectroscopic method
Secondary and tertiary structure

ABSTRACT

The gram-positive bacteria *Corynebacterium pseudotuberculosis*, the causative agent of caseous lymphadenitis in livestock significantly reduces productivity and often causes death. The adenine/guanine-specific DNA glycosylase (MutY) prevents mutations in the DNA of the pathogen and a unique feature of the MutY protein family is the $[4Fe–4S]^{2+}$ cluster that interlinks two protein subdomains. MutY from *C. pseudotuberculosis* was expressed in *E. coli* and purified, the CD experiments indicate a high content of α-helices and random coiled secondary structure and a typical near-UV CD fingerprint for the $[4Fe–4S]^{2+}$ cluster. EDTA and copper sulfate possess a strong destabilizing effect on the $[4Fe–4S]^{2+}$ cluster. UV–vis and fluorescence spectroscopy results demonstrate that between pH 3.0 and 4.0 the integrity of the $[4Fe–4S]^{2+}$ cluster is destroyed. To investigate the thermal stability of the protein differential scanning calorimetry and fluorescence spectroscopy were used and the T_m was determined to be 45 °C. The analysis presented provides information concerning the protein stability under different physio-chemical conditions.

1. Introduction

Corynebacterium pseudotuberculosis (*C. pseudotuberculosis*) is a gram-positive bacterium which together with mycobacterium, nocardia and rhodococcus forms the 'CMNR group' of potential animal and human pathogens [1]. *C. pseudotuberculosis*, a facultative intracellular parasite is the causative agent of caseous lymphadenitis (CLA) in equids, sheep and goats (biovar ovis) and also to a lesser extent in horses and cattle (biovar and equus). Infection by *C. pseudotuberculosis* in sheep and goats leads to considerable economic loss due to significantly reduced yields in wool and milk production, weight loss, carcass condemnation and death due to the formation of abscesses in superficial and visceral lymph nodes and caseous necrosis of the lymphatic glands [2,3]. This pathogen is capable of survival and growth in macrophages thus evading detection by the host immune system [4,5]. Infections due to *C. pseudotuberculosis* are predominantly observed in sheep and goats and infections by this pathogen, although rare, have been reported to occur in humans [6–8]. In macrophages, *C. pseudotuberculosis* is exposed to an environment rich in reactive oxygen and nitrogen species (ROS and RNS, respectively) [9] in addition to those it endogenously generates during metabolism. These molecules interact with DNA ultimately causing different types of damage including the formation of modified bases, formation of abasic sites, and strand breaks, with cytotoxic or mutagenic effects on the cell [10,11]. Organisms have evolved various defense systems to protect their genomes from oxidative DNA damage; the base excision repair (BER) mechanism is the major repair pathway for the oxidized DNA bases and is initiated by DNA glycosylases. 7,8-dihydro-8-oxo-2′-deoxyguanosine (8-OxoG), one of the most stable oxidized purines, has the most deleterious effects because it can mispair with adenine during DNA replication [12,13]. The adenine/guanine-specific DNA glycosylase (MutY) [EC 3.2.2] plays an important role in the BER pathway and prevents DNA mutations resulting from the presence of the oxidatively damaged 8-OxoG. This guanosine derivate can mispair with 2′-deoxycytidine 5′-triphosphate or with 2′-deoxyadenosine triphosphate during DNA replication, forming C*8-oxoG and A*8-oxoG mispairs. If uncorrected, the A*8-OxoG mispairs can result in deleterious C:G to A:T transversions.

Abbreviations: CLA, caseous lymphadenitis; ROS, reactive oxygen species; RNS, reactive nitrogen species; MutY, adenine/guanine-specific DNA glycosylase; IPTG, isopropyl-β-D-thiogalactopyranosid; CD, circular dichroism spectroscopy; DSC, differential scanning calorimetry; UV–vis, ultraviolet–visible spectroscopy; Trp, tryptophane; REES, red edge excitation shift

* Corresponding author at: Centro Multiusuário de Inovação Biomolecular, Departamento de Física, Universidade Estadual Paulista (UNESP), Rua Cristóvão Colombo 2265, São Jose do Rio Preto, SP 15054-000, Brazil. Tel.: +55 17 32212460; fax: +55 17 32212247.
E-mail address: arni@sjrp.unesp.br (R.K. Arni).

http://dx.doi.org/10.1016/j.bbagen.2014.11.014
0304-4165/

Protein Expression and Purification 112 (2015) 15–20

Contents lists available at ScienceDirect

Protein Expression and Purification

journal homepage: www.elsevier.com/locate/yprep

Expression, purification and characterization of cold shock protein A of *Corynebacterium pseudotuberculosis*

Antje Lindae [a], Raphael J. Eberle [a], Icaro P. Caruso [a], Monika A. Coronado [a], Fabio R. de Moraes [a], Vasco Azevedo [b], Raghuvir K. Arni [a,*]

[a] Multiuser Center for Biomolecular Innovation, Departament of Physics, Universidade Estadual Paulista (UNESP), São Jose do Rio Preto-SP 15054-000, Brazil
[b] Laboratório de Genética Celular e Molecular, Instituto de Ciências Biológicas, Universidade Federal de Minas Gerais, Av, Antônio Carlos, 6627 – Pampulha, CP 486, CEP 31, Belo Horizonte, MG 270-901, Brazil

ARTICLE INFO

Article history:
Received 24 February 2015
and in revised form 27 March 2015
Available online 20 April 2015

Keywords:
C. pseudotuberculosis
Cold shock protein
Spectroscopic methods
Secondary structure
Folding and refolding proteins

ABSTRACT

The gram-positive bacterium *Corynebacterium pseudotuberculosis* is the causative agent of different diseases that cause dramatically reduced yields of wool and milk, and results in weight loss, carcass condemnation and also death mainly in sheep, equids, cattle and goats and therefore globally results in considerable economical loss. Cold shock proteins are conserved in many bacteria and eukaryotic cells and they help to restore normal cell functions after cold shock in which some appear to have specific functions at normal growth temperature as well.

Cold shock protein A from *C. pseudotuberculosis* was expressed in *Escherichia coli* and purified. The thermal unfolding/refolding process characterized by circular dichroism, differential scanning calorimetry and NMR spectroscopy techniques indicated that the refolding process was almost completely reversible.

Introduction

Corynebacterium pseudotuberculosis (*C. pseudotuberculosis*) belongs to the heterogeneous CMNR-group of pathogens, a cluster of gram-positive bacteria including *Mycobacterium*, *Nocardia*, and *Rhodococcus* species besides *Corynebacterium* [1]. It is the causative agent of caseous lymphadenitis (CLA),[1] a disease encountered in sheep, goats, and equids and to a minor extent in horses (ulcerative lymphangitis) and cattle (cutaneous excoriated granulomas) as well and leads to drastically reduced yields of wool and milk, weight loss, carcass condemnation and eventually death. It thus results in considerable economic loss in related production areas all over the world [2,3]. Rare cases of infection have also been reported in humans [4]. As a facultative intracellular parasite the bacterium is capable of survival and growth in macrophages and is thus able to evade detection by the host immune system [5].

Although *C. pseudotuberculosis* is a mesophilic bacterium, growing optimally at 37 °C, its genome includes *csp* genes, coding for cold shock proteins (Csp). In many bacteria a reduction in the ambient temperature results in the concomitant increase of the production of cold shock proteins 2- to 100-fold whereas, normal protein production levels are decreased drastically [6]. Their first known function is the enhancement of DNA transcription to support the expression of other cold shock induced genes, for example *hns* or *gyrA* [7–9]. This is achieved by binding of the cold shock proteins to short stretches of single stranded DNA with high affinity and specificity [10–13]. However, some cold shock proteins have been reported to bind to ssRNA in an unspecific manner as well, leading to the suggestion that cold shock proteins can also function as RNA chaperones [14] and prevent the formation of cold-induced mRNA secondary structures [15]. Both mechanisms help to preserve cell viability during cold shock and to restore normal cell function.

To date many cold shock protein homologs in different bacteria have been identified, including *Escherichia coli* CspA, *Bacillus subtilis* CspB, *Bacillus caldolyticus* CspB, and *Salmonella typhimurium* CspE, to cite only a few examples. Csps share a cold shock domain (CSD) which is comprised of a five-stranded β-barrel and their structures have been solved by using either X-ray crystallography [16–19] or NMR-spectroscopy [20]. Significant sequence and structural similarity are shared with the CSD of eukaryotic Y-box

* Corresponding author at: Centro Multiusuário de Inovação Biomolecular, Departamento de Física, Universidade Estadual Paulista (UNESP), Rua Cristóvão Colombo 2265, São Jose do Rio Preto-SP 15054-000, Brazil. Tel.: +55 17 32212460; fax: +55 17 32212247.
E-mail address: arni@sjrp.unesp.br (R.K. Arni).

[1] *Abbreviations used:* CLA, caseous lymphadenitis; CspA, cold shock protein A; IPTG, isopropyl-β-D-thiogalactopyranosid; CD, circular dichroism; DSC, differential scanning calorimetry; NMR, nuclear magnetic resonance.

http://dx.doi.org/10.1016/j.pep.2015.04.006
1046-5928/

Biochemical and Biophysical Research Communications 467 (2015) 171–177

Contents lists available at ScienceDirect

Biochemical and Biophysical Research Communications

journal homepage: www.elsevier.com/locate/ybbrc

Crystal structure of *Staphylococcus aureus* exfoliative toxin D-like protein: Structural basis for the high specificity of exfoliative toxins

Ricardo B. Mariutti [a], Tatiana A.C.B. Souza [b], Anwar Ullah [a], Icaro P. Caruso [a], Fábio R. de Moraes [a], Leticia M. Zanphorlin [c], Natayme R. Tartaglia [d, e, f], Nubia Seyffert [d], Vasco A. Azevedo [d], Yves Le Loir [e, f], Mário T. Murakami [g], Raghuvir K. Arni [a, *]

[a] Multi User Center for Biomolecular Innovation, Department of Physics, IBILCE/UNESP, São José do Rio Preto, SP, Brazil
[b] Carlos Chagas Institute, FIOCRUZ-PR, Curitiba, PR, Brazil
[c] Bioethanol Science and Technology Laboratory (CTBE), National Center for Research in Energy and Materials, Campinas, SP, 13083-970, Brazil
[d] Cellular and Molecular Genetics Laboratory, Institute of Biological Sciences, Federal University of Minas Gerais, Belo Horizonte, MG, 270-901, Brazil
[e] INRA, UMR1253 STLO, Science et Technologie du Lait et de l'œuf, F-35042 Rennes, France
[f] Agrocampus Ouest, UMR1253 STLO, F-35042 Rennes, France
[g] Brazilian Biosciences National Laboratory (LNBio), National Center for Research in Energy and Materials, Campinas, SP, 13083-970, Brazil

ARTICLE INFO

Article history:
Received 12 August 2015
Accepted 19 August 2015
Available online 20 August 2015

Keywords:
Exfoliative toxin D-like protein
Staphylococcus aureus
Crystal structure
Toxin-mediated staphylococcal syndromes

ABSTRACT

Exfoliative toxins are serine proteases secreted by *Staphylococcus aureus* that are associated with toxin-mediated staphylococcal syndromes. To date, four different serotypes of exfoliative toxins have been identified and 3 of them (ETA, ETB, and ETD) are linked to human infection. Among these toxins, only the ETD structure remained unknown, limiting our understanding of the structural determinants for the functional differentiation between these toxins. We recently identified an ETD-like protein associated to *S. aureus* strains involved in mild mastitis in sheep. The crystal structure of this ETD-like protein was determined at 1.95 Å resolution and the structural analysis provide insights into the oligomerization, stability and specificity and enabled a comprehensive structural comparison with ETA and ETB. Despite the highly conserved molecular architecture, significant differences in the composition of the loops and in both the N- and C-terminal α-helices seem to define ETD-like specificity. Molecular dynamics simulations indicate that these regions defining ET specificity present different degrees of flexibility and may undergo conformational changes upon substrate recognition and binding. DLS and AUC experiments indicated that the ETD-like is monomeric in solution whereas it is present as a dimer in the asymmetric unit indicating that oligomerization is not related to functional differentiation among these toxins. Differential scanning calorimetry and circular dichroism assays demonstrated an endothermic transition centered at 52 °C, and an exothermic aggregation in temperatures up to 64 °C. All these together provide insights about the mode of action of a toxin often secreted in syndromes that are not associated with either ETA or ETB.

1. Introduction

Staphylococcus aureus, the Gram-positive bacterial pathogen, triggers a wide spectrum of infection and is the primary causative agent of pyogenic infections which can result in septicemia, osteomyelitis and meningitis, is encountered in humans and approximately 35% of the population are carriers. It is also found in warm-blooded animals [1] and is a major causative agent of mastitis in ruminants, causing thus huge economic losses in the milk production [2].

S. aureus secretes different exfoliative toxins (ETs) that result in toxin-mediated staphylococcal syndromes. These disorders range from localized bullous impetigo to staphylococcal scalded skin syndrome (SSSS) in which superficial skin blistering and exfoliation follow widespread painful erythema [3]. Thus far, four different serotypes of exfoliative toxins ETA, ETB, ETC, and ETD have been identified [4] and three of them (ETA, ETB, and ETD) are related to human infection [5]. Some ET and ET-like proteins are also found associated to skin infections in animal hosts and show cleavage specificity against human or animal desmogleins [6].

* Corresponding author. Departamento de Física, Universidade Estadual Paulista (UNESP), São José do Rio Preto, 15054-000, SP, Brazil.
E-mail address: arni@sjrp.unesp.br (R.K. Arni).

http://dx.doi.org/10.1016/j.bbrc.2015.08.083
0006-291X/

Biochemical and Biophysical Research Communications 468 (2015) 365–371

Contents lists available at ScienceDirect

Biochemical and Biophysical Research Communications

journal homepage: www.elsevier.com/locate/ybbrc

Crystal structure of mature 2S albumin from *Moringa oleifera* seeds

Anwar Ullah [a, **], Ricardo Barros Mariutti [a], Rehana Masood [a], Icaro Putinhon Caruso [a], Gustavo Henrique Gravatim Costa [b], Cristhyane Millena de Freita [b], Camila Ramos Santos [c], Leticia Maria Zanphorlin [d], Márcia Justino Rossini Mutton [b], Mario Tyago Murakami [c], Raghuvir Krishnaswamy Arni [a, *]

[a] Multiuser Center for Biomolecular Innovation, Department of Physics, IBILCE/UNESP, São Jose do Rio Preto, SP, Brazil
[b] Departamento de Tecnologia, FCAV/UNESP, Campus de Jaboticabal, Brazil
[c] Brazilian Biosciences National Laboratory (LNBio), National Center for Research in Energy and Materials, Campinas, SP, 13083-970, Brazil
[d] Brazilian Bioethanol Science and Technology Laboratory (CTBE), Brazilian Center for Research in Energy and Materials (CNPEM), Campinas, SP, Brazil

ARTICLE INFO

Article history:
Received 7 October 2015
Accepted 17 October 2015
Available online 23 October 2015

Keywords:
Moringa oleifera seeds
2S albumin
Flocculating activity
Crystal structure

ABSTRACT

2S albumins, the seed storage proteins, are the primary sources of carbon and nitrogen and are involved in plant defense. The mature form of *Moringa oleifera (M. oleifera)*, a chitin binding protein isoform 3-1 (m*Mo*-CBP$_3$-1) a thermostable antifungal, antibacterial, flocculating 2S albumin is widely used for the treatment of water and is potentially interesting for the development of both antifungal drugs and transgenic crops. The crystal structure of m*Mo*-CBP$_3$-1 determined at 1.7 Å resolution demonstrated that it is comprised of two proteolytically processed α-helical chains, stabilized by four disulfide bridges that is stable, resistant to pH changes and has a melting temperature (T_M) of approximately 98 °C. The surface arginines and the polyglutamine motif are the key structural factors for the observed flocculating, antibacterial and antifungal activities. This represents the first crystal structure of a 2S albumin and the model of the pro-protein indicates the structural changes that occur upon formation of m*Mo*-CBP$_3$-1 and determines the structural motif and charge distribution patterns for the diverse observed activities.

1. Introduction

Moringa oleifera (*M. olifera)* a hardy, drought resistant tree, native to the foothills of the Himalayas is widely cultivated in subtropical and tropical regions since the bark, leaves, seeds and roots are rich in vitamins and mineral salts and are widely used in herbal medicine [1], as a dietary supplement [2], for the extraction of edible oil [3], as natural flocculants for water purification [4,5] and more recently, as flocculants in the industrial production of alcohol from sugar cane [6].

A number of cationic peptides and low molecular weight basic proteins have been isolated from the crude extract of *M. oleifera* seeds [7,8]. One of these, the chitin binding protein (*Mo*-CBP$_3$), is a 14 kDa thermostable protein has been the focus of a disproportionately large number of studies since it is widely used for water purification and also possess antigungal and antibacterial activities [9].

Mo-CBP$_3$ belongs to the 2S albumin family of proteins that are synthesized as precursors, which are then proteolytically cleaved to form the mature protein. Four isoforms of this precursor have been isolated from *M. oleifera* seeds namely *Mo*-CBP$_3$-1, *Mo*-CBP$_3$-2, *Mo*-CBP$_3$-3 and *Mo*-CBP$_3$-4, which differ from each other by only a few amino acid residues [9]. The *Mo*-CBP$_3$-1 precursor (p*Mo*-CBP$_3$-1) consists of 163 amino acids including the N-terminal signal peptide and the linker peptides. Solution structures (NMR) of several 2S albumin precursors have been deposited with the Protein Data Bank (http://www.rcsb.org) and the only crystal structure currently available is that of the sweet protein, Mabinlin II (*Capparis masaikai* Levl., PDB ID: 2DS2) [10].

The crystal structure of mature *Mo*-CBP$_3$-1 (m*Mo*-CBP$_3$-1), a typical 2S seed storage albumin determined at 1.70 Å resolution provides a model for understanding the diversity of the structures of this large family of albumins, serves as a model for the structures of the precursors and indicates the structural basis for the observed flocculating activities.

* Corresponding author.
** Corresponding author.
E-mail addresses: anwar.ms90@yahoo.com (A. Ullah), arni@sjrp.unesp.br (R.K. Arni).

http://dx.doi.org/10.1016/j.bbrc.2015.10.087
0006-291X/

Send Orders for Reprints to reprints@benthamscience.ae

712 *Protein & Peptide Letters*, 2015, *22*, 712-718

Preparation and Characterization of Monomodal Grapevine Virus A Capsid Protein

Vinícius S. Santana[1#], Ricardo B. Mariutti[1#], Raphael J. Eberle[1], Anwar Ullah[1], Icaro P. Caruso[2] and Raghuvir K. Arni[1,2,*]

[1]*Multiuser Center for Biomolecular Innovation &* [2]*Departament of Physics, Universidade Estadual Paulista (UNESP), São Jose do Rio Preto-SP, 15054-000, Brazil*

R.K. Arni

Abstract: Grapevine virus A (GVA), a flexible filament of approximately 800 nm in length is composed of capsid subunits that spontaneously assembles around a positive sense genomic RNA. In addition to encapsidation, plant viruses capsid proteins (CPs) participate in other processes throughout infection and GVA CP is involved in cell-to-cell translocation of the virus. A protocol was developed to obtain low-molecular weight GVA-CP that is not prone to aggregation and spontaneous assembly and this was characterized by circular dichroism and dynamic light scattering. These results indicate the suitably of GVA-CP for X-ray crystallographic and NMR studies that should lead to the elucidation of the first three-dimensional structure of a flexible filamentous virus from the *Betaflexiviridae* family.

Keywords: Capsid protein, CD spectroscopy, dynamic light scattering, grapevine virus A, protein characterization, secondary structure.

1. INTRODUCTION

Grapevine virus A (GVA), a member of the *Vitivirus* genus [1], belongs to the *Betaflexiviridae* family [2] and is the etiological agent of Kober stem grooving, a member of the rugose wood disease complex, which is spread by propagation materials and mealy bugs. This disease is of considerable economic relevance to viticulture since it causes irreversible alterations to the susceptible grapevine, often resulting in the delay of budding in spring, reduction of grape yield and quality and, in some cases, complete destruction of affected vines [3].

The virus is a flexuous filament of about 800 nm in length containing a positive single-stranded RNA of 7349 nucleotides, excluding the poly(A) tail at the 3' terminus. The GVA genome consists of five open reading frames (ORF 1 to 5) and the coat protein (CP) is the only structural protein encoded by ORF4 [4]. In addition to encapsidation, plant viral coat proteins participate in practically every stage of the viral cycle, from multiplication to dissemination [5,6]. In an attempt to determine the role of GVA genes, mutations were inserted in every ORF [7], and the effect on viral replication, gene expression, symptoms and viral movement were examined. Mutation on ORF4 restricted viral movement, thus suggesting that the coat protein is required for cell-cell translocation of the virus.

Structural information regarding GVA CP is not available and the mechanism by which this protein participates in encapsidation and virus translocation is as yet poorly understood. Only a single crystal structure of the CP of flexible filamentous Papaya Mosaic virus (PMV) (PDB: 4DOX) that belongs to the *Alphaflexiridae* family, genus *Potexvirus*, has been determined [8].

Viral coat proteins tend to spontaneously self-assemble into virus-like particles that resemble the wild-type viruses [9-13] even in the absence of any other viral components [14,15]. The challenge to determine the crystal structure of a filamentous virus CP is the production of a low-molecular-weight capsid protein that is not prone to aggregation or spontaneous self-assembly.

We present the expression and a three-step purification method to produce highly pure, low-molecular-weight GVA CP in *Escherichia coli* suitable for functional and structural studies.

2. MATERIAL AND METHODS

2.1. In Silico Analysis

Sequence alignments of different viral CP proteins were performed with the ClustalW2 online Tool [16] and the secondary structure of the protein was predicted with the PSIPRED server [17,18].

2.2. Cloning of the CP gene

To construct the plasmid containing the CP gene, the cDNA was prepared from the isolated viral RNA. The GVA CP gene was amplified by PCR using the forward (5'-ATA GAA TCC GGT GAA AAT TTA TAT TTT CAA GGT GCA CAC TAC GCC AAG AGG-3') and reverse (5'-ATA AAG CTT CTA TAT CTC GAC AGC CTG-3') oligonu-

*Address correspondence to this author at the Centro Multiusuário de Inovação Biomolecular, Departamento de Física, Universidade Estadual Paulista (UNESP), Rua Cristóvão Colombo 2265, São Jose do Rio Preto-SP, 15054-000, Brazil; Tel: +55-17-32212460; Fax: +55-17-32212247;
E-mail: arni@sjrp.unesp.br
#Both authors contributed equally to this work.

1875-5305/15 $58.00+.00